DESIGN OF A MICROFLUIDIC CARTRIDGE FOR MALARIA DIAGNOSIS

A Dissertation

by

KOKOU SERGE DOGBEVI

Submitted to the Office of Graduate and Professional Studies of
Texas A&M University
in partial fulfillment of the requirements for the degree of

DOCTOR OF PHILOSOPHY

Chair of Committee,	Gerard L. Coté
Committee Members,	Melissa Grunlan
	Daniel Alge
	Jun Kameoka
Head of Department,	Michael McShane

December 2020

Major Subject: Biomedical Engineering

ABSTRACT

Malaria remains one of the deadliest diseases of the 21st Century, with 405,000 deaths annually. The visualization of stained blood smears with white light microscopy is still the gold standard for a proper diagnosis. Due to the difficulty of preparing consistent, high quality blood smears, effective malaria diagnosis remains challenging at the point of care (POC). Malaria diagnosis at the POC could be improved through the development of an automated smear preparation cartridge. In this work, materials for an automated smear preparation were developed and tested using bulk modifying polydimethylsiloxane (PDMS) with a poly(ethylene oxide) (PEO)-containing surface modifying additive (SMA). The modification was done at different concentrations, resulting in an increase in surface hydrophilicity as the concentrations of the SMA increased. The modified PDMS was optimized for the design of microfluidic cartridge for the generation of an automated, uniform, and repeatable blood smear by testing different SMA concentrations (3, 5, and 7 wt%) and blood volumes (0.3, 1, and 2 µl). Pillars were added at various locations throughout the channel, which served to prevent channel collapse and provide uniform cell distribution. With a target of cell uniformity (e.g. monolayer and cell density per area of 400-700 unique cells/ 0.024 mm^2 field of view), the combination of 5 and 7 wt% SMA, 4.7 ± 0.1 µm height and 0.3 µl of blood was shown to provide a good quality smear within 15 min. Also, using flow control, a wet whole blood staining protocol was developed in the microchannel for automated staining at the POC. A 3X concentration Giemsa stain was created and diluted with DI water yielding 10% 33%, 50% concentrations and was

tested to see which one worked best for staining malaria parasites. Although the results showed that for the 50% concentration the parasites were more distinguishable, this concentration also caused a crenation problem. Thus the 33% concentration showed the best contrast without crenation of RBCs. Further tests showed that the consistency for the 33% protocol was also good and that the parasites stained with 33% are equally or even more distinguishable than parasites from typical glass smear protocol.

DEDICATION

To my family and friends

To my loved ones, may the grace of God be with you. Thank you for all your sacrifice these past years.

ACKNOWLEDGEMENTS

First, I would like to give grace and thank God for everything.

I would like to thank my advisor, Dr. Gerard Coté, for his support and guidance throughout my Ph.D. program. Dr. Cote, thank you for being patient with me, for your encouragement, mentoring me, and providing me opportunities to grow.

I would also like to thank my committee members Dr. Melissa Grunlan, Dr. Daniel Alge, and Dr. Jun Kameoka, for their support and counsel throughout the course of my research.

I also want to thank all the past and current members of the OBSL lab and Dr. Bryan Ngo. I want to thank each one of you for everything you taught me, for your moral support, friendship, motivation, and guidance.

Thanks to Texas A&M University for providing me a place to learn and grow.

Finally, I want to thank my family (wife and child), my mother and my friends. Thank you for your support, patience, and motivation.

CONTRIBUTORS AND FUNDING SOURCES

Contributors

This work was supervised by a dissertation committee consisting of Dr. Gerard Cote (chair), Dr. Melissa Grunlan, and Dr. Daniel Alge of the Department of Biomedical Engineering and Dr. Jun Kameoka of the Department of Electrical Engineering.

All work for the dissertation was completed by the student, under the advisement of Dr. Gerard Cote from the Department of Biomedical Engineering.

Funding Sources

The graduate study was supported by a fellowship from Louis Stokes Alliances for Minority Participation (LSAMP) from National Science Foundation (NSF), a grant from the National Science Foundation (#1402846), the TEES Center for Remote Health Technologies and Systems, and the Texas A&M Biomedical Engineering Graduate Trainee Fellowship.

TABLE OF CONTENTS

Page

LIST OF FIGURES

Page

LIST OF TABLES

Page

CHAPTER I

INTRODUCTION

1.1 Motivation and Significance

Malaria remains a major global health burden with 405,000 deaths and 228 million cases in 2018 (1, 2), as well as 3.2 billion people at risk (3). The heartbreaking and outrageous part of malaria is that it kills mostly children. In 2018, around 67% of the malaria-related deaths were of children under the age of 5, and 94% of those children were from Africa (2, 3). Rapid diagnostic tests (RDTs) have recently been developed for the detection of malaria in the field to help screen for malaria, but they lack sensitivity and the ability to define parasitemia (i.e. the quantitative content of parasites per microliter of blood), which is needed for comprehensive diagnosis (4-6). Thus, the gold standard for diagnosis is still the examination of stained, smeared blood samples with white light microscopy (4, 7, 8). The examination of a stained blood smear with light microscopy has three steps: 1) Uniform generation of a blood smear (9, 10); 2) fixation and staining or simply staining (5); and 3) the examination of the stained smear under the microscope, which also has 3 sub-steps (e.g. parasite detection, identify parasite species, and determine parasitemia level (11, 12)). Each of these steps are challenges for malaria diagnosis, especially at the point of care (POC). They require a trained technician, which is often unavailable in remote areas (5, 9, 10, 13). Among those three steps, the smear preparation is the most important part, with the staining step coming in a close second, because the quality of the stained smear affects the rest of the examination process. Because the process of malaria diagnosis based on microscopy can be very time consuming, depending

on the level of expertise, as well as expensive (3, 5, 11, 12, 14), many efforts have been done to alleviate these problems. Specifically, parasitemia, which is the quantitative content of parasites in the blood, is a time-consuming, labor-intensive endeavor that requires counting the cells and parasites and calculating the percentage per microliter of blood (15). It gives the doctor an indicator of the severity of the disease, and its lack of accuracy can lead to poor treatment or even death (6, 16). This workload prevents a fast and effective diagnosis. As a result, doctors often will over or under diagnose the disease and start patients on specific malaria medication at a particular dose before they can determine whether they even have the disease or what the severity of the disease is (4, 17) if they do have it. Those situations can lead to death or to parasites' becoming resistance to the drug. Knowing early the severity of the disease can help doctors make an accurate diagnosis and provide the correct treatment. To this end, research has been done in developing automated software to detect parasites and reduce the time for determining parasitemia without the need of high-level experts, but the software is still unavailable for use in the field because of its lack of sensitivity and specificity (6, 18). This lack of sensitivity and specificity is due, in part, to the lack of good smear quality and uniformity across trained technicians (10, 19, 20). Little to no efforts have been made to develop automated smear makers, especially for use at the POC (21, 22). Smear quality and uniformity can vary both within and between trained technicians (10, 23, 24). As a result, the software may work for the smear from one technician but may not work for smears developed by another technician. Thus, a reproducible automated smear and staining microfluidic chip is of great interest to solve this lack of smear uniformity, particularly at

the POC. In general, point-of-care microfluidic chips have also shown the potential to meet many, if not all, of the ASSURED criteria guide created by the World Health Organization (WHO) for the development of diagnostic devices for use in developing countries (25). Specifically, the ASSURED criteria stands for devices that are Affordable, Sensitive, Specific, User-friendly (minimal expertise necessary), Robust and rapid (results accessible in under 30 min), Equipment-free, and Deliverable to remote areas (25, 26). By developing such a faster and easier to use microfluidic chip that produces more uniform smears at the POC, diagnosis can be done quickly, treatment can be more effectively administered with reduced parasite resistance, and more lives can be saved.

1.2 Background

1.2.1 Malaria disease and parasite transmission cycle

Malaria is a serious and often fatal disease transmitted by female mosquitoes of the genus Anopheles that are infected with the malarial parasite (27). The disease results in estimated mortality of 405,000 deaths, 228 million cases in 2018, and there are 3.2 billion people at risk of acquiring the disease, with 67 % of the deaths being children under age of 5 according to WHO (1, 2). Although there are 173 species of malaria, in humans only four different species of parasites can cause malaria: Plasmodium (P.) – falciparum, vivax, ovale, and malariae (28, 29). P. knowlesi is still considered zoonotic malaria, which can affect humans but there is no evidence that the parasite is being naturally transmitted from human to human via the mosquito, without the natural intermediate host (e.g. macaque monkeys, genus *Macaca*) (28, 30).

The development of malaria parasites occurs through two hosts (the mosquito and the human) and through many stages and cycles as depicted in **Figure 1** (31). Soon after the parasite enters the human body it travels to the liver and develops into hepatic schizonts, which contain up to 30,000 merozoites each (27). The merozoites are then released into the bloodstream. From there, they go through the erythrocyte cycle during which the merozoites invade the red blood cells (RBCs), develop into immature (ring) trophozoites, and then into mature trophozoites, which mature into schizonts containing 8 to 32 new merozoites. At maturity, the RBCs rupture and release merozoites into the bloodstream which invade new RBCs and start a new cycle (3, 27, 32-34). Some merozoites can also develop into male and female gametocytes, which are then picked up by other female mosquitoes of the genus Anopheles (27, 32, 34). Although the gametocytes do not cause the disease directly, they go through multiple cycles inside the mosquitoes (e.g. mosquito stages) to transmit the disease to another person (32, 34) and this restarts another Human cycle.

In humans, the liver stage of the development of the parasite, in general, is around 5-15 days (3, 16, 27). However, the P. vivax and P. ovale can stay dormant in the liver for many years. This state is called hypnozoites (29, 34, 35) and P. vivax has been reported to have a 30 year hypnozoites stage (34). The erythrocyte cycle is around 2 days for P. falciparum, P. vivax, and P. oval; 24 hours for P. knowlesi and 3 days for P. malariae (16, 30, 33, 36). During this stage, the parasites grow, consume the RBCs' hemoglobin, produce a byproduct called hemozoin and rupture the RBCs (37-39). The erythrocyte stage causes the symptoms for malaria when RBCs are being lysed (32-34). Because many

merozoites go through the erythrocyte cycle, it can increase the severity of the disease by making the patient anemic. However, it is possible to have malaria parasites in the bloodstream and be asymptomatic of the disease (3, 16, 27).

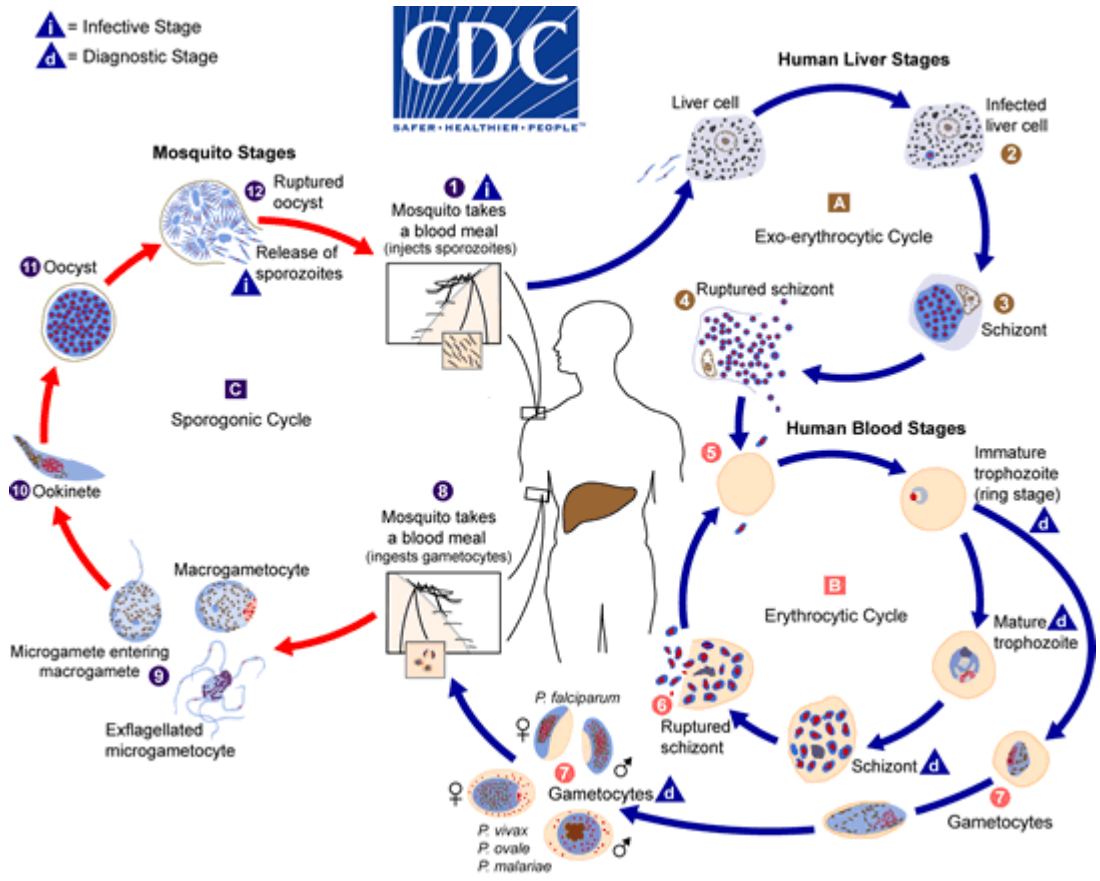

Figure 1. Malaria parasites life cycle Reprinted with permission from (CDC, 2020)

1.2.2. Malaria Species

Malaria disease is usually categorized as uncomplicated malaria and complicated or severe malaria. Uncomplicated malaria can sometimes be asymptomatic for patients

who are immune or can cause symptoms which are generally nonspecific to malaria (e.g. fevers, headaches, nauseas, vomiting, chills, lassitude, fatigues, abdominal, anorexia, etc.) (3, 16, 27). Complicated or severe malaria causes symptoms such as comas (i.e. cerebral malaria), seizures, metabolic acidosis, severe anemias, hypoglycemia, acute renal failures or acute pulmonary edemas, and vital organ dysfunctions. Malaria is so deadly because it can progress from uncomplicated to severe very quickly, within 48 hours (16, 27). However, not all the species of malaria parasites have the same level of severity that is considered deadly.

Each of these species have their own unique characteristics, with P. falciparum as the most dangerous of the 5 since it leads to the most malaria deaths (5, 28). It is often found worldwide in a tropical and subtropical regions, but mostly in Africa (29, 30). P. falciparum can cause a life-threatening disease because it infects all RBCs with a high level of parasitemia by multiplying rapidly (40). In addition, it can sequester in the capillary vessels and lead to occlusion over time (30, 41, 42). This can affect brain capillaries and cause a severe condition called cerebral malaria that can lead to coma or death in few days (8, 32, 35). P. vivax is mostly found in Asia, Latin America, and some parts of Africa (29, 30, 32), and is the cause of most malaria cases (43); However, many Africans are immune to the parasites because most Africans are Duffy negative (32, 43, 44). The Duffy antigen is a protein receptor for malaria parasites, but most Africans do not have it, thus becoming Duffy negative. Although the maximum parasitemia of P. vivax is usually < 2 % and mostly infects young RBCs (40), in high prevalence it has been reported to be fatal and behave like P. falciparum with an inflammatory response,

dyserythropoiesis, and severe anemia caused by RBCs fragility. It can also be retained by the spleen or cause renal failure, severe thrombocytopenia, and sometimes coma (8, 35, 43). Furthermore, the liver stage of P. vivax (hypnozoites) can cause a relapse of the disease. For that reason, a patient with P. vivax will need 2 different treatments (43, 45), one treatment to clear the parasites from the bloodstream and one treatment to clear the parasites from the liver. P. ovale is found in Africa, mostly in West Africa, and western Pacific islands (30, 32, 46). Similar to P. vivax, P. ovale has a low maximum parasitemia (< 2%), prefers to infect young RBC's (40, 46, 47), and also has a liver hypnozoites stage that can cause a relapse of the disease (30, 32, 47). Thus, the required treatment is similar to that of P. vivax. Despite the similarities, P. ovale is able to infect people who are Duffy negative (30, 32, 46) but P. ovale is not as life threatening as P. vivax (47). P. malariae is found worldwide in tropical or subtropical areas (30, 32), has a maximum parasitemia that is usually < 2%, and mostly infects old RBCs (40, 48). P. malariae is not as dangerous as P. falciparum and does not have a hypnozoites stage like P. Vivax. However, it can cause a chronic infection that lasts a lifetime if untreated and, in some cases, it can cause nephrotic syndrome, a long-lasting serious complication of the chronic infection (30, 32, 48). P. knowlesi is located throughout Southeast Asia and is the only zoonotic malaria that affects humans (40, 49, 50). Because of its short 24-hour RBC cycle, P. knowlesi can be life threatening similar to P. falciparum. It can infect all RBCs and its parasitemia can be very high, which is why it can develop rapidly from uncomplicated to severe malaria (40, 49, 50).

Early, fast, easy, and more importantly, a comprehensive diagnosis for all malaria species is still unavailable, especially at the POC (51, 52). Although there are many medications to treat malaria, and many efforts have been made to improve diagnosis, people are still dying from the disease. This is, in part, because complications can arise due to late diagnosis and/or misdiagnosis, which is due to an excessive workload and lack of equipment and high-level experts at the POC. Thus, there remains a need to find a different way to diagnose or to improve upon the gold standard of malaria diagnosis.

1.2.3. Malaria diagnosis requirements and methods

Researchers have identified three main requirements for malaria diagnosis: 1) parasite detection 2) species identification and 3) the determination of the parasitemia (53). There are multiple methods used for the diagnosis of malaria: bright field or fluorescence microscopic observation of a blood smear, Polymerase Chain Reaction (PCR)-based diagnosis, Rapid Diagnostic Test (RDT) and others (3, 5, 29).

1.2.3.1. A symptomatic-based diagnosis method

A symptomatic-based diagnosis of malaria is the main method used for malaria diagnosis. This method is based on the patient's clinical signs and symptoms during a physical examination by the Community Health Workers (CHWs) or at home in a rural areas (5, 54, 55). This diagnosis method is the main method used because over 70% of patients with malaria symptoms (e.g. fever) do not go to the hospital (54) and instead diagnose and treat themselves at home with traditional medicine or over the counter

antimalaria drugs purchased at local shops (54, 56, 57). Patients usually only go to the health community centers if their home treatment failed (54). The diagnosis in the health community center is based on clinical signs and symptoms because the center does not have the proper equipment and/or personnel for a proper diagnosis. Although health community centers helps save lives, the clinical diagnosis is based on the medical expertise of the CHWs, and thus usually has a low sensitivity and specificity (5, 54, 55) because malaria is not the only disease with symptoms such as fever, headache, nausea, vomiting. Diseases such as yellow fever and Q fever, influenza, cold, and other common infections have similar symptoms (5, 58).

1.2.3.2. Examination of a stained blood smear with white light microscopy

Basic white light microscopic observation of blood smears by a trained technician is the current gold standard for malaria diagnosis (4, 7, 8). This technique requires multiple steps that need to go well for a proper and fast diagnosis. The first step is the blood smear preparation, which can either be thick or thin (59). For thick smear preparation, 3 drops of blood (~ 6 µL) are placed on a glass slide and spread using the corner of another slide or an applicator stick to a size of 12 mm diameter (60-62). Another way to spread the thick smear is to use the corner of the slide to create small scratches in the underlying slide (60). This method is called the scratch method and it helps improve the adherence of the smear to the slide without affecting the morphology of the cells.

There are three main methods used for thin smear preparation: the manual wedge method, the manual coverslip method, and the automated method (13, 22, 63, 64). The

manual wedge method is the most commonly used and involves using a cover slide or microscope slide to push and spread around 2 µl of blood on the top of another slide at an angle between 30 to 40 degrees. Despite being the favored technique because of its easy to handle advantage, the wedge method has some drawbacks, including a high degree of variability across smears prepared by either one expert using the same blood, or smears across experts, (13, 23, 24). In the coverslip method, a sample of blood is placed between two coverslips or between a slide-glass and a coverslip, which are placed crosswise to each other so that they have eight-star corners (13). The coverslip on top is moved to spread the blood and uniformly distribute the cells. The coverslip method is harder to implement, so it is not often used.

Generating a good quality thin blood smear is a challenge in hematology diagnosis, particularly at the POC and automated smear preparation could improve the smear quality. The manual method for smear preparation is labor intensive and requires a trained technician, who is often unavailable in developing countries and at the POC (9, 10, 13). As reported by various researchers, a good quality and repeatable smear is important and plays an essential role in the proper detection, classification, and differential counting of blood cells in manual or digital microscopy (10, 19, 20). Riedl et. al. indicates that manual smear preparation is insufficient for a proper and reproducible detection and classification of blood cells and that a semi and fully automated slide preparation would be better (19). Thus, automated smear preparation devices were investigated and developed (21, 22). The automated smear method uses many techniques to create the smear, such as a microfluidic, a spinning, a wedge, or a coverslip technique. Some automated smear methods have a

better WBC distribution than the wedge method, less variation within smear, less labor and time for the operation, and are as easy to handle as the wedge method (10, 13, 21, 23). However, there is still variation across smears of different automated devices and these devices are only available for laboratory use and cannot be used at the point of care (21).

Typically, in malaria diagnosis, both thin and thick smears are required for a rapid and proper diagnosis. Both types of smears have their advantages and disadvantages. The thick smear procedure lyses RBCs and uses a large volume of blood, so it is useful for parasite detection and sometimes parasitemia (60, 62). However, because cells are lysed during the procedure, parasite morphologies are sometimes affected, and thus the thick smear is difficult to use for species identification (60). Thin smears**,** on the other hand**,** use a small volume of blood, 1-2 µl usually, and no cells are lysed during the procedure. Because of this, the process can be used for all steps of the diagnosis procedure, especially for species identification (62). While a thick smear is used for species identification in samples of low parasite density (61), a thin smear is typically used for parasite detection in samples of high parasite density. This is because the thin film doesn't lyse the cells and uses less blood volume, so parasite detection would take more time at low parasite densities. Thus, both smears are often used in harmony toward a faster diagnosis.

After a blood smear is generated, the next step involves fixing and staining, with the former only applying to a thin smear. There is chemical as well as physical methods that are used for fixing a blood smear. The chemicals that are generally used are formaldehyde, glutaraldehyde, acetone, ethanol, methanol, or a combination of them depending on the application (65, 66). Physical methods include heating, microwaving,

and cryo-preservation (freeze-drying). Of these options, the gold standard technique is to use a 100% methanol solution (64). The fixing protocol in the gold standard technique is simple, usually summarized as the insertion of the dry smear slide into an absolute methanol solution for at least 30 seconds, and differs from the stain to stain (64). While Giemsa staining requires fixing in absolute or 100% methanol beforehand, in a Leishman protocol, the fixing is part of the staining protocol because Leishman has 100% methanol in its solution (67). For the Giemsa stain, fixation beforehand allows the methanol to open the cellular membranes of the cells for the stain to get into the cell. It also helps cell morphology conservation over a long period of time and influences the color of the stain (68).

A stain is generally used for the contrast of cellular components, study of cell morphology or changes in the cell, and identification of intracellular components. For malaria diagnosis, Romanowsky stains, such as Field's and JSB stain, Giemsa, Leishman, and Wright stains are considered the gold standard (67). Similar to the importance of the quality of the smear, the quality of the stain is invaluable in the diagnosis, characterization, and monitoring of various clinical diseases such as malaria (9, 69). There has been inconsistency in the stain quality for malaria diagnosis because staining quality depends on the skill level of the expert, chemical staining, fixation, and the quality of the smear (70). Bad staining is usually shown by the presence of artifacts and/or improper color and contrast for the cells (9, 54, 66). Because the role of the stain is to enhance the contrast of cellular component for better diagnosis, a bad stain can conversely lead to error in the

diagnosis (54, 69-71), which can lead to improper treatment, parasites' resistance to antimalaria drugs, death and socioeconomic burden (42, 54, 71-73)

The visualization of the blood smear under a microscope allows the technician to go through the malaria diagnosis requirement steps (detection, species identification, and parasite counting for parasitemia). The parasite detection, which is usually done with a thick smear, gives proof that the patient has malaria. After confirming the presence of malaria in the blood, the technician tries to identify the species of malaria by looking at the morphology of the parasite. Each of these requirements is very important. Parasite detection and species identification could sometimes be difficult to accomplish, particularly with lesser skilled technicians or low parasite density. If the presence of parasite cannot be confirmed because of low parasite density, it could lead to a false negative diagnosis. Error from the technician could also lead to a false positive, (72, 74). False positive or false negative diagnosis could lead to severe consequence such death or parasites resistance (4, 72, 74, 75). Identifying the spices of the malaria parasites is also sometimes difficult (4, 5) and important because each species has its own treatment (8, 16). Thus, getting the species wrong could lead to the wrong treatment which could lead to death or parasite resistance (4, 16, 76). Parasitemia calculation is a time-consuming, labor-intensive endeavor that requires counting the cells and parasites and calculating the percentage per microliter of blood. There are rules to follow when counting the cells for the parasitemia calculation (62, 77). These rules only apply if the presence of a parasite has been confirmed either through microscopy or RDT. The rules depend on if thick film or thin film is used. Because a thick smear doesn't have an RBC, WBC count is used for

the parasitemia calculation. If you count greater than 100 or more parasites with 200 WBCs, then one stops and report the results per 200 WBCs. However, if one counts less than 100 parasites then they should continue counting until they reach 500 WBCs and use the results to calculate the parasitemia per 500 WBCs. The parasitemia equation or the parasites per µl of blood's equation for WBCs is equation 1 (62, 77).

$$\text{Parasites /µl of blood} = \frac{\boldsymbol{number\ of\ parsites\ counted} \times \mathbf{8000}\ \boldsymbol{WBCs/\mu l}}{\boldsymbol{number\ of\ WBCs\ counted}} \qquad (1)$$

The thin smear rule on the other had uses RBC count for the parasite's density calculation. If the parasitemia is high (e.g., > 10%) one examines 500 RBCs; if it is low (e.g., <1%) one examines 2,000 RBCs (or more) and stops counting when 5000 RBCs have been counted or when one examines about 20 fields of view assuming they have around 250 RBCs per field (62, 77). Most technicians prefer the rule based on the WBC count because it is easier, however, automated software uses thin smears, so they prefer the rule based on RBC count. It is also important to note that if one counts 100 or more parasites in each field of view of a thick smear, the parasite density calculation should be done with a thin smear. The equation for RBCs parasites density calculation is equation 2 (62, 77).

$$\text{Parasites /µl of blood} = \frac{\boldsymbol{number\ of\ parsites\ counted} \times \mathbf{5000000}\ \boldsymbol{RBCs/\mu l}}{\boldsymbol{number\ of\ RBCs\ counted}} \qquad (2)$$

In summary, the microscopy gold standard has a sensitivity of 5-10 parasites/µl for a thick smear when examined by a high-level expert and if the quality of the smear, stain, and equipment are on the highest level possible (16, 78). However, the average sensitivity for thick smear examination reported is around 50 parasites/µl (28, 41, 79), and this sensitivity increase to 100 parasites /µl or more when diagnosed in the field (4, 16, 28). On the other hand, the sensitivity for a thin smear is >200 parasites/µl when examined by a high level expert and > 500 when examined by a low level expert (80). The process, in general, is considered time-consuming, expensive, and requires an expertise at each step for proper diagnosis and is unavailable in the rural area because of lack of expertise. In addition, the examination of 100 fields of view at least is required to claim a negative slide for a thick smear (4, 27, 28, 79) and at least 300 fields of view for a thin smear (28, 77).

Although considered the gold standard, the challenges of each step in the microscopy diagnosis process calls for continued research to overcome some of these challenges. For example, to improve sensitivity, fluorescence stains were developed for malaria diagnosis (81, 82). Among them, Quantitative Buffy Coat (QBC) has been considered successful enough to be used in some areas for malaria diagnosis.

1.2.3.3 Quantitative Buffy Coat (QBC)

The QBC technique is a microscopic detection method that stains the parasites' deoxyribonucleic acid (DNA) in micro-hematocrit tubes with fluorescent dyes, e.g., acridine orange (5, 41, 83). The process is similar to the bright field gold standard procedure, except that instead of the preparation of a smear, the blood is collected in a

hematocrit tube containing acridine orange and anticoagulant. The blood in the tube is centrifuged at 12,000 g for 5 min and examined under a fluorescence microscope (5, 81, 83). The process is fast because it eliminates the smear preparation step, and its staining process is short (27). As a fluorescence technique, it is a very sensitive method and can detect >5 parasites/ul (5), however, it lacks specificity and is not suitable for species identification and parasite density calculation (5, 37, 41).

1.2.3.4 Rapid Diagnosis Test (RDT)

The RDT was developed to overcome the complexity of the gold standard process and for use in the field. RDTs are immunochromatographic lateral flow devices that detect specific antigens of malaria parasites. RDTs can either detect the Plasmodium lactate dehydrogenase (pLDH) expressed by all human malaria species and/or the histidine-rich protein 2 (HRP2) expressed by P. falciparum (5, 14, 84). Since 1990, the WHO has recognized RDTs as a method for malaria diagnosis because they are fast, easy to use, and do not require a trained technician nor any other equipment (5, 14). Since then, there have been 332 RDTs developed and tested by 2018 (84). RDTs are currently used in conjunction with the gold standard process because they cannot provide parasites' density/µl nor provide the species in mixed infections (5). Thus, they are mostly used as a screening tool. However, they are very useful and can be more sensitive than microscopy in rural areas where trained technicians do not exist (4, 5, 85). Their sensitivity has been reported as variable in some remote areas. The sensitivity limit is typically 100 parasite/µL. However, they can have false positives because HRP2 are usually still in the

blood for several weeks even after malaria is cured**.** The RDT false-negative diagnosis is due to malaria antigen gene deletion or mutation (4, 7), but sometimes because of its detection limit, and they are often not reliable for non-falciparum infection (4).

Besides the microscopy method and RDT, there are also molecular methods developed for malaria diagnosis such as polymer chain reaction (PCR).

1.2.3.5 Polymerase Chain Reaction (PCR)

PCR is a molecular method based on the amplification of the malaria parasite DNA. Malaria PCR is also considered a gold standard method for mix parasite detection, species identification and low level parasite detection because it is more sensitive and more specific than the microscopy gold standard technique, RDT, and QBC (5, 41, 85, 86). It has a detection limit of >1 parasite/ μL compared to 50 for the microscopy gold standard and 100 for RDT (5, 41). Because of its high sensitivity and specificity, PCR is useful for detecting drug resistant parasites and correctly diagnosing mixed infections (5, 41). Despite all the advantages of PCR, it is still not widely used because it is hindered by complex methodology. It is very expensive, requires a highly trained technician (5), and requires quality control and equipment maintenance frequently. Thus, PCR is difficult to implement in developing countries, especially at the POC (5, 85, 87).

In addition to the methods described here, there are several others for malaria diagnosis which are summarized in **Appendix A Table A1** (5).

1.2.4. Malaria treatment

There is a close relationship between malaria diagnosis requirements, methods, and treatments. Examination with white light microscopy remains the gold standard because it provides information on all 3 requirements which is vital for proper treatment. As mentioned earlier, malaria is categorized as uncomplicated and complicated or severe (16, 88).

1.2.4.1 Complicated malaria

Complicated malaria is subdivided into groups based on the species: Severe falciparum malaria, severe vivax, and severe knowlesi malaria (16, 88). The falciparum malaria is defined as severe if one or more of the following in **Appendix A Table A2** occur (16). Severe falciparum malaria is treated with intravenous or intramuscular artesunate for at least 24 h and followed by oral treatment (16, 86). It is important to note that the dose for oral treatment depends on if the person is a child, adult, or pregnant (8, 16, 86). Besides P. falciparum, P. vivax and P. knowlesi are the only other species that produce a complicated malaria condition (16, 86).

Treatment of severe vivax malaria is similar to that of severe falciparum malaria, but without parasite density thresholds because the parasitemia level of P. vivax is not usually high (16). Having a parasite density threshold as high as the one P. falciparum malaria would be misleading. The severe P. knowlesi is defined as severe falciparum but with two key differences summarized in **Appendix A Table A3** (16). The parasites' density of 100,000/µl is equivalent to 2% parasitemia (16, 87), which is lower compared

to P. falciparum hyperparasitemia level requirement of > 10% (16). This indicates that P. knowlesi is more severe at low parasitemia than P. falciparum at the same level of parasitemia. Secondly, Jaundice symptom from plasma or serum bilirubin > 50 µmol/L (3 mg/dL) with a parasite count > 20,000/µL, which is a key difference between severe P. knowlesi and P. falciparum

There are many factors that define severe falciparum malaria, such as parasitemia level, anemia, hypoglycemia, coma, and seizure, which are clinical signs of cerebral malaria (8, 16). However, most of them are a combination of clinical signs and the level of parasite density. Although the treatment for severe malaria is almost the same for all severe malaria, regardless of the species with parenteral treatment, the requirement for severe malaria diagnosis is species dependent based on different levels of parasite density for P. falciparum and P. knowlesi and not the parasite density requirement for P. vivax (16, 88). These requirements indicate the importance of the malaria diagnosis requirements, such as species identification and determination of parasitemia level. Thus, despite having few drawbacks, the examination of a stained blood smear with microscopy and PCR remained the gold standard because only they can accurately provide all 3 malaria diagnosis requirements.

1.2.4.2 Uncomplicated malaria

Every patient diagnosed with malaria that does not meet the criteria for severe malaria is considered to have uncomplicated malaria (16). Uncomplicated malaria is subdivided into multiple groups based on species: uncomplicated P. falciparum malaria,

uncomplicated P. vivax, P. ovale, P. malariae, and P. knowlesi, and mixed malaria infections (16). The uncomplicated P. falciparum is subdivided into uncomplicated P. falciparum malaria and special risk groups such as the first trimester of pregnancy, infants less than 5kg, patients co-infected with HIV, non-immune travelers, and uncomplicated hyperparasitemia and uncomplicated non-special risk group (17). Patients with uncomplicated P. falciparum malaria and who don't belong to any special risk group are usually treated with a combination of drugs including one or more of the following: artemether + lumefantrine, artesunate + amodiaquine, artesunate + mefloquine, dihydroartemisinin + piperaquine, artesunate + sulfadoxine–pyrimethamine (SP) (16, 73).

Patients in the special risk group follow a specific treatment designed for them. Similar to severe malaria, the value of knowing the species and parasite density is used to determine the severity of the disease. Although every malaria species has its specific uncomplicated malaria treatment, most of the malaria species treatments are similar to P. falciparum treatment and differ only in regard to parasite drug resistance or the absence of a specific treatment (16).

In summary, malaria remains a major global health burden. Many diagnosis methods have been developed, however, all them have some flaws. They either can cannot fulfill the malaria diagnosis requirements, require complex methods for easy and fast diagnosis, especially at the POC in a rural area, require a trained technician which are unavailable, and/or are costly. Despite all the efforts done to solve these issues, some problems such as smear preparation and staining at the POC are still lacking. These issues

could be partially addressed by creating an automated microfluidic device for smear preparation and staining for POC diagnosis.

1.2.5. Microfluidic overview

Microfluidic systems have been shown to have the potential for developing devices for POC diagnosis. For more than half a century, microfluidic technology advancement has been driven largely by application needs and demands (89). Today, one of the primary demands for microfluidics is to advance diagnosis from the laboratory into field work, while solving the problems such as sample transportation and sample preparation. Thus, many efforts have been made to include sample preparation in microfluidic systems (90-92). While some researchers focus on the development and creation of microfluidic devices, others focus on the research and development of materials that help advance many microfluidic applications (92-94). Two major trends, such as powerful microscale research platforms and low-cost portable analyses, have been the focus of many researchers (93). As the areas of microfluidic applications increase, there is continued interest in investigation of different materials to accommodate that demand. **Appendix A Table A4** summarizes a list of different materials for different microfluidic applications (89, 93). In order to better understand the materials used for a microfluidic and to provide better guidance for the choice of material for specific applications, many studies investigate various features such as hydrophilicity/hydrophobicity, modulus, surface charge, optical transparency, channel profile, etc (89, 93, 95). **Appendix A Table A5** shows a summary of studies on different material features (93).

The design of low-cost portable analyses microfluidic devices has shown its potential in biological, chemical and medical applications (93). One of the main paths of this growth is the development of POC diagnostic devices. The path of the design of low-cost portable analyses has not been easy. Most current devices still require pumps, syringes, and tubing connections to help fluid flow through the channels (96-98). Although these methods work well for lab-based applications, they have many negative features for field work or POC applications. Field driven requirements favor simple techniques, such as capillary flow transport that can eliminate complicated sample interface connections and reduce the large dead volume of fluids associated with syringes, tubing, and pumps. Field work microfluidic chips should be easy to use and not need any significant hands-on operation time (92, 98, 99). To solve these problems, researchers have been developing pumpless capillary flow system (90, 97, 100-104). The research for the development of pumpless capillary flow systems focused of the development of hydrophilic materials and microfluidic designs that allow flow without external force (90, 97, 100-104).

Given the above significance and background showing the need for a uniform smear and staining POC device that follows much of the ASSURED criteria for malaria diagnosis, three studies toward the design of a pumpless microfluidic system were performed as described in the next three chapters, namely; Chapter 2) Pumpless, self driven, microfluidic channels with controlled blood flow using an amphiphilic silicone, Chapter 3) Whole blood smears prepared via a pumpless microfluidic for POC applications and Chapter 4) Brightfield and fluorescent staining of microfluidic cartridge generated thin peripheral blood smears.

CHAPTER II

PUMPLESS, "SELF-DRIVEN" MICROFLUIDIC CHANNELS WITH CONTROLLED BLOOD FLOW USING AN AMPHIPHILIC SILICONE*

2.1 Overview

A silicone microfluidic system that enables the pumpless, controlled flow of blood represents a significant advancement for the improvement of diagnostics and biological research. Such a system would be especially useful toward developing a single use, optical imaged point-of-care (POC) device. While readily used to prepare microfluidics via soft lithography, silicones inhibit capillary flow of blood due to their extreme hydrophobicity. Herein, Sylgard 184 was conveniently modified with a surface modifying additive (SMA) to produce microfluidics having "on-demand" surface hydrophilicity leading to pumpless capillary blood flow. The SMA is a poly(ethylene oxide) (PEO) silane amphiphile composed of a cross-linkable silane (Si–H) end group, an oligodimethylsiloxane (ODMS) tether, and PEO segment: HSi-$ODMS_{30}$-*block*-PEO_8-OCH_3. The SMA was incorporated at different concentrations into the silicone (5, 7, and 14 wt %) and resulting films as well as corresponding microchannels were assessed for key properties relevant to a single use, POC device to analyze blood. Overall, the SMA did not compromise light propagation or increase autofluorescence, which are important parameters for permitting the eventual use

*Reprinted with permission from "Pumpless, "Self-Driven" Microfluidic Channels with Controlled Blood Flow Using an Amphiphilic Silicone" by Dogbevi KS, Ngo BKD, Blake CW, Grunlan MA, Coté GL., ACS Applied Polymer Materials. 2020. Copyright 2020 American Chemical Society

of optical detection and imaging methods for analysis of blood within a microfluidic channel. While incorporation of the PEO-silane amphiphile SMA led to an expected decrease in modulus, this did not result in collapse of the channels. The SMA caused a dramatic increase in water-driven surface hydrophilicity, particularly at higher concentrations. As a result of the surface restructuring effect, the modified silicones enabled the pumpless flow of blood through microfluidic channels. Moreover, channel height as well as SMA concentration was useful in controlling the speed of blood flow.

2.2 Introduction

Microfluidics, by offering fluid flow control for a microscale device, have vast potential to impact medicine and biology.(105) Most microfluidic technologies rely on pumps, syringes, and tubing connections to help push fluid through the channels.(96, 98) While enabling controlled flow, these increase liquid and analytic reagent consumption (due to large dead volumes) and also generate bubbles.(98, 106) In addition, pump-actuated microfluidic systems are typically bulky and require expensive equipment.(98, 99, 106) Recently, a low-cost portable pressure pump was created from a silicone sponge and shown to achieve rapid release of but not controlled flow of water into a microfluidic device.(107) A capillary-driven, pumpless, microfluidic system is more suitable for use as part of a POC device as it would eliminate bulky equipment and complicated sample interface connections as well as reduce the large dead volumes of the fluids. (98, 106) This approach is also ideal for one-time use applications.(90, 108) In particular, a pumpless

microfluidic that would control the flow of blood would enable the development of assays and drug screening platforms, and biomimetic 'organ-on-a-chip' systems. (96, 108, 109) Additionally, if also optically transparent, a single use, optical imaged POC diagnostic could be developed for numerous bloodborne diseases (e.g. malaria, anemias, sickle cell diseases, thrombocytopenia, thrombocytosis, leukemia, lymphoma, and iron deficiency).

While capillary forces may be leveraged to induce pumpless flow of a liquid through a microchannel, flow control remains a challenge. As a result, pump-actuated microfluidics continue to be designed and used due to their precision flow control capability.(108, 110) To achieve capillary flow, materials approaches(97, 100, 102-104, 111) as well as more complex microfluidic designs(99, 108, 109, 112-115) have been explored, but only a few have achieved flow control.(99, 100, 108, 109, 115) For most liquids, control of capillary flow is characterized by its flow velocity.(108, 109, 116-118) In the case of blood capillary flow, the speed of the blood flow to reach the final destination (i.e. flow velocity) and the coagulation time of blood must be considered.(119, 120) These are both related to the hydrophilicity and wettability of the material with which the blood interacts.(103, 121) Capillary pressure or Brownian motion,(122-124) both related to surface hydrophilicity,(123-125) are suggested to drive microfluidic capillary flow, including for blood. Hydrophilic surfaces also reduce cellular adhesion to contribute to the enhanced flow of blood as well as reduced coagulation times.(121, 124)

Since first demonstrated for soft lithography by Whitesides,(104) most microfluidic channels are conveniently prepared from a polydimethylsiloxane (PDMS) elastomer (i.e. silicone). However, because of its extreme hydrophobicity, capillary action by aqueous

liquids, including blood, is inhibited.(103, 112, 126) In addition to poor flow control, silicone microfluidic channels are prone to adsorption of proteins and small molecules as well as whole blood thrombosis.(100) While a channel with a higher height/width aspect ratio may better facilitate flow, the low modulus of silicones makes wider channels prone to collapse at low aspect ratio (generally, <0.1).(127-129) Alternatively, pillars have been incorporated into silicone-based microfluidic channels to inhibit channel collapse and to improve capillary flow.(112, 114) However, based on their potential for simplicity, most approaches used to create pumpless microfluidic flow have focused on making the surfaces of silicone hydrophilic.(97, 100, 102-104, 111) For instance, plasma treatment in an air or oxygen environment is known to induce their hydrophilicity (i.e. water contact angle, $\theta < \sim 30°$) but undergo rapid hydrophobic recovery when maintained in air ($\theta \sim 79$ ° in ~15 min and ~ 93 ° in ~45 min).(104) Efforts have been made to limit hydrophobic recovery of silicones after plasma treatment, including storage in DI water(111, 130) and thermal annealing.(131) However, these techniques are of limited efficacy. For instance, hydrophobic recovery of plasma-treated silicones occurs within hours to days after removal from water and within days to weeks post-heat treatment.(101, 132) Other methods to impart surface hydrophilicity have been reported, namely relying on surface modification processes applied to an already formed silicone microfluidic.(107, 126, 133) For instance, a poly(vinyl alcohol)/glycerol layer-by-layer (LbL) coating was deposited onto the surfaces of silicone microfluidics.(97) While hydrophilicity ($\theta \sim 6°$) was maintained for ~90 days, a higher surface roughness resulted(101) which can negatively influence flow behavior, biological adhesion, bubble generation, and optical

imaging.(134) Several reports have included the use of amphiphilic copolymers based on poly(ethylene oxide) (PEO) [or poly(ethylene glycol), PEG] for surface modification of silicone microfluidics. For instance, triblock PEO-PPO-PEO copolymers have been applied to several surfaces, demonstrating subsequent reduced cellular adhesion but only a modest improvement in wettability by water ($\theta \sim 73$ ° to 63°),(135) anticipated to be insufficient for pumpless flow. Silicone microchannels were prepared with surfaces modified with commercial non-ionic and ionic copolymer surfactants by first forming surfactant thin films (via a masking technique) on the inner walls of the of the mold.(126) While pumpless flow of water was achieved for silicone microchannels modified with a PEO-PDMS-PEO triblock copolymer ($\theta \sim 22$ °) and surface hydrophilicity stable upon storage in air (11 days), the fabrication process was >48 hr and flow rate could only be controlled by channel geometry.

"On-demand" surface hydrophilicity, achieved with a surface modifying additive (SMA), represents a convenient approach to prepare pumpless silicone microfluidic channels with controlled blood flow. A SMA may be readily blended into the silicone prior to formation of the channels via conventional soft lithography. For a pumpless microfluidic in POC blood applications, it is essential that, upon contact with blood, the SMA rapidly migrates to the surface to induce hydrophilicity and subsequent capillary blood flow. If SMA concentration could further regulate blood flow rate, this would offer additional utility. Also essential is a lack of compromise of silicone modulus (to prevent channel collapse) and transparency (for subsequent optical imaging). Given its hydrophilicity and associated anti-biofouling behavior, poly(ethylene oxide) (PEO) [or

poly(ethylene glycol), PEG] has been extensively evaluated for silicone modification.(136-141) However, conventional bulk modification of silicones with PEO is limited. For instance, hydrophobic recovery is observed for condensation-cured or "RTV" silicones prepared with PEO-silanes (e.g. triethoxysilyl-propyl PEO monomethyl ether [$(EtO)_3Si$-$(CH_2)_3$-PEO_n-OCH_3] (139, 140) and for addition-cured silicones prepared with allyl PEO monomethyl ether [CH_2=$CHCH_2$-PEO_n-OCH_3].(141) Hydrophobic recovery is also observed for silicones surface-grafted with allyl PEO monomethyl ether.(139, 141) Several reports have utilized an amphiphilic "PDMS-PEO" copolymer as an SMA to create hydrophilic silicone microchannels, but none have yet demonstrated controlled blood flow. For instance, incorporation of a commercial PDMS-PEO copolymer (MW = 600 g/mol; 60-70% PEO) into a silicone induced water-driven surface hydrophilicity ($\theta \sim 0^\circ$ to 80° in 25- 45 min), indicates a relatively slow surface segregation of their polymers.(142) This surface hydrophilicity was maintained after lengthy storage in air (20 months). However, because of the slow surface segregation of their polymers to increase surface hydrophilicity only water flow rate control with SMA concentration (0.25, 0.5 wt%) was demonstrated and proper blood flow would be hard to achieve. In another example, a commercial PDMS-*graft*-PEO (MW = 600 g/mol; 75% PEO) was used to create silicone microfluidics and demonstrated improved surface hydrophilicity ($\theta \sim 22^\circ$ to 81° in 200 seconds) and facilitated capillary flow of water.(100) However, because the sample was not used to create a microchannel, but used as a coversheet for a microchannel, it was only able to control water flow rather than blood

with their SMA. Additionally, transparency was not demonstrated, and modulus values were noted to be compromised at higher SMA levels but not quantified.

In this work, microchannels were formed with silicone modified with an SMA towards achieving controlled capillary flow of blood based on SMA concentration. We have demonstrated that PEO-silane amphiphiles, bearing an oligodimethylsiloxane (ODMS) tether [α-$(EtO)_3$-$(CH_2)_3$-$ODMS_m$-*block*-PEO_n-OCH_3], are highly effective SMAs for RTV silicones.(143, 144) These modified silicone films underwent rapid, water-driven migration of PEO segments to the surface, creating hydrophilic surfaces with high wettability and resistance to plasma protein adhesion. This effect was also not lost with prolonged storage in air. Moreover, the transparency of the modified silicones was not compromised which is essential to enable subsequent optical detection and imaging.(144) This is in contrast to the increase in opacity of silicones modified with traditional, non-amphiphilic PEO such as for PEO divinyl ether (PEO-DE).(145) While these ethoxy-terminated PEO-silane amphiphile SMAs effectively modified RTV silicone films, microfluidics are typically prepared via soft lithography with platinum (Pt)-cure PDMS (e.g. Sylgard 184).(144, 146, 147) These addition-cure silicones are based on the crosslinking of silane (Si-H) and vinyl (-$CH=CH_2$) groups which occurs with limited shrinkage. Thus, in this work, Sylgard 184 was bulk-modified with a silane-terminated PEO-silane amphiphile (HSi-$PDMS_{30}$-PEO_8) at varying concentrations (5, 7 and 14 wt%). The resulting amphiphilic silicones (***5%-, 7%-*** and ***14% PEO-PDMS***) were evaluated in terms of their resulting optical properties, modulus and surface wettability versus the unmodified Sylgard 184 (***unmodified silicone***). The amphiphilic silicones were also used

to prepare microfluidic channels and the capillary flow of whole blood was subsequently assessed in terms of flow speed (**Figure 2**). The impact of SMA concentration on the speed of blood flow was evaluated as was channel height. Given that such microfluidics may be stored for periods of time prior to use, key properties such as modulus and surface wettability were assessed after prolonged storage in air.

2.3 Materials and Methods

2.3.1 Materials.

SU-8 2007 and SU-8-5 were purchased Microchem. Allyl methyl PEO (Polyglykol AM 450, M_n = 292–644 g mol^{-1} per manufacturer's specifications; M_n = 424 g mol^{-1} (per ^{1}H NMR end group analysis) was provided by Clariant. Octamethylcyclotetrasiloxane (D_4) and tetramethyldisiloxane (TMDS) were purchased from Gelest. $ODMS_{30}$ (M_n = 2354 g mol^{-1} per ^{1}H NMR end group analysis) was prepared as reported.(148) Triflic acid, rhodium (I) tris(triphenylphosphine) chloride (Wilkinson's catalyst), hexamethyl-disilazane, tridecafluoro-1, 1, 2, 2-tetrahydrooctyl-1-trichlorosilane, and solvents were obtained from Sigma-Aldrich. All solvents were dried over 4-Å molecular sieves prior to use for hydrosilylation reactions. Sylgard 184 was purchased from Ellsworth Adhesives. Fluoresbrite® fluorescent polystyrene latex beads (diam. 6.1 μm, 2.6 wt% in water; "Polychromatic Red Microspheres" per manufacturer) and "non-fluorescent" polystyrene latex beads (diam. 1.00 μm, 5 wt% in water) was purchased from Polysciences, Inc. and Sigma, respectively. Glass microscope slides (75 × 25 × 1 mm^3) were purchased from

Fisher Scientific. Freshly collected whole bovine blood (citrated) was provided by the Texas A&M College of Veterinary Medicine.

2.3.2 Methods

2.3.2.1 Synthesis of PEO-silane amphiphile (HSi-PDMS$_{30}$-PEO$_8$).

HSi-PDMS$_{30}$-PEO$_8$ was synthesized as previously reported using a regioselective hydrosilylation reaction of ODMS$_{30}$ and allyl methyl PEO$_8$.(148) Briefly, a difunctional ODMS$_{30}$ with terminal silane (SiH) groups was synthesized using a triflic acid catalyzed equilibrium ring-opening polymerization of D_4 and TMDS. Next, the product was reacted for 8 hr with allyl methyl PEO$_8$ (1:1 molar ratio) and Wilkinson's catalyst in toluene at 75 – 80 °C to form the amphiphilic product. ^{1}H NMR of the purified product, a clear and colorless liquid, agreed with that previously reported.

2.3.2.2 Preparation of amphiphilic silicone microfluidic chips and corresponding films.

Blending of PEO-silane amphiphile with Sylgard: The Sylgard 184 "base" was added with the Sylgard 184 "curing agent" at a 10:1 wt ratio in a plastic cup. To this was added HSi-PDMS$_{30}$-PEO$_8$ at 0 wt% (***unmodified silicone***), 5 wt% (***5% PEO-PDMS***), 7 wt% (***7% PEO-PDMS***), or 14 wt% (***14% PEO-PDMS***) (based on total weight of Sylgard base and curing agent). This final mixture (~20 g) was blended using a spatula in the 70 °C water bath for ~3 min.

Fabrication of microfluidic chips: SU-8 2007 and SU-8-5 were used for the master mold fabrication(149) and the channel height measured using Dektak profilometry. A single master mold contained four microchannels of the same dimensions. Master molds were prepared with different channels height (4.6, 10 and 14 μm). All channels were 15 mm long and 250 μm wide. The master molds were coated with a release agent (trideca-fluoro-1, 1, 2, 2-tetrahydrooctyl-1-trichlorosilane) and then placed in a 60 °C oven. A designated, aforementioned silicone mixture (~9 g) was removed from the 70 °C water bath and then poured onto the pre-heated, treated master mold. Next, the filled master mold was placed into a vacuum oven (60 °C, 36 mm Hg, 10 min) to degas the silicone mixture and the temperature then increased to 110 °C for 1 hr to cure the silicone. The specimens were stored at room temperature (RT) for ~5 days. During this time, an inlet and outlet (diameter = 3 mm) of the mold was created using a biopsy punch, reducing the channel length to 13 mm (**Figure 2**). The mold was bonded to a plasma cleaned microscope glass slide (Harrick; sequential vacuum [10 min], oxygen [2 min], plasma [2 min] and 110 °C oven [2 hr]). The resulting microfluidic chips were thus comprised of four equivalent D-shaped channels wherein the curved portion (facing the bottom) was comprised of the silicone and the flat portion (facing the top) was the glass surface (**Appendix B Figure S1**). Microfluidic chips were stored on a bench top in a covered Petri dish and tested the next day.

Fabrication of films*:* Analogous silicone films were also prepared for materials testing. A designated silicone mixture (12-13 g) was removed from the 70 °C water bath and

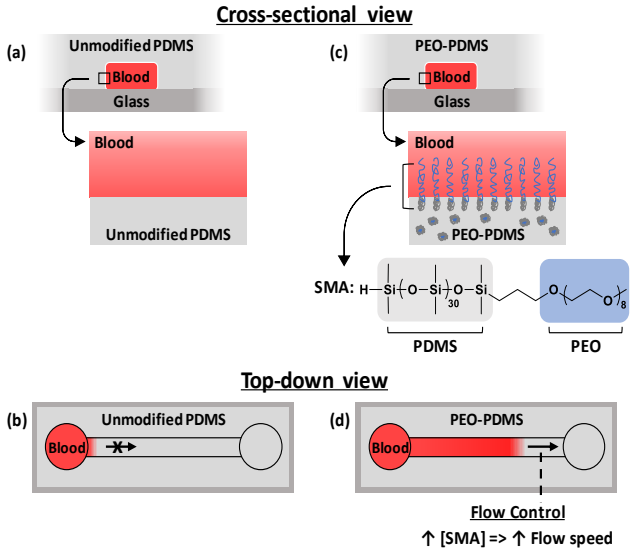

Figure 2. Following deposition of blood into the inlet of the microfluidic channel: (a) For unmodified PDMS (i.e. Sylgard 184), (b) minimal flow is achieved due to the hydrophobicity of the silicone. (c) For amphiphilic silicone "PEO-PDMS" (i.e. Sylgard modified with PEO-silane amphiphile surface modifying additive, SMA), migration of hydrophilic PEO segments to the surface-blood interface blood occurs and (d) results of capillary flow.

deposited onto a pre-heated (60 °C), levelled Petri dish (diameter = 90-100 mm) and placed into a vacuum oven for degassing (60 °C, 36 mmHg, 10 min) followed by curing at 110 °C for 1 hr. Specimens were stored on a bench top in a covered Petri dish and tested within 24 hr after preparation or, in the case of contact angle analysis and modulus, up to 6 months. After removal from the glass substrate, 6 mm diameter discs were cut from free-standing films and were utilized for light attenuation, autofluorescence and modulus measurements. Thickness of films were measured with an electronic caliper (thickness = 1.3 ± 0.7 mm).

2.3.2.3 Characterization of amphiphilic silicone material properties

***Light attenuation measurements*.** The light attenuation of films was measured as follows. Briefly, discs (N = 3; diameter = 6 mm) were cut from a free-standing film with a biopsy punch. The specimens were placed in Greiner 96-well, flat bottom, transparent polystyrol plate reader wells and absorbance (350 to 950 nm wavelength) was measured (Tecan Infinite M200 Pro). A baseline value was taken from the blank microplate well and subtracted from sample values. The attenuation coefficient (in mm^{-1}) was calculated by dividing the subtracted baseline value by the thickness of the specimen. All films were tested in triplicate (N = 3).

Autofluorescence, fluorescence and brightfield measurements*.** The autofluorescence of ***14% PEO-PDMS films (N = 3) was tested at three excitation wavelengths (358, 488 and 557 nm) (emission filter ranges of 417 – 477, 517 – 537, and 604 – 644, respectively) across 255 pixels (Zeiss Axio Vert.A1 microscope with an Axiocam 503 mono camera). The difference in pixel intensity of the ***14% PEO-PDMS*** film (on top of a glass microscope slide) versus a glass microscope slide "control" was used as an indicator of autofluorescence. The autofluorescence of an ***unmodified silicone*** (on top of a glass microscope slide) was also measured. Both the ***unmodified silicone*** and ***14% PEO-PDMS*** sample autofluorescence were normalized to the glass control. After the autofluorescence test, (1 µl volume) of 6.1 µm fluorescent beads was allowed to flow through a microfluidic channel of ***14% PEO-PDMS*** (channel height = 14 µm) and imaged at the wavelength

shown to have the highest auto-fluorescence (358 nm) using a 20x/0.4 objective. In order to assess brightfield resolution, an aqueous solution of non-fluorescent 1.00 μm beads (volume = 1 μL) were allowed to flow through a microfluidic channel of ***14% PEO-PDMS*** (channel height = 4.6 μm) and the beads imaged using a 40x/0.55NA objective. After the image of the beads was acquired, Image J software was used to plot the full width at half maximum (FWHM) of the bead.

Modulus measurement. The compressive modulus of modified, amphiphilic silicones and the ***unmodified silicone*** control films were performed at room temperature (RT) on an Instron 3345. Film discs were placed between two parallel plates and compressed to a separation of 1 mm and with an average preload force of ~0.00066 N. The modulus was calculated from the linear portion of the resulting stress versus strain curve up to 25% strain (R-squared values ≥ 99%).(150, 151) The ***silicone control***, ***5%-, 7%-*** *and* ***14% PEO-PDMS*** films were tested at t = 0 (i.e. within 24 hr post-fabrication) and ***14% PEO-PDMS*** was also tested at t = 2 wks, 1 mo, 3 mo, and 6 mo. All films were tested in triplicate ($N = 3$).

Static water contact angle measurements. The static water contact angle (θ_{static}) of modified silicones (coated on glass substrates) (***5%-, 7%-*** and ***14% PEO-PDMS***) were measured using a CAM-200 goniometer (KSV instruments) equipped with autodispenser, video camera, and Attension Theta analysis software. The θ_{static} of a sessile drop of DI water (5 μL) was measured at 15 sec and 1 min. Measurements were taken at t = 0 (i.e. within 24 hr post-fabrication) and at several time points thereafter (2 wk, 1 mo, 3 mo, and 6 mo) for ***14% PEO-PDMS***. Between measurements, specimens were stored in a

desiccator. The average and standard deviation values reported for θ_{static} are based on triplicate measurements made on different areas of the same sample. Additionally, to verify a lack of variability, three independent films with the highest concentration of amphiphile (***14% PEO-PDMS)*** were prepared and contact angle analysis likewise performed (t = 0) at 15 sec, 1 min and 3 min.

Capillary flow speed of blood. A designated microfluidic chip was placed onto a levelled microscope stage with the microscope slide surface on the bottom and the microscope objective (Nikon Eclipse TE2000-S; 20X/0.4) positioned at the outlet of the microchannel. Using a micropipette, blood (volume = 5 µL) was placed at the inlet and a timer was simultaneously started. Blood flow was monitored and the total time (t) it took the blood to flow down a channel length (13 mm) and reach the outlet was recorded. Two different types of tests were performed to evaluate the impact of the microfluidic channel parameters on capillary flow speed: (i) *Flow speed as a function of channel height:* Three microfluidic chips were prepared with ***7% PEO-PDMS*** having three different channel heights (4.6 µm, 10 µm and 14 µm). (ii) *Flow speed as a function of SMA concentration:* Three microfluidic chips were prepared with ***5%-, 7%-*** and ***14% PEO-PDMS*** having a constant channel height (14 µm). All tests were conducted in triplicate ($N = 3$). In addition, videos of the capillary flow of blood (volume = 5 µL) through a ***14% PEO-PDMS*** microchannel (h = 14 µm, w = 250 µm) were captured (Nikon Eclipse TE2000-S; 20X/0.4).

Statistical analysis. Data is reported as the mean ± standard deviation of triplicate measurements (N = 3). Data set mean values were compared in GraphPad Prism via ANOVA followed by a Tukey's post-hoc test

2.4 Results and Discussions

Preparation of microfluidic chips and films. The PEO-silane amphiphile SMA was incorporated at three different concentrations into the Sylgard 184: 5 wt% (*5% PEO-PDMS*), 7 wt% (*7% PEO-PDMS*), or 14 wt% (*14% PEO-PDMS*); these represented relatively "low", "intermediate" and "high" concentrations, respectively. Preliminary screening of SMA concentrations revealed that *14% PEO-PDMS* produced a very hydrophilic surface by contact angle analysis and so was chosen as the upper limit due to the potential of even higher concentrations to reduce optical transparency and modulus. Thus, *7%- and 5% PEO-PDMS* are intermediate and low concentrations relative to the highest concentration. Importantly, these concentrations resulted in differences in surface hydrophilicity that were predicted to alter the rate of blood flow comparison. It was observed that, due to its viscosity, achieving a homogeneous mixture of the Sylgard 184 with the SMA required modest heating. Thus, during mixing, the vessel was subjected to a 70 °C water bath and subsequently degassed in a 60 °C vacuum oven (36 mm Hg). Because this brief heating improved mixing, improved transparency and reduced cure times also resulted. Prior to formation of microfluidic channels with modified silicone, the impact of addition of the PEO-silane amphiphile SMA on optical, surface and mechanical properties were first evaluated by preparing films on a glass substrate (Petri dish). The

uniformity of the modified, amphiphilic silicones was visually confirmed in the resulting microfluidic chips and films (**Figure S1 and S2**).

Optical properties. To probe the utility of optical detection of blood within microfluidic channels created with the amphiphilic silicones, a series of measurements were conducted. First, we sought to verify that the amphiphilic silicones did not substantially increase light attenuation (i.e. transmission loss), defined as the reduction in intensity of a light beam with respect to distance travelled through the transmission medium.(152) Versus the *unmodified silicone*, the average light attenuation was not increased for *7% PEO-PDMS* free-standing films but increased for *14% PEO-PDMS* (up to ~0.04 mm^{-1} at lower wavelengths of ~400 nm) (**Figure 3**). In other words, for a 1 mm thick film, only a 0.5% to 5% reduction (95% to 99.5% transmission) was seen across the ultraviolet to near

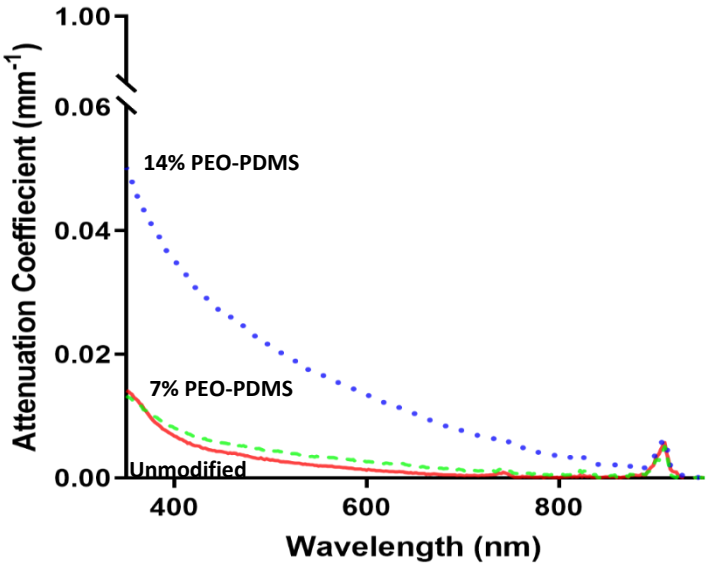

Figure 3. Comparison of light attenuation coefficient values for unmodified silicone and amphiphilic silicones modified with PEO-silane amphiphile SMA (7%- and 14% PEO-PDMS). All samples were tested in triplicate (N = 3).

infrared wavelength range with the maximum reduction occurring below the normal visible imaging and detection range at the lower ultraviolet wavelengths.

Because the components of blood within a microfluidic channel may be fluorescently stained for subsequent optical imaging, autofluorescence of the amphiphilic silicones could potentially compromise imaging and resolution. Based on the slight increase in light attenuation at lower wavelengths, we evaluated the autofluorescence of ***14% PEO-PDMS*** at three different excitation wavelengths (**Figure 4**). Compared to the glass control, the mean pixel intensity of the ***14% PEO-PDMS*** increased by 1.5x, 1.1x

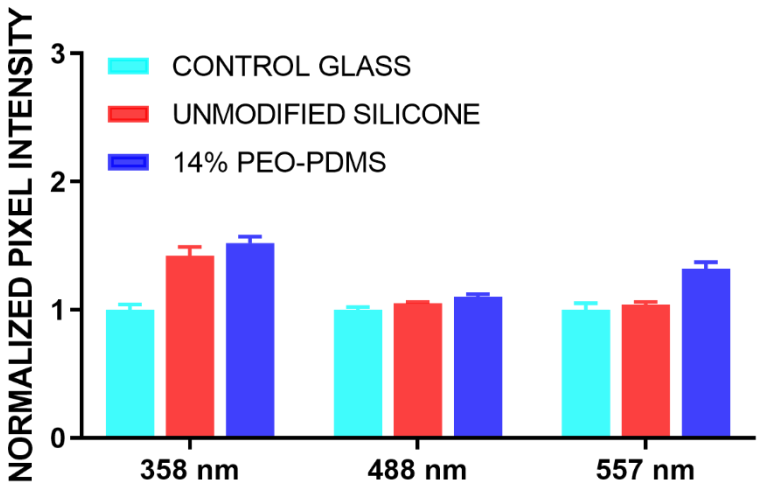

Figure 4. Autofluorescence for unmodified silicone and 14% PEO-PDMS normalized to the control glass. All samples were tested in triplicate (N = 3).

and 1.3x at 358, 488, and 557 nm, respectively. In the case of the ***unmodified silicone***, the pixel intensity increased by 1.4x, 1.1x and 1.1x, respectively, for these excitation wavelengths. Thus, the increase in autofluorescence of the ***14% PEO-PDMS*** is rather similar to that of the ***unmodified silicone*** and very low overall.

To assess fluorescent testing potential, an aqueous solution of fluorescent beads (diam. = 6.1 µm) were allowed to flow through a ***14% PEO-PDMS*** microfluidic channel (height = 14 µm) and imaged at 358 nm (i.e. wavelength that produced the greatest increase in autofluorescence). These beads were observed to be easily distinguishable as expected given the overall low autofluorescence of ***14% PEO-PDMS*** (**Figure 5**). Lastly, to assess brightfield resolution potential, an aqueous solution of non-fluorescent beads

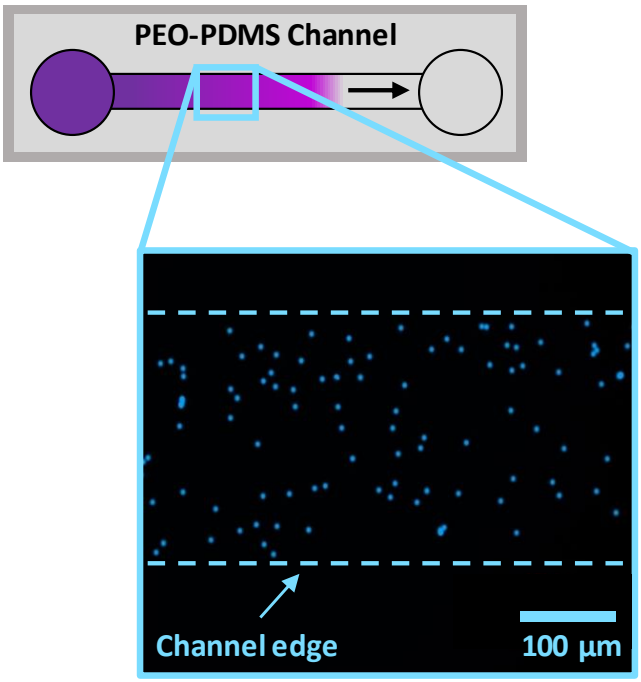

Figure 5. Fluorescent beads (diam. = 6.1 µm) were imaged when flowed through a 14% PEO-PDMS microfluidic channel (height = 14 µm).

(diam. = 1.00 µm) were allowed to flow through a ***14% PEO-PDMS*** microfluidic channel and imaged. The FWHM of the beads was determined by Image J to be approximately 1.1 ± 0.2 µm, within an average of 10% of their actual size.

Modulus measurements*.** Because microfluidic channels are prone to collapse for low modulus materials, particularly for low aspect ratio channels as used herein,(127-129) we assessed the impact of the addition of the PEO-silane amphiphile SMA to the Sylgard 184. Initially (i.e. at t = 0 h), the ***unmodified silicone had a modulus of 4.8 ± 0.6 MPa, similar to previous reports (150) (**Figure 6a, Appendix B Table S1**). As the concentration of SMA was increased, the modulus of ***5%-, 7%-*** and ***14% PEO-PDMS*** concomitantly decreased. This

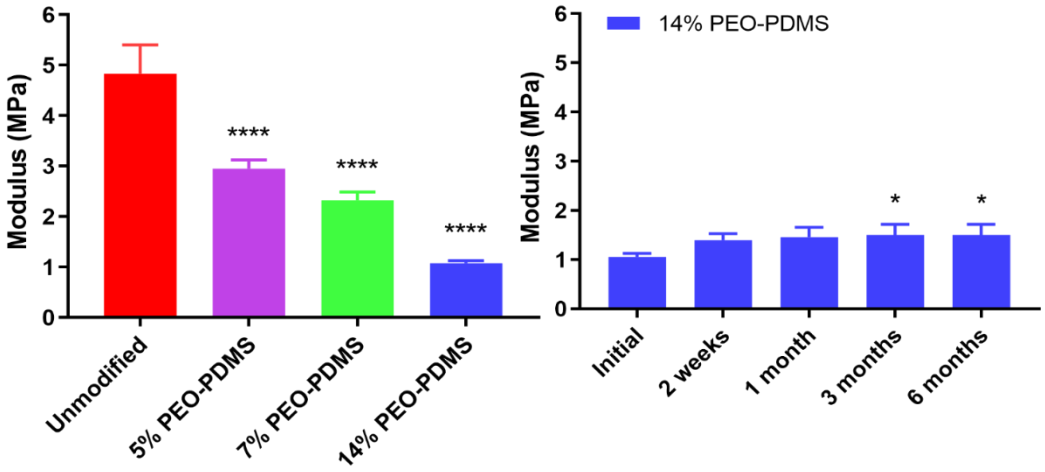

Figure 6. Modulus of unmodified silicone and amphiphilic silicones modified with increasing amounts of PEO-silane amphiphile SMA (5%-, 7%- and 14% PEO-PDMS). **** denotes a significant difference relative to the unmodified silicone, $p < 0.0001$. (b) Modulus of 14% PEO-PDMS over a period of 6 months. * denotes a significant difference relative to the initial, $p < 0.05$. All samples were tested in triplicate (N = 3).

plasticization effect was expected as, following crosslinking, the PEO segments of the SMA exist as “dangling free ends”. This effect was likewise observed in earlier work wherein a condensation cured silicone system was modified by ethoxy-terminated PEO-silane amphiphiles.(153) For ***14% PEO-PDMS***, the modulus was observed to increase after 2 weeks but, statistically, ceased to continue to increase during a 6-month period (**Figure 6b; Appendix B Table S2**). This increase is attributed to curing of the silicone that can occur over longer periods of time. In any case, even for the silicone formulation with the highest SMA (i.e. ***14% PEO-PDMS***) and the lowest modulus, channel collapse was not observed via brightfield microscopy and based on the flow observed (**Figure. 5**).

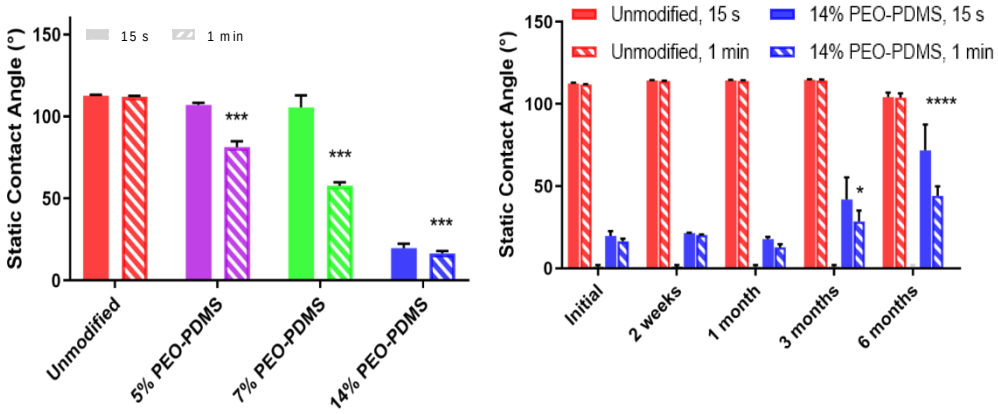

Figure 7. (a) θstatic values of deposited water droplets (recorded at 15 sec and 1 min) on unmodified silicone and amphiphilic silicones modified with increasing amounts of PEO-silane amphiphile SMA (5%-, 7%- and 14% PEO-PDMS). *** denotes a significant difference relative to the unmodified silicone, $p < 0.001$. (b) θstatic values of deposited water droplets (recorded at 15 sec and 1 min) on unmodified silicone and 14% PEO-PDMS over a period of 6 months. * denotes a significant difference relative to initial, $p < 0.05$ and **** denotes a significant difference relative to the initial, $p < 0.0001$. Reported values are based on triplicate measurements (N = 3) made on different areas of the same sample.

Static water contact angle measurements. Essential to pumpless capillary flow of blood is the ability of the PEO-silane amphiphile SMA to invoke rapid and substantial water-driven surface hydrophilicity by the migration of PEO segments to the surface interface (**Figure. 2**). While previously demonstrated in RTV cure silicone,(143, 144) this had not been established in an addition-cure silicone like Sylgard 184 used herein. Thus, temporal measurement of θstatic values of deposited water droplets (recorded at 15 sec and 1 min) were used to assess rate and extent of this process in the amphiphilic silicones. In a first series of measurements, θstatic values were recorded immediately after fabrication (t = 0) (**Figure 7a, Appendix B Table S3**). As expected, the unmodified silicone was extremely hydrophobic (θstatic ~ 112°). However, as the PEO-silane amphiphile SMA was added at increased concentrations, surface hydrophilicity was increased. For 5% PEO-PDMS and 7% PEO-PDMS, the surfaces were initially hydrophobic (θstatic, 15 sec ~ 107 ° and 105 °, respectively) but rapidly became increasingly hydrophilic (θstatic, 1 min ~ 81° and 58°, respectively). Notably, at the highest concentration of SMA, 14% PEO-PDMS rapidly achieved hydrophilicity ($\theta_{static,\ 15\ sec}$ ~ 20° and $\theta_{static,\ 1\ min}$ ~ 16°). The substantial reduction in θ_{static} at early timepoints (i.e. 15 s and 1 min) demonstrates the rapid and extensive restructuring of the SMA's PEO segments to the aqueous interface. This was anticipated to be essential to achieving capillary blood flow in a microchannel. A similar analysis was performed on three replicate films of ***14% PEO-PDMS*** (t = 0) and a lack of variability confirmed the reproducibility of these types of films (**Appendix B Table S4**).

Since microfluidic devices may be stored for long periods of time prior to use, the retention of this water-driven surface hydrophilicity was evaluated for ***14% PEO-PDMS*** after prolonged storage (in air) (**Figure 7b, Appendix B Table S5**). During the first one month, surface hydrophilicity did not substantially change. At 3 and 6 months, contact angles progressively increased, but the surfaces remained hydrophilic ($\theta_{static,\ 1\ min} < 50°$). This decrease in surface hydrophilicity may be due to absorption of water during storage which we have previously shown to produce this effect in condensation cured silicones modified with PEO-silane amphiphiles.(148)

Capillary blood flow rates. A series of two experiments were conducted to elucidate the extent to which the amphiphilic silicone microchannels could regulate the speed of capillary blood flow. For all experiments, the same blood volume (5 µL) was utilized in order to fill a 3 mm diameter channel inlet and to ensure that the pipette pressure did not contribute to differences in flow and the gravity effect at the inlet is the same across channels. Channel height is known to impact flow rate, with the speed of flow increasing with a larger height: width aspect ratio.(123) Thus, **7*% PEO-PDMS*** was first used to prepare three microfluidic chips of different channel heights (4.6, 10 and 14 µm) such that the aspect ratio increased with a greater channel height. Indeed, the average blood flow time (from inlet to outlet) decreased as channel height increased (t = 33.3 ± 1.5, 19.3 ± 0.6, and 13.3 ± 0.6 sec, respectively) (**Figure 8a, Appendix B Table S6**). Moreover, these experimental results are comparable to the theoretical model when using the equation developed by Jong et al.(123) for this range of heights with an R-squared (R^2) value of ~ 0.987 (**Appendix B Figure S3**). Blood flow did not occur in similar channels prepared

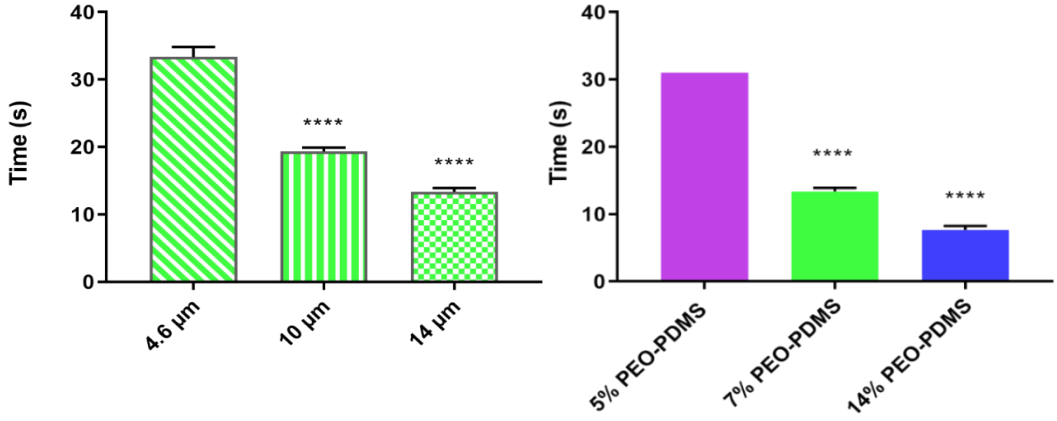

Figure 8. Pumpless flow time of whole blood through: (a) 7% PEO-PDMS microfluidic channels of different channel heights and (b) 14 µm height microfluidic channels of different 5%-, 7%- and 14% PEO-PDMS microfluidic channels (height = 14 µm). For (a) **** denotes a significant difference relative to the "4.6 µm" sample ($p < 0.0001$). For (b) **** denotes a significant difference relative to 5% PEO-PDMS sample ($p < 0.0001$). All samples were tested in triplicate (N = 3). For 5% PEO-PDMS, the flow time was 31 sec for all three samples such that no error bar is shown.

from ***unmodified silicone***. In the second set of experiments, the channel height was maintained (14 µm) but the concentration of the PEO-silane amphiphile was systematically increased (***5%-, 7%-*** and ***14% PEO-PDMS***). As SMA concentration increased, capillary flow times of blood decreased (31.0 ± 0.0, 13.3 ± 0.6, 7.7 ± 0.6 seconds, respectively) (**Figure 8b, Appendix B Table S7**). This correlates well with the observed differences in water-driven surface hydrophilicity that increases with higher levels of the PEO-silane amphiphile SMA (**Figure 7a**). Representative videos of capillary blood flow are shown in Supporting Information (Video S1, S2). Video S2 shows that even after 30 min of flow, blood cells were still moving and hence there was no thrombi formation, indicating a lack of adhesion to the modified silicone or to the glass cover.

2.5 Conclusion

In this work, it was demonstrated that a controlled, pumpless capillary flow of blood could be achieved for microfluidic channels prepared with amphiphilic silicones. Specifically, Sylgard 184, a commonly used silicone for soft lithography of microfluidics, was bulk modified with a PEO-silane amphiphile. This SMA was comprised of a crosslinkable silane (Si-H) end group, an oligodimethylsiloxane tether, and PEO segment: HSi-ODMS$_{30}$-*block*-PEO$_8$-OCH$_3$. This SMA was incorporated at varying concentrations (5, 7 and 14 wt%) to produce the resulting amphiphilic silicones (*5%-*, *7%-* and *14% PEO-PDMS*). Both microfluidic channels of varying heights (4.6, 10 and 14 μm) as well as corresponding films were prepared to assess blood flow as well as key material properties. Several optical properties were assessed based on the anticipated future fluorescent and brightfield POC imaging of blood within a microfluidic channel. Compared to the unmodified Sylgard 184 (*unmodified silicone*), the amphiphilic silicones exhibited only a slight increase in light attenuation and almost no autofluorescence, even at the highest concentration of SMA (i.e. *14% PEO-PDMS*). Moreover, fluorescent and absorptive microparticles within these channels were easily imaged and their size could be accurately quantified. While the modulus decreased with increasing levels of PEO-silane amphiphile SMA, this did not contribute to any observed channel collapse, despite their low aspect ratios. Contact angle analysis of deposited water droplets confirmed the anticipated migration of SMA PEO segments to the surface to induce hydrophilicity. This effect was more pronounced as the concentration of SMA increased and was furthermore largely

retained even following prolonged storage in air. Pumpless capillary blood flow was confirmed for microfluidic channels of varying heights prepared from the amphiphilic silicone with the intermediate concentration of SMA (i.e. *7% PEO-PDMS*). As expected, a decreased channel height led to longer blood flow rate. Additionally, microfluidic channels of the same height (14 μm) were shown to produce increased blood flow rates as the concentration of SMA increased. This increased blood flow rate with SMA concentration correlated to the observed increase in water-driven surface hydrophilicity. Thus, this amphiphilic silicone system offers a simple yet effective method to enable the production of optically transparent microfluidic channels with the ability for controllable, pumpless, flow of blood, specifically useful for POC blood imaging applications

CHAPTER III

A THIN WHOLE BLOOD SMEAR PREPARED VIA A PUMPLESS MICROFLUIDIC

3.1 Overview

A pumpless, capillary microfluidic cartridge would enable the convenient generation of an automated, uniform, and repeatable blood smear for potential point-of-care (POC) applications. Herein, such a system was created and flow control optimized for uniform cell distribution by modifying poly(dimethyl siloxane) (PDMS) with a surface modifying additive (SMA) at 3, 5, and 7 wt% and by varying whole blood volume (0.3, 1, and 2 µl). The channel height, width, and length were 4.7 ± 0.1 µm, 250 µm, and 16 mm respectively and, to avoid channel collapse and provide more uniform flow and cell distribution, pillars were added within the channel. Specifically, flow control was assessed by how it affected the blood speed, flow stop time, and cell distribution. The targets were flow speed of ≤ 3 min, stop time of ≤ 10 min and uniformity (monolayer) with cell density per area of 400-700 unique cells/ 0.024 mm2 field of view. When varying SMA concentration, samples at 5 and 7 wt% with 0.3 µl of blood gave better blood flow and a better-quality smear compared to the 3 wt%. The variation of blood volume with 5 wt% SMA as volume increased from 0.3 µl to 1 µl to 2 µl resulted in a decrease of smear quality. A good quality smear in terms of monolayer and density per area was proven to be repeatable across different channels within one chip and across different chips for 5 wt% SMA, 4.7 ± 0.1 µm height, 0.3 µl of blood.

3.2 Introduction

The peripheral blood smear is invaluable in the diagnosis, characterization, and monitoring of various clinical diseases such as malaria, anemias, sickle cell diseases, thrombocytopenia, thrombocytosis, leukemia, lymphoma, and iron deficiency (9, 69, 154, 155). For these diseases, the blood smear is often used for observation of cell morphology and differential counting of blood cells (9, 23, 154, 155). The manual examination of stained blood smear with light microscopy has three steps: 1) Smear preparation; 2) fixation and staining or simply staining; and 3) the examination of the stained smear under the microscope. Among those three steps, the smear preparation is arguably the most important since the quality of the smear affects the rest of the process (staining and the examination). A good quality blood smear is defined as one that is uniform in terms of cell density (monolayer) and cell density per area (9, 10, 13). However, blood smear uniformity is highly variable from one person across days and from person to person (10, 23, 24) . The primary manual method of blood smear preparation is the manual wedge method (13, 22, 63, 64). It uses a cover slide or microscope slide to push and spread ~1-2 µl of blood on top of a slide at a 30 – 40 º angle. However, this method's drawbacks include a high degree of variability across smears prepared by either one expert using the same blood, or smears across experts (23, 24), making it insufficient for accurate and reproducible diagnosis, characterization and monitoring of blood-based diseases (21-23). A semi- or fully automated smear preparation device is considered better for accurate and reproducible diagnosis, characterization and monitoring of blood-based diseases. Automated smear preparation devices (21, 24, 26, 27) use a centrifugal force to spread the

blood cell over an area (64). Some exhibit a better white blood cell (WBC) distribution, less variation within smears, and less labor and time for operation (10, 13, 21). However, there is still variation between smears from different automated devices and most are only available for laboratory use and cannot be used at the POC (21). Thus, there is a need for a blood smear preparation method that can minimize variation while maintaining uniform cell distribution and one that can be used without a high level of expertise at the POC.

Microfluidics platforms are being developed primarily to provide low-cost, adaptable, rapid, and easy-to-use detection platforms for various biological analytes at the POC. They can provide a platform for detection with high resolution and sensitivity, have small device footprints, and allow for the use of small sample volumes. Microfluidics provide the potential for simplicity that is required for use in underserved areas and developing countries (156, 157). A few researchers have tried to design a microfluidic chip for blood smears (70, 158, 159). Among them, only Horning et al. has designed a chip that can do a smear and staining process at the POC (ref-37). Even though this microfluidic chip can generate a smear with good sensitivity for fluorescence staining, it lacks resolution when using bright field imaging for diagnosis of diseases such as malaria or others, which require bright field imaging (70). Although a microfluidic cartridge for smear preparation has the potential to provide a good platform for POC diagnosis in the developing countries and could solve some of the aforementioned problems with current methods used in the developing countries, it is not easy to implement because capillary flow control without a pump is hard to achieve. In addition, microfluidic capillary flow and its use in the

development of diagnostics for bloodborne diseases to create smears with uniform cell distribution have not been well studied (108).

Microfluidic blood flow control, often reported as flow velocity, is a key feature for capillary-driven, pumpless systems and many researchers have sought to accomplish this challenging control task using more complex microfluidic designs (99, 108, 109, 115). Specifically, there are numerous variables such as material selection, chip design parameters (e.g. pillars and channel height), and blood volume which can help generate better flow control as well as a uniform smear. In an earlier study by our group, it was shown that pumpless aqueous flow control could be acquired for microfluidic chips prepared with a silicone (Sylgard 184) bulk modified with a surface-modifying additive (SMA) (ref). Specifically, the SMA was an amphiphilic PEO-silane amphiphile bearing an oligodimethylsiloxane (ODMS) tether [α-$(EtO)_3$–$(CH_2)_3$–$ODMS_{30}$-*block*-PEO_8–OCH_3] and a poly(ethylene oxide) (PEO) segment (HSi-$PDMS_{30}$-PEO_8)(160). The modified silicone underwent rapid, water-driven migration of PEO segments to the surface to create hydrophilicity and wettability. For blood applications, it is important to take into account blood coagulation time because blood tends to coagulate fast when it comes into contact with materials outside the body and the data should be collected before that happens (119, 120)**.** The time for creating the smear is also important in the context of the overall diagnosis time because the World Health Organization's (WHO) ASSURED criteria recommends that a diagnosis procedure should be done in under 30 min at the POC (25). Thus, the flow speed (time it takes for blood to flow from inlet to outlet) and the flow stop time (time it takes for the blood to stop flowing) before analysis need to be controlled

and minimized. Both times together should be ≤ 15 min which allows 15 min for the automated analysis. Volume is another variable that affects flow control toward creating a good quality smear. Theoretically for most fluids and in most situations the flow speed increases as the volume of the fluid increases based on flow rate equation (123). In addition, it has been reported that blood volume/hematocrit can affect the smear quality. Specifically, the higher the blood volume and hematocrit the higher the probability for cells to be overlapped creating a bad quality smear (64, 161, 162). Thus, accounting for or controlling the blood volume is needed to produce a high-quality smear in the microchannel with proper cell density and uniform cell distribution.

It has also been shown that pillars can be used to enhance capillary flow in microchannels (112, 113, 163), including providing better blood separation where pillars are used to redistribute cells to a more uniform pattern (164). In addition, pillars have been used to minimize channel collapse (165-167). Changes in cell distribution depend on the gaps between the pillars. Literature suggests that the gap between pillars should be as small as possible but still allow the cells to pass through for better cell distribution (168). Also, the use of pillars for blood separation has shown that gaps between pillars that are too small can block cells and clog the gap (169, 170). Kaminaga et. al. recommended that the optimal gap to prevent clogging and allow for a good cell distribution should be chosen base on the cell size (5-8 μm for bovine or human RBCs) or stiffness (168). Although that recommendation works well for a pump microfluidic platforms, it is not large enough for a capillary pumpless system. The reduced forces pushing the blood cell through the pillars should also be taken into account for a capillary pumpless system. Kaminaga et. al.

showed a good cell distribution after traveling 1 to 2 mm down the channel from the pillars (168). Although this was useful in some applications, it is a problem for applications with a longer channel that require uniform cell distribution down the entire channel. Following the theory of how blood can exhibit multi-phase, non-homogeneous characteristics with flow profile depending on hematocrit, shear stress, shear rate, aggregation, flow rate, and the dilution medium (169), conclusions can be made that uniform cell distribution would not be achieve down the entire channel with just one set of pillars at the inlet. Such applications would need pillars at different sections of the channel to redirect and redistribute the blood cells as the blood travels down the channel and would also serve to prevent channel collapse if distributed at certain locations down the channel. Such applications would also take into account that flow speed decreases exponentially as channel length increases (123), so the force at the middle and end of the channel needs to be strong enough to push the blood through the pillar gap distance chosen. Although the number of rows required, for better cell distribution was not discussed, the principle of using pillars for cell distribution that was shown by Kaminaga et. al. (168) and the research showed that cells would be better distributed as one increased the number of pillar rows . These qualities show that pillars can be useful in the design of a cartridge for providing stability and creating a uniform thin smear preparation as they facilitate flow control.

In this paper, a pumpless microfluidic cartridge was created and used to rapidly produce a uniform thin blood smear. A doped material to increase hydrophilicity and introduction of pillars to provide both stability and flow control down the channel. The appropriate blood volume, the pillar location, channel size and doping material

concentration of amphiphilic silicone were adjusted to yield optimized capillary flow for ultimate robust uniform blood smear creation for diagnostic applications at the POC.

3.3. Materials and Methods

3.3.1 Materials.

Allyl methyl PEO (Polyglykol AM 450, Mn = 292–644 g mol-1 per manufacturer's specifications; Mn = 424 g mol-1 per proton (1H) nuclear magnetic resonance (NMR) end group analysis) was provided by Clariant. Octamethylcyclotetrasiloxane and tetramethyldisiloxane were purchased from Gelest. $ODMS_{30}$ (Mn = 2354 g mol-1 per 1H NMR end group analysis) was prepared as reported (148). Triflic acid, rhodium (I) tris(triphenylphosphine) chloride (Wilkinson's catalyst), hexamethyldisilazane, tridecafluoro-1, 1, 2, 2-tetrahydrooctyl-1-trichlorosilane, and solvents were obtained from Sigma-Aldrich. All solvents were dried over 3 Å molecular sieves prior to use. Sylgard 184 was purchased from Ellsworth Adhesives, and SU8-5 from Microchem. Glass microscope slides (75 × 25 × 1 mm3) were purchased from Fisher Scientific. Freshly collected whole bovine blood (citrated) was provided by the Texas A&M College of Veterinary Medicine (160)

3.3.2 Methods

Synthesis of PEO-silane amphiphile (HSi-$PDMS_{30}$-PEO_8). HSi-$PDMS_{30}$-PEO_8 was synthesized as previously reported using a Wilkinson's-catalyzed regioselective hydrosilylation reaction of $ODMS_{30}$ and allyl methyl PEO_8 (1:1 molar ratio) (148). ^1H

NMR of the purified product, a clear and colorless liquid, was in agreement with that previously reportedSmear analysis. The generation of a smear monolayer (i.e. thin smear) was defined as described by Nourbakhsh et al. (7) In brief, the smear was considered thick if more than half of the red blood cells (RBCs) are overlapped in a field view. The cells should not be flattened unless for an acceptable reason such as disease or lack of hemoglobin. Rouleau formation and agglutination found in the presence of cold agglutinins or with elevated globulin and plasma fibrinogen will be considered acceptable (6). For this paper, every smear discussed is a thin smear. Additionally, no staining was involved and counting was done on all cells as a whole with a focus on RBCs using ImageJ software to outline and count the cells. For the analysis of the smear quality for experiments in this paper, all images were visualized to check if the smear was thin or thick and spot checked manually to ensure the ImageJ software was accurately counting the cells.

Design and chip fabrication. The channel's mask design includes pillars as described by Kaminaga et al. (168) but four different placements of these pillars down the channel were selected to uniformly distribute the cells down the entire channel length and keep the channel from collapsing. The mask includes four microfluidic channels, which are 16 mm long from the center of the inlet to the center of the outlet and 250 µm in width. The complete channel design is shown in **Figure 9**. Within each channel, pillars (50 µm diameter, 10 µm gap between pillars) were designed at the inlet, outlet, as well as two location roughly 4 mm and 8 mm from the inlet. The pillars at the inlet and outlet cover approximately 1.6 mm, which is about 30 columns of pillars. There are two sets of pillars

after the inlet with 3 columns in each set. A standard SU8-5 process was used to fabricate the master mold following the procedure described by by Thangawng et. al.(149). The Dektak profilometry was used to measure the channel height. After the master mold microfabrication process, the master mold was coated with tridecafluoro-1, 1, 2, 2-tetrahydrooctyl-1-trichlorosilane for easy removal of the mold. The mold was fabricated using the following protocol. The Sylgard 184 "base" was added with the Sylgard 184 "curing agent" at a 10:1 ratio. To this HSi-PDMS30-PEO8 was added at 3 wt% (3% PEO-PDMS), 5 wt% (5% PEO-PDMS), and 7 wt% (7% PEO-PDMS) based on the total weight of the Sylgard base and curing agent. Samples were mixed in a Flacktek speed mixer for 15 seconds at 1000 rpm, ramped manually to 3000 rpm over 15 seconds, and then mixed at 3000 rpm for 4 minutes. The sample mixture was removed from the Flacteck and mixed while being heated in a 70 ℃ water bath before pouring into a 60 ℃ preheated master mold. The sample was desiccated for 13 min to remove the air bubbles and cured at 130 ℃ for 1.5 hr. The mold was removed from the master mold after it cured and was stored at room temperature for 5 days. During this time the mold was prepped by creating an inlet and outlet using a 5 mm biopsy punch. Once prepped, the mold was bonded to glass using an oxygen oven plasma cleaner (Harrick Plasma PDC-001) with the following protocol: sequential vacuum (10 min), oxygen (2 min), plasma (2 min), and 110 □C oven (2 hr). After bonding, chips were stored for at least 24 hr at room temperature (RT) to allow for the plasma effects to dissipate prior to use in experiments. The chips had channel dimensions of approximately 4.7 μm height, 250 μm width, and 13 mm length (after inlet and outlet biopsy).

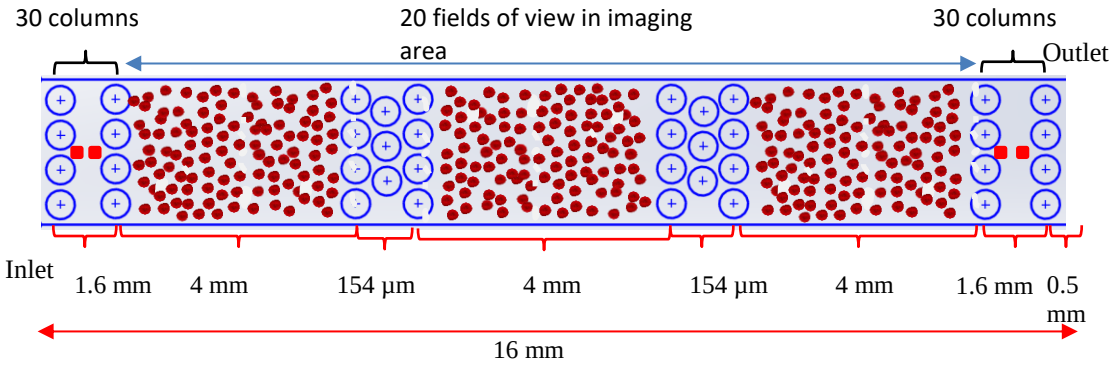

Figure 9. Chip mask design and dimensions: Chip mask design and dimensions. BLUE CIRCLES: Pillars. RED CIRCLES: Red blood cells (RBCs). (Note: Pillar number depicted in specified length is not actual number. Actual number = 30)

Study Variables

Blood volume. To evaluate the potential effects on cell distribution, several blood volumes were used for testing within the channels. Three channels on the same 5% PEO-PDMS chip were used to compare the effects of 0.3 µl, 1.0 µl, and 2.0 µl of blood. The volume of blood was added to the inlet and the time it took to reach the outlet was recorded. Additionally, the time required for the blood to stop moving once added to the channel was recorded and will be referred to as the flow-stop-time (FST). A microscope (Nikon eclipse 11 TE2000-S) with a 20x/0.4 NA objective was used to monitor blood flow towards the outlet and the continuous flow of the blood until it stopped flowing. Once the blood stopped, 20 fields of view were imaged at random positions across the channel outside of the pillar areas from the outlet to the inlet within the imaging area of the channel using a 40X/50 NA objective. This procedure was implemented for each blood volume in their respective channels on the chip. This analysis was repeated with 2 additional chips

to get a triplicate result. Three separate variables and their relationships to one another were tested in the experiment: 1) blood volume as a function of flow speed (flow control), 2) blood volume as a function of FST, and 3) the effects of blood volume, flow speed and FST on cell distribution. The collection of images allowed for the determination of cell distribution through cell counting using the software ImageJ. Once all data was collected it was analyzed to see if a thin smear had been achieved in each field of view. Then cell distribution was investigated within each channel and was compared to the other channels of same volume along with the other channels containing the different volumes of blood.

PEO-silane amphiphile concentration. Chips were made using 3 wt%, 5 wt%, and 7 wt% SMA concentration. For each varying SMA concentration chip, 0.3 µl of blood was loaded at the inlet of the channel and the Nikon microscope was used to monitor the flow. The blood flow speed and flow stop time were recorded to see how they changed within each channel on a chip and across separate chips. These quantities were also used to see how their variation affected the smear quality in terms of aggregation, cell distribution, and the formation of a monolayer. Thus, the relationship of SMA concentration to flow speed and flow stop time was studied in conjugation with how they affected the cell distribution. Each chip had 3 channels that were tested. Once the blood stopped flowing, images of 20 fields of view outside of the pillar areas were acquired within the imaging area and were analyzed as previously described in section 2 of the materials and methods to see if all images showed a thin smear. The cells from each field of view were counted using the ImageJ software to investigate the cell distribution within each individual channel on a chip and compared relative to each other. The comparison

analysis between the three SMA concentrations focused on the thin smear capability of the channel and cell distribution. This was done for all 3 different SMA concentrations in the chips. A final conclusion was made to decide which SMA concentration was best with regard to creating an automated thin smear that can produce a uniform cell distribution.

Chip-to-chip variability. Two 5% PEO-PDMS chips were made the same day using the same master mold. Once the chips were made, they were prepared and bonded together using the same plasma protocol. Blood was pipetted into the inlet at 0.3 µl and allowed to travel down the channel. The blood flow speed, flow stop time, and cell distribution were recorded. This was performed using a Nikon microscope as noted in section 4 of the methods. This was repeated for 3 different channels on the same chip and on two separate 5 % PEO-PDMS chip. After the blood stopped flowing, the 40x objective of the microscope was used to acquire 20 fields of view of the channel from outlet to inlet outside of the pillar locations. The images were then analyzed by counting the number of cells per field of view using the ImageJ software to investigate the cell distribution per field of view within a channel and across all 3 channels on the same chip and then across the 2 chips.

Blood variability. Two 5% PEO-PDMS chips were made, prepped, and bonded the same way as described in the previous experiment. In order to test how the addition of blood variability to chip variability can affect the variation and repeatability, blood was drawn from 2 different sources and tested. We will refer to them as blood A and blood B. In both blood types, 0.3 µl of blood was loaded in each of the three channels of a chip. The blood flow speed and flow stop time were recorded. After the blood stopped flowing,

images of 20 fields of view were acquired outside the pillar area using the 40x objective of the microscope. The images acquired for this experiment were analyzed using ImageJ software for to show how the cell distribution, blood flow speed, and flow stop time varied from chip to chip and how it varied from patient to patient.

3.4 Results and Discussion

***Design and chip fabrication*.** To acquire a high-quality smear with a monolayer of cells, uniform cell distribution, and no flattened cells, the microfluidic cartridge design as well as dimensions needed to be investigated. The height of the channel was manipulated to control flow and to acquire a monolayer of cells without causing channel collapse. Based on the height of RBCs (~2 μm) and allowing for the possibility of the channel bowing, a target height of 4.7 μm was set. The profilometry results indicated that channels with heights of 4.7 ± 0.1 μm were achieved. As the aspect ratio of the channel was extremely low (h:w <0.1), pillars were added at various sections of the channel to prevent collapse in addition to providing a more uniform cell distribution. **Figure 10A,** acquired from a 5 % PEO-PDMS chip, shows that, in the absence of pillars, the channel can collapse and prevent blood from flowing. If collapse does not occur and blood still flows, it can still lead to a nonuniform cell distribution as depicted in **Figure 10B**. Taking the size of the blood cells into account, a 10 μm gap was chosen for this application. Further, knowing that the channel was ~250 μm in width and the pillar gap was around 10 μm, the size of the pillars was calculated to be approximately 50 μm with 4-5 rows of pillars used to produce uniform distribution for those between the inlet and outlet (**Figure**

9). We hypothesized that pillars are needed at the inlet/ outlet and in two loctations on either side of the middle of the channel following the theory that the blood flow profile can have non-homogeneous characteristics even after introduction of inlet pillars for longer channel lengths. The presence of the pillars in the middle of the channel has been shown to redirect flow and get cells to distribute uniformly laterally across the channel. Based on minimizing the potential for channel collapse and optimizing and to produce uniform smear throughout the channel length it was decided that the pillar sections should be 4 mm apart (i.e. equally distributed down the channel). This was validated as shown in **Figure 10C**, which shows that at ~6 mm from the channel entrance without using pillars in the middle of the channel the cells were not-uniformed distributed but rather tended to have more cells closer to the outer edges of the channel. Thus pillars were added at 4 mm and 8 mm from the inlet pillars of the channel for a consistent and repeatable flow redirection that leads to uniform cell distribution and minimized the possibility of a collapse within the channel (166, 168, 170). Kaminaga et. al. showed 4 columns of pillars in his design (168). The choice of the number of columns at the inlet and outlet was primarily influenced by having enough columns to prevent collapse and not obstruct flow because the inlet and outlet are more prone to collapse due to atmospheric forces. For the middle, we choose 3 columns because we wanted to use as few columns as possible to increase the amount of space for microscopic imaging within the channel, to provide a good flow velocity throughout the channel without the need for pumping and also still provide adequate cell distribution. Too many columns would obstruct the flow and block the imaging area, while too few would not provide adequate cell distribution. **Figure 10D**

acquired from a 5 % PEO-PDMS chip shows that, with the right size and placement of pillars and the proper gaps, that uniform cell distribution can be achieved across the entire channel.

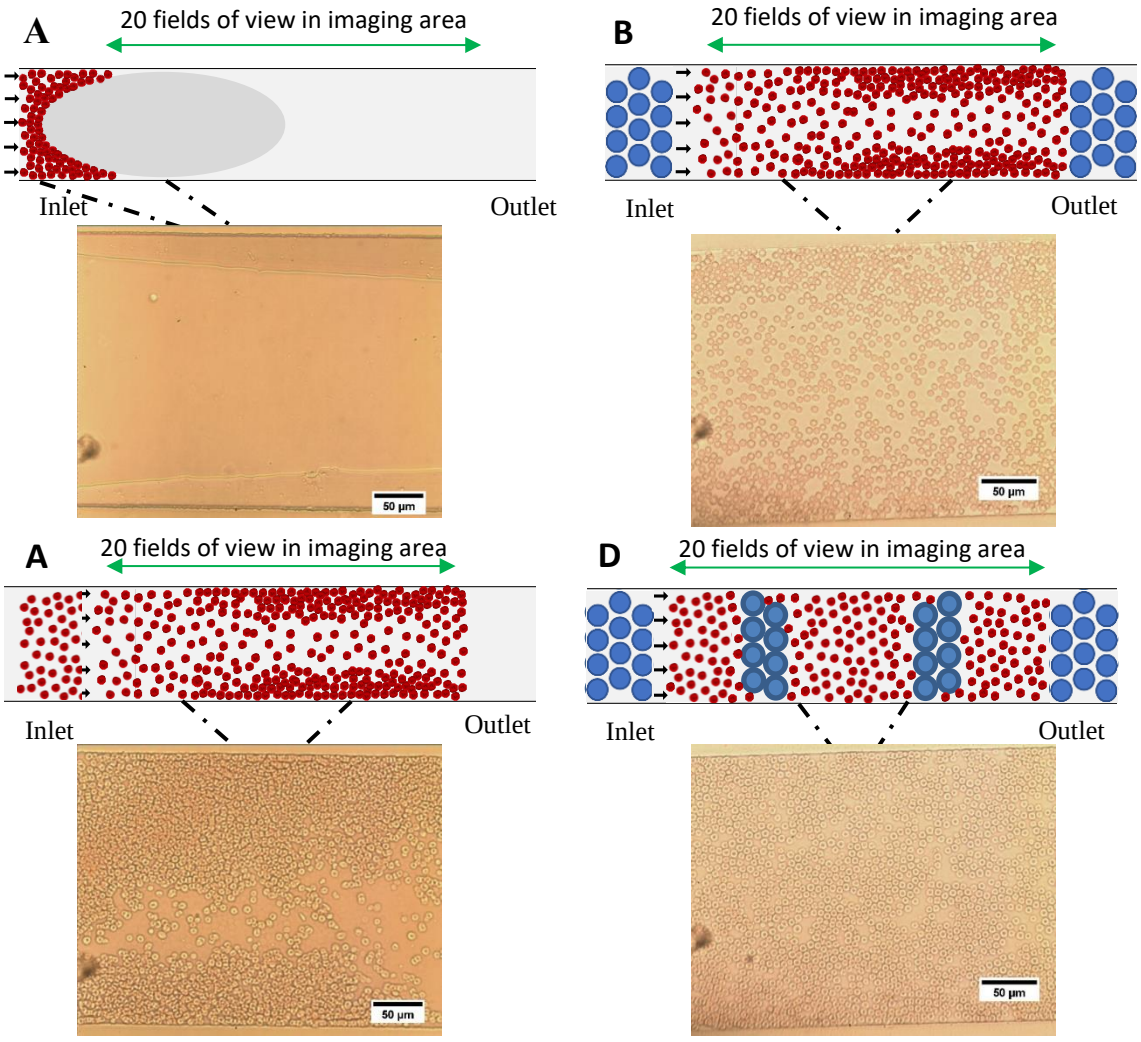

Figure 10. For 5% PEO-PDMS chips with 0.3 µL of blood, schematic of channel design and representative images: (A) no pillars with channel collapse, resulting in no blood flow, (B) no pillars without channel collapse, resulting in non-uniform cell distribution, (C) pillar sections at inlet and outlet, resulting in non-uniform cell distribution and (D) pillar sections at inlet, outlet, and interior, resulting in a uniform cell distribution (i.e. thin smear).

Blood flow control and cell target numbers per field of view. Blood volume and SMA concentration variables can help control the blood flow and monolayer cell distribution. In our previous work, flow control using 5 % PEO-PDMS, 7 % PEO-PDMS, and 14 % PEO-PDMS with 5 µl was tested (160). From the results, we concluded that < 5 µl of blood may provide a better-quality smear and, to test lower blood volumes, that 5 % PEO-PDMS would be a good starting point. This is because for a good quality smear, the average number of red blood cells (RBCs) per field of view for human blood for a 1000X magnification (0.025 mm^2) has been found to be around 250 cells (171). Bovine blood has around 5-7 million RBCs per/µl (comparable to humans) but the RBC size is smaller at around 5-6 µm in disk diameter (172) (rather than the 6-8 micron for humans), which can be translated into higher cells per unit area (i.e. 320-480 cells per 0.025 mm^2)(171). However, in the field using an automated microfluidic smear technology with less fields of view available, having more cells per area would be useful and helpful for faster diagnosis, providing the smear is uniform and the separation is sufficient for the automated software to detect the cells and parasites (62, 171). Theoretically, assuming an area of view of 0.024 mm^2 and a bovine blood RBCs size of 6 µm, the maximum for the field should be no more than 700 cells. With that number of cells in the field, the cells should be packed together with slight gaps between each cell to allow for software counting. A smear with higher numbers of cells (i.e. over 800) will result in no gap between the cells, no way to count them effectively with an automated system and hence an overall poor-quality smear. Such a poor-quality smear with a high cell density can lead to poor diagnosis, particularly false negatives or false positives for instance in the case of

malaria diagnosis (69, 71). Further, smears with overlapping cells can also lead to an inaccurate diagnosis when using manual or automated methods, especially if the diagnosis requires cell counting such is the case for parasitemia in malaria (15).

Blood volume variation. It has been shown that the monolayer cell distribution can be altered with a change in blood volume causing the smear quality to be less than adequate (64, 161, 162). Because a blood smear done on glass typically uses 1 µl of blood, the values chosen to be tested were 0.3 µl, 1 µl, and 2 µl. For all 3 chips, the result of this experiment showed that the blood flow speed increased as the blood volume increased from 0.3 µl to 1 µl. However, it decreased for 2 µl (**Table 1**). Intuitively, as the volume increased one would think the speed would increase because of flow rate equation (123, 173), but as the volume increases the hematocrit increases also and, in this case based on the aspect ratio of the microfluidic channel, it reached a level where it became an obstacle for the flow. Specifically, the higher number of cells were not able to move freely in this narrow channel making it difficult for the blood to flow faster. The blood flow stop time, on the other hand, increased as the blood volume used increased (**Table 1**).

In terms of blood smear cell distribution, the imaging took place at the time the blood flow stopped and for all three of the 0.3 µl channels did not present thick smear qualities in the imaging area. Also, the field of view did not have large numbers of cells making it easier for the software to count the cells. However, there were some rouleaux formations (i.e. stacks or aggregations of red blood cells that form because of the unique

Table 1: 5 % PEO-PDMS chips (1-3) with variable blood volume deposited to inlet.

Channels of Chip 1	**Blood Volume (µL)**	**Flow time** (inlet to outlet) **(min)**	**Flow stop time (min)**	**Number of cells per field of view**
1	0.3	1:25	6:32	530 ± 16
2	1	1:09	12:45	539 ± 26*
3	2	1:47	>20	564 ± 18*
Channels of Chip 2	**Blood Volume (µL)**	**Flow time from inlet to outlet (min)**	**Flow stop time (min)**	**Number of cells per field of view**
1	0.3	1:07	7:55	523 ± 18
2	1	0:59	13:41	539 ± 31*
3	2	1:30	>20	584 ± 30*
Channels of Chip 3	**Blood Volume (µL)**	**Flow time from inlet to outlet (min)**	**Flow stop time (min)**	**Number of cells per field of view**
1	0.3	0:49	6:31	547 ± 20
2	1	0:42	11:59	528 ± 28*
3	2	0:55	>20	532 ± 18*

*An accurate cell count could not be obtained in some images due to cell proximity &/or overlap in the absence of a generated thin smear.

discoid shape of the cells in vertebrates) in some of the images. Rouleaux formations are considered acceptable in situations like this because of cold agglutinins (13). The images from the 1 µl of blood channels did not present any thick smear qualities in the imaging area, but there were a few images with large amounts of cells that were close to each other making it difficult to count them. The images from the 2 µl experiment had a few images that were characteristic of a thick smear and some images had a high quantity of cells making it difficult to count them. After the cells were counted, cell distribution analysis

was done to see how the cells' distribution varied within a channel, across channels of the same chip, and across chips. **Figure 11** shows an example of a 0.3 µl image containing an optimal number of cells for counting along with no thick smear qualities. This is compared to a 1 µl image with high numbers of cells close to each other and hence hard to count as well as a 2 µl image showing a thick smear. From the blood volume experiment, we concluded 0.3 µl blood volume with 5 % PEO-PDMS are the best combination in terms of both flow control and for providing a good quality smear.

PEO-silane amphiphile variation. From the blood volume test, we concluded that 0.3 µl flow control with 5 % PEO-PDMS gave a good quality smear and thus 0.3 µl will be used for further testing the concentration variation of the PEO-PDMS. Specifically, since SMA concentration influences hydrophilicity and hence affects flow speed and

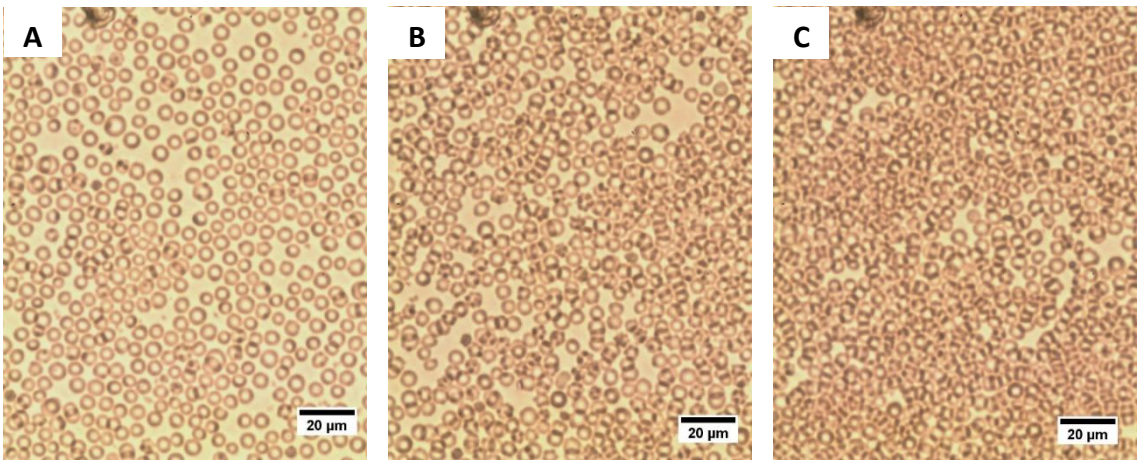

Figure 11. For 5% PEO-PDMS chips, representative images: (A) With 0.3 µL of blood, thin smear generated and cell counting possible, (B) with 1 µL of blood, thin smear generated and increased cell proximity disrupts cell counting, and (C) with 2 µL of blood, thin smear not generated and further increased cell proximity disrupts cell counting.

smear quality (64, 162, 174), different SMA concentrations, 3 wt% and 7 wt%, above and below 5 wt% were tested in combination with 0.3 µl blood volume. The results of the flow speed and flow stop time are shown in **Table 2.** The results showed that both the flow speed and stop time decreased as SMA concentration increased from 3 to 7 wt%. This was anticipated as one would expect faster flows with higher hydrophilicity but it is noted that from 5 to 7 wt% the rate of the stop time is lower than the rate of decrease in stop time when going from 3 to 5 wt%. In terms of the blood smear, the 3 wt% has a few thick smear images in the imaging area and a few thin smear images with large amounts of cells making it difficult for the software to count them. The 5 wt% did not have any thick smear images or images with too many

Table 2: *3*-, *5*- and 7*% PEO-PDMS* chips (1-3) with 0.3 µL of blood deposited to inlets.

Channels (3) of *3% PEO-PDMS* chip	**Flow time from inlet to outlet (min)**	**Flow stop time (min)**	**Number of cells per field of view**
Ave (1-3)	6:22 ± 0:3	8:54 ± 0:31	510 ± 28*
Channels (3) of *5% PEO-PDMS* chip	**Flow time from inlet to outlet (min)**	**Flow stop time (min)**	**Number of cells per field of view**
Ave (1-3)	2:30 ± 0:27	6:03 ± 1:03	523 ± 16
Channels (3) of *7% PEO-PDMS* chip	**Flow time from inlet to outlet (min)**	**Flow stop time (min)**	**Number of cells per field of view**
Ave (1-3)	0:33 ± 0:04	5:56 ± 0:51	541 ± 27

*An accurate cell count could not be obtained in some images due to cell proximity &/or overlap in the absence of a generated thin smear

cells, but there were some with rouleaux formations as noted in the results section 2.1. As for the 7 wt%, there were no thick smear images and only a few images had too many cells with no rouleaux formations. **Figure 12** shows the images of a smear obtained from a 3, 5, and 7 wt% PEO-PDMS chip. From both blood flow control experiments in which both blood volume and SMA concentration were varied, it can be concluded that a combination of 0.3 µl blood volume with 5 and 7 wt% SMA concentration are acceptable in terms but that the 5% was slightly better in smear quality with only a slight increase in stop time.

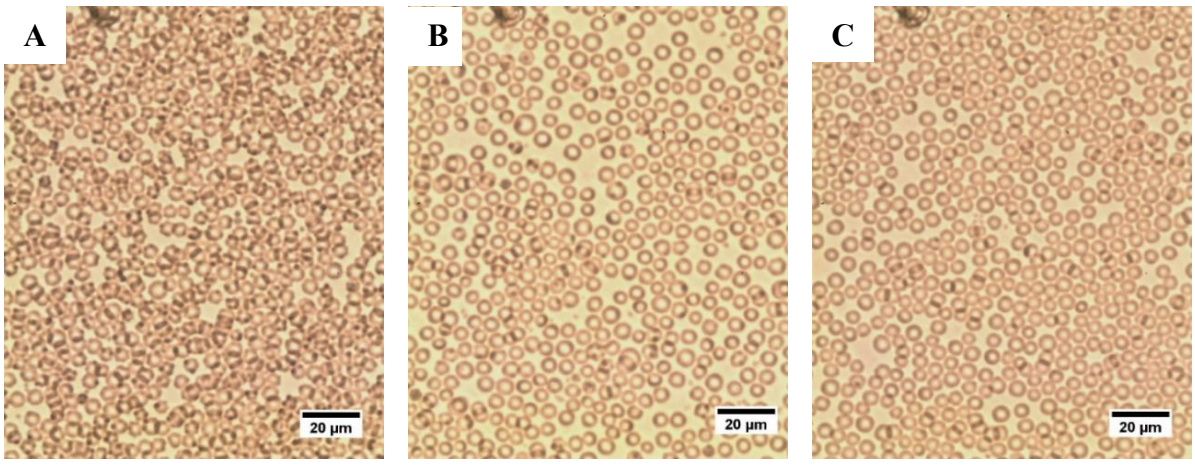

Figure 12. For chips prepared with varying concentrations of PEO-silane amphiphile SMA additive and treated with 0.3 µL of blood, representative images: (A) a 3% PEO-PDMS chip, unacceptable thin smear generated and increased cell proximity disrupts cell counting, (B) a 5% PEO-PDMS chip, thin smear generated and cell counting possible, (C) a 7% PEO-PDMS chip, thin smear generated with some cells proximity that disrupts some cell counting

Chip to chip variability. One of the biggest challenges in smear preparation, in particular manual smears, is the reproducibility since there is wide variation both from a single person across days and for different people (10, 23, 24). This variation is often a

function of the physical or mental state of the person on a given day (e.g. whether they are feeling tired or have the proper mental state to do a good job). In addition, the person's ability also affects the smear quality, particularly the person at the POC in rural areas. The SMA concentration and blood volume tests above showed that a combination of 0.3 µl of blood volume with 5 wt% PEO-PDMS chip gave a good smear quality and reasonable flow. Thus, the 0.3 µl with 5 wt% PEO-PDMS chip was used in these studies to test the repeatability of the chip. As depicted in **Figure 13**, the smears for all channels on both chips were single layered. The cell count and density distribution within a channel, across different channels of the same chip, and across different chips were within ~5% of each other, which is considered well below the acceptable by WHO standards, which only require less than 25% (175). For chip 1, the cell counts and standard deviations for channels 1, 2, and 3 were 461 ± 17, 449 ± 16, and 451 ± 15 respectively. For chip 2 they were 447 ± 19, 439 ± 17, and 456 ± 23. The average cell count and standard deviation for chip 1 and chip 2 are respectively 453 ± 6 and 447 ± 9. The blood flow speed and the blood flow stop time for both chips are summarized in **Table 3**. As shown in **Table 3**, within a chip both of flow time and flow stop time are within 5% and across chips the flow time is also within 5%, however, across chips the flow stop time did vary by 25% (nearly 2 minutes) but both were below the 10 minutes targeted for a POC diagnostic device.

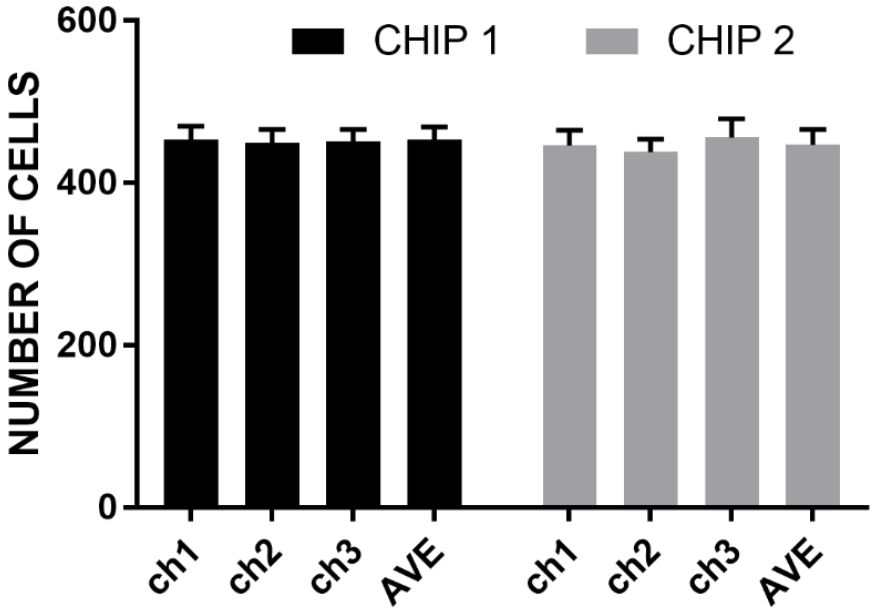

Figure 13. Cell count within a channel and across channels for chip 1 and chip 2 acquired with the same blood

Table 3: Two 5% PEO-PDMS chips treated with 0.3 µL of blood deposited to inlets.

Channels (3) of *5% PEO-PDMS* "chip-1"	**Flow time from inlet to outlet (min)**	**Flow stop time (min)**	**Number of cells per field of view**
Ave (1-3)	1:14 ± 0:08	7:30 ± 0:34	454 ± 16
Channels (3) of *5% PEO-PDMS* "chip-2"	**Flow time from inlet to outlet (min)**	**Flow stop time (min)**	**Number of cells per field of view**
Ave (1-3)	1:09 ± 0:11	9:06 ± 0:08	447 ± 19

Patient blood variability across chips. Another variable that affects the smear variation and reproducibility is the blood used for the smear because different patients could have different blood variations. Specifically, often the patients' blood variability lies within hematocrit levels, blood viscosity differences, diseases, and the possibility of Rouleau and agglutination formation. All of these variables can affect the smear quality. The flow speed and the flow stop time is shown in **Table 4**. The results showed that all flow speeds and flow stop times for both were in the range of previous data results and all the smears were thin smears. With regard to the cell density, the cell count from two blood samples is different (**Figure 14**) and there was a higher variation within a chip compared to the previous results of **Figure 13**. Thus, this does show that as the blood changes, the number of cells per field of view across the chip could be different; however, both still had a uniform cell distribution within and across all channels of the chip. Further, these results are similar to the standard manual glass blood smear (64), where the blood variables affect the quantity of cells per area and the flow rate, but, as noted, the microfluidic generated smear, both blood types show good quality smear and cell count for diagnosis.

As mentioned earlier, every patient has a different blood characteristics. Although we cannot test for every blood condition, in Appendix C four common blood situations are analyzed using the blood viscosity flow model and described in terms of how they can effect smear quality namely; low hematocrit/low blood viscosity, high hematocrit/high viscosity, healthy hematocrit/low viscosity, and healthy or normal blood hematocrit/high viscosity. These conditions can lead to or arise from various diseases or conditions such as anemia, kidney failure, erythrocytosis, polycythemia vera, and hypergammaglobulinemia. The blood viscosity model showed that even with a blood viscosity 5 times the normal, the flow times are still in the range of

our experiment data. Although we did not test for all the different types of blood, this study still has an essential value because, in a situation for example, where the smear quality shows less red blood cells per field of view could indicate to the doctor that the patient's blood is anemic or has problems and that the doctor should investigate the blood quality further.

Table 4: Blood variation experiment done with 5% PEO-PDMS chip and 0.3 µl of blood.

Channels (3) of *5% PEO-PDMS* "chip-1"; blood from "donor-A"	**Flow time from inlet to outlet (min)**	**Flow stop time (min)**	**Number of cells per field of view**
Ave (1-3)	1:35 ± 0:03	8:05 ± 0:56	511 ± 39
Channels (3) of *5% PEO-PDMS* "chip-2"; blood from "donor-B"	**Flow time from inlet to outlet (min)**	**Flow stop time (min)**	**Number of cells per field of view**
Ave (1-3)	1:22 ± 0:08	7:47 ± 0:22	625 ± 42

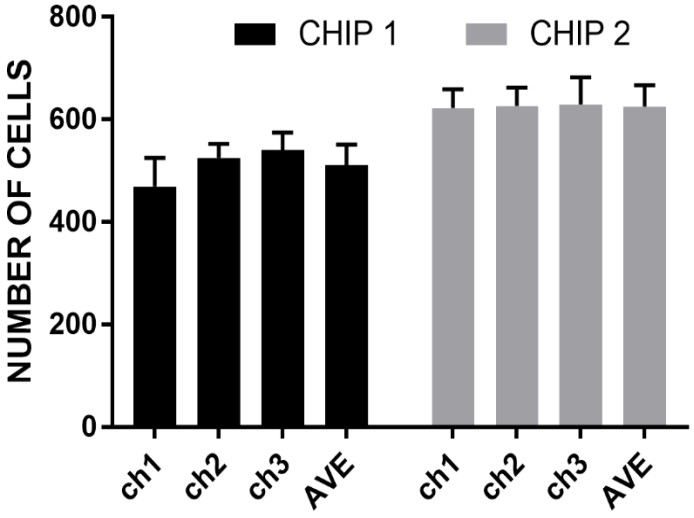

Figure 14. Cell count within a channel and across channels for chip 1 and chip 2 acquired with different blood

3.5 Conclusion

The design of a capillary flow, pumpless, microfluidic cartridge to replicate whole blood smears for ultimate POC applications was demonstrated in this paper. A master mold with pillars at the inlet, outlet, and either side of the middle of the channels was made using an SU8-5 process. Microfluidic chips were made from Sylgard 184 modified with an **H-PDMS$_{30}$-PEO$_8$** SMA at different concentrations (3, 5, and 7 wt%) to provide varying hydrophilicity. The flow of 0.3 µl of blood into chips of 3, 5, and 7 wt% PEO-PDMS showed that the 5 wt% and 7 wt% samples gave adequate smear quality with the 5% providing slightly better results and the 3 wt% sample providing poor results. Specifically, the 5 and 7 wt% PEO-PDMS had smears with cell monolayers and no thick smear images were seen in the imaging area of the channel. In contrast, the 3 wt% PEO-PDMS had areas that could be considered as a thick smear. Different blood volumes (0.3, 1, and 2 µl) were also added into 5% PEO-PDMS channels to generate blood smears. The results show that the smear quality decreased as the blood volume increased due to the microfluidic aspect ratio. The 0.3 and 1 µl volumes produced smears with cell monolayers; however, the 1 µl sample had a few areas with densely packed cells, which made it difficult to count the cells properly. The 2 µl samples were worse, with a few regions that could be considered as thick smears within the imaging area. The repeatability from chip to chip with the same patient's blood was excellent. Specifically, the resulting blood smears had cell monolayers

and the cell counts from channel to channel and chip to chip that were in the range of 5% considered acceptable by the WHO, which only requires 25%. When comparing blood smears generated from blood samples of different patients, variation in cell counts were observed, as is common due to inherent differences in patient blood (e.g. hematocrit, viscosity, etc) Overall, this capillary flow-controlled microfluidic cartridge has the potential for use as an automated whole blood smear preparation, particularly for POC diagnostic applications

CHAPTER IV

BRIGHTFIELD AND FLUORESCENCE STAINING OF MICROFLUIDIC CARTRIDGE GENERATED THIN PERIPHERAL BLOOD SMEARS

4.1 Overview

Proper staining of peripheral blood smears is essential for the accurate characterization, diagnosis, and monitoring of various diseases such as malaria and various anemias by increasing contrast of intracellular components and biomarkers Herein, wet Romanowsky and fluorescence staining protocols are adapted for use in flow-controlled microchannels, allowing automation of stained whole human blood smears at the point-of-care. A 3X concentration Giemsa stain was created and diluted with DI water to 10% 33%, 50% concentration, and Acridine Orange fluorescence stain at 12µg/mL were tested on human blood samples containing malaria parasites to assess utility and optimal protocols. Giemsa staining at 33% dilution showed an optimal blend of contrast and preservation of cellular morphology, while 50% dilutions showed significant cellular crenation and 10% dilutions did not show desired contrast in brightfield imaging. Fluorescence staining at 12µg/mL using Acridine Orange shows that parasites can be clearly seen with reduced signal intensity when compared to gold-standard staining protocols. The wet smear protocol also showed inverted contrast of red blood cells and background when compared to gold-standard in fluorescence imaging. These results demonstrate that peripheral blood can be successfully stained in a simple, one-step

procedure for multiple imaging modalities prior to use in a microfluidic smear-generating cartridge.

4.2 Introduction

Peripheral blood smears are essential to the characterization, diagnosis, and monitoring of various diseases such as malaria, anemias, sickle cell diseases, thrombocytopenia, thrombocytosis, leukemia, lymphoma, and iron deficiency (9, 69, 154, 155). These smears can be used to diagnose, characterize, and monitor diseases either manually or using automated microscopic techniques to observe cell morphology and differential blood cell counts (9, 23, 154, 155). The general use of peripheral blood smears involves three primary steps: 1) formation; 2) fixation/staining; and 3) examination. Smear preparation is the process of physically manipulating a blood sample to form a thin layer of cells with proper thickness, shape, and density. Fixation and staining use various chemicals to accomplish some combination of sample inactivation, permeabilization, adhesion to a substrate, and augmentation with a contrast-enhancing stain prior to examination. This work presents simple staining protocols used to enhance the contrast of such auto-generated smears, with applicability for use in remote locations and at the point-of-care (POC).

One common use of blood smears in remote locations is for the microscopic diagnosis of malaria. To prepare a conventional thin smear, a small drop of patient blood is deposited onto a microscope slide, where it is immediately “wiped” across the surface of the glass to form a monolayer of cells using a second slide (176). This process requires

significant practice and skill, and there is variability in the quality of smears created (177). After a thin film has been formed and dried, it will be fixed using either physical or chemical techniques (178). Fixative chemicals include formaldehyde, glutaraldehyde, acetone, ethanol, methanol, or combinations; while physical methods are heating, microwaving, and cryo-preservation (freeze-drying) (65, 66, 178, 179). Most typically, the smear will be submerged in 100% methanol for 30-60 seconds immediately prior to staining to effectively permeabilize, preserve, and prepare the sample for stain uptake (64). Some stains, such as Leishman Stain, include fixative agents in their composition and allow for a single-step fixation/staining procedure (67). Exact fixation protocols can vary to account for differences in stain concentration, temperature, osmolarity, and materials used (180). A proper fixation technique will result in smears that preserve cellular morphology and allow for stain uptake by the sample to produce the desired contrast (179, 180).

While various types of stains may be used to enhance features of peripheral blood smears, this work focuses primarily on the use of Romanowsky-type stain used for brightfield imaging and Acridine Orange (AO) stain used for fluorescence imaging. Variations in traditional staining protocols arise from variables such as staining compounds, time, concentration, buffers used, pH balance, and age, all of which must be controlled to produce smears with the desired enhanced contrast (9, 70). Romanowsky and Giemsa-Romanowsky stains are fundamentally a combination of eosin and methylene blue derivatives which create a wide range of blue, purple, and pink hues. Some common examples of these stains include Giemsa, Field's, JSB, Wright's, and Leishman stains,

which can be used in numerous distinct ways depending on the sample type and desired effect (66, 67). It is important to note that the presence of multiple staining compounds is required to create purple hues in what is known as the "Romanowsky effect" within the granules of neutrophils, chromatin, and other cellular matter. Azure B, a methylene blue derivative, is a small molecule and can stain quickly, while eosin, the pigment mainly responsible for the purple color, is three-times bigger and takes longer to diffuse across the cell's membrane, creating a time-hue interdependency that must also be considered (66). When used in peripheral blood smears, the Romanowsky effect is especially visible wherever DNA is present, which causes *Plasmodium* parasites to appear with high contrast due to the lack of DNA in erythrocytes.

Similarly, the use of fluorophores in peripheral blood smears has been shown to be viable for parasitic contrast enhancement within red blood cells (RBC's), with some studies claiming greater sensitivity with the use of fluorescent stains when compared to brightfield-chromophores (181-185). Acridine Orange is a cell-permeant stain that bonds to DNA and RNA via intercalation with emission peaks of 526nm and 650nm, respectively. It has been used previously in malaria research and diagnosis due to its combination of function, cost, and stability. Use of both brightfield and fluorescent stains require that a balance is achieved between maximizing stain-target binding and saturating the sample such that binding specificity and contrast is lost (9). In Romanowsky stained blood smears, under-staining results in highly transparent samples with poor contrast, and over-staining results in nearly homogenous light absorption across entire cells such that little to no chromatic variance between targets and the cellular background can be seen.

Fluorescently stained smears, which are imaged through filters to block all non-signal light, do not emit sufficient photons to generate a discernable signal when under-stained, and overstaining results in fluorescence being seen in sample background, cellular membranes, and condensed debris, creating washed-out images.

The complexities of staining protocols and diversity of applications thus require that customized protocols must often be adapted for each unique circumstance. Poor smear preparation, fixation, and staining should be avoided whenever possible to mitigate diagnostic errors which can lead to the improper drug prescription, increased morbidity & mortality, and undue socio-economic burden (42, 54, 69-71, 73). With diagnostic errors oftentimes attributed to stain quality, automated staining devices have been developed but are typically unsuitable for use at the point-of-care (POC), away from centralized laboratories (21, 70). Thus, there is a need for a automated or semi-automated staining platform technology and simple protocols that can incorporate a diverse set of sample stains for use at the POC (9, 70).

Microfluidic systems have been proposed for use at the POC in developing countries because they promise low-cost, adaptable, rapid, and easy-to-use detection platforms for various biological analytes (156, 157). While many groups attempt to accomplish complex laboratory functions such as staining on a single chip, many devices require auxiliary technologies to operate and fail to meet the World Health Organization's ASSURED criteria or FDA simple test guidance (25, 186). Li et al. showed that blood smears can be stained in a microchannel with the use of pumps and valves to accommodate the staining procedure, however, their complex design produced stains with many artifacts

(159). Horning et al. designed a POC blood smear staining device on a paper microfluidic cartridge, however the lengthy drying times associated with their protocol would not meet the WHO's ASSURED criteria, which requires that the diagnosis procedure be done under 30 min (14, 32). Additionally, the use of paper-fluidics causes difficulty in achieving the necessary microscopy resolution for accurate disease diagnosis. Our previous works have shown blood flow can be controlled using capillary forces in a microfluidic chip made from a bulk modification of Sylgard 184 with poly(ethylene oxide) (PEO) – poly(dimethyl siloxane) (PDMS) (HSi-$PDMS_{30}$-PEO_8) based on surface-modifying additives (SMAs) (160). SMA concentration adjustments allow us to create thin blood smears and to dictate flow rates and the time to flow cessation. Control of flow rates is especially important as it allows for customization of the cellular density in the smear and adjustment of the time required for a sample to be ready for analysis.

As a closed system, it is difficult for smears in microchannels to dry between reagent steps as in most standard staining protocols. Thus, such methods are not feasible in microchannels and stresses the need for a different staining protocol altogether. In this paper, we propose the development of wet Romanowsky fluorescence staining protocols for whole human blood for use in a microfluidic cartridge for POC diagnosis of hematology disease such as malaria. The staining procedure allows for samples to be ready for analysis in under 20 min, with results similar to those achieved using traditional glass-slide staining protocols.

4.3 Materials and Methods

4.3.1 Materials

Allyl methyl PEO (Polyglykol AM 450, M_n = 292–644 g mol^{-1} per manufacturer's specifications; Mn = 424 g mol^{-1} per proton (^1H) nuclear magnetic resonance (NMR) end group analysis) was provided by Clariant. Octamethylcyclotetrasiloxane and tetramethyldisiloxane were purchased from Gelest. $ODMS_{30}$ (M_n = 2354 g mol^{-1} per ^1H NMR end group analysis) was prepared as reported (56). Triflic acid, rhodium (I) tris(triphenylphosphine) chloride (Wilkinson's catalyst), hexamethyldisilazane, tridecafluoro-1, 1, 2, 2-tetrahydrooctyl-1-trichlorosilane, and solvents were obtained from Sigma-Aldrich. All solvents were dried over 3 Å molecular sieves prior to use. Sylgard 184 was purchased from Ellsworth Adhesives, and SU8-5 from Microchem. Glass microscope slides (75 × 25 × 1 mm3) were purchased from Fisher Scientific (160).

4.3.2 Methods

A Giemsa powder and Acridine Orange powder purchased from Millipore-Sigma were used for all brightfield and fluorescence stain solution preparations, respectively. Giemsa 3X concertation stock solution was made using the protocol described by Bain et al, modified to use 300 mg of Giemsa powder was mixed with 10 ml of absolute methanol (187). The mixture is put on a hot plate at 50 degrees for 15min. After that the stock was put on a mixer for at least 12 hours to break clumps of Giemsa from the stock. Following that, the stock was filtered using 4 µm and 2 µm paper filters. The filtered stock is left sitting for at least 24 hours before use. Acridine orange stock solution was made as a 96

μg/mL suspension of AO in PBS pH 7.2. Microfluidic thin-smear generating cartridges were prepared on 0.17mm microscope cover glass according to protocols as first described in our previous work, a summary of which can be found in **Appendix D**. Cultures of P. falciparum parasites were cultured in vitro and reconstituted to mimic physiological properties of unaltered human blood according to full details as given in **Appendix D**

***Experimental setup*.** To test the hypothesis that microchannels can be used to create a well-stained, stable, repeatable thin smear of cells for brightfield and fluorescence microscopic analysis, a small amount of stained parasitized human blood samples were deposited at the inlet of the micro channels and allowed to flow from the inlet to the outlet of the channel, creating a thin monolayer of cells. After the stained blood stopped flowing inside the channel, a Nikon Eclipse Ti-2 microscope with 60x oil-immersion objective was used to take images of the cells from the outlet to the inlet at 0.5 mm increments, and the images were catalogued for later analysis.

Staining Protocols. Gold-standard reference smears for both brightfield and fluorescence stains were created on glass microscope slides according to published procedures (176, 182-184, 188). While the gold-standard staining methods use previously dried and fixed thin smears, staining for use in a microchannel-generated thin smear requires staining to be done in liquid-phase suspension. It was found that the fluorescence staining procedures were significantly simpler to adapt to liquid-phase staining than the Giemsa-type brightfield procedures. Fluorescence stain solutions were created by diluting

AO to desired concentrations in 1x PBS. For brightfield staining, it was found that a 3X Giemsa stain stock concentration was optimal, which was then diluted with DI water to create 10%, 33%, and 50% stain solutions. The upper and lower concentrations for staining were selected based on Gold-Standard procedures typically using a 10% dilution, and deformations in cellular morphology that appeared above 50% concentration. To create stained blood samples, stain solutions were mixed with reconstituted parasitized blood in 1:2 (stain:blood) ratios by volume in 2mL centrifuge tubes. The combined sample and stain were mixed by hand for 30 seconds then set aside under a light-shielding covering for 10 minutes to incubate at room temp. After 10 minutes, 0.5µL of sample was transferred to the inlet of the microfluidic channels, and imaging began after cells stopped flowing in the channels after 4.31 ± 0:39 in. The incubation time for the AO on the other hand was for 6 minutes before it was loaded in the microchannel

Image Analysis. Image analysis was performed to compare staining quality, which was defined as the quantitative feature separability of parasites from both intracellular and extracellular backgrounds. Fluorescence images were monochromatic, while brightfield images contained standard red, green, and blue data. Images from each mode of imaging were processed similarly, with parasitic, RBC, and background features segmented using masks that were commonly applied to all images taken for individual single staining procedures. In fluorescence images, parasitic, RBC, and background features were segmented using Nikon BR Elements software based on the presence of intensity thresholded local maxima in the imaging field, and the intensities of these features were

analyzed for separability and repeatability. For brightfield images, MATLAB was used to segment parasites, RBC's, and background using hue, saturation, and value (HSV) units. Feature differentiability was determined from the average HSV values of each feature's pixel population. When plotted in cylindrical HSV colors pace, the distance between population clusters were compared, with higher distance values indicating that features were more differentiable. The quantitative variance of stained features was used to assess overall repeatability both within and between images gathered from each individual smear. Throughout all portions of image analysis, cellular morphology was qualitatively assessed to ensure that no crenation, lysis, or significant morphological deformations occurred at any point during the tests.

4.4 Results and Discussions

***Brightfield Staining*.** For Giemsa stained samples, HSV values for smear background were found to be (238, 5%, 78%) for the 10% dilution, (244, 6%, 80%) for the 33% dilution, and (236, 7%, 78%) for the 50% dilution. These values each result in very similar shades of gray. HSV values of the RBCs were (237, 5%, 78%), (194, 3%, 71%), (147, 4%, 72%) for 10%, 33% and 50% dilutions, respectively. Qualitatively, the color of the RBC's in the 10% dilution appeared as a lighter shade of gray than the similarly darker shades of 33% and 50%. HSV values for malaria parasites were (210, 40%, 66%), (216, 48% 67%), and (220, 53%, 66%) for 10%, 33%, and 50% respectively, with all values representing comparable blue colors (**Figure 15**).

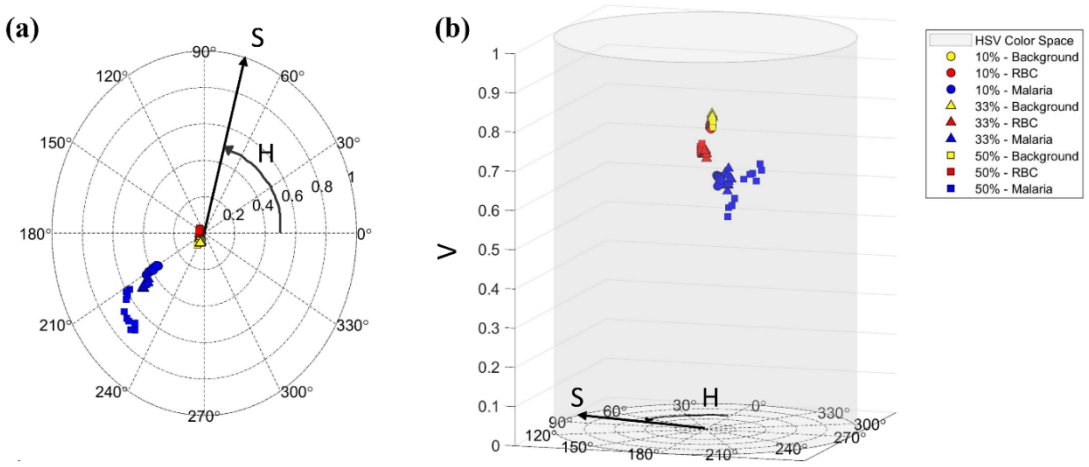

Figure 15. Average HSV colors for mal aria parasites (blue), background (yellow), and RBCs (red) in 10 brightfield images within (a) two dimensional hue and saturation space and (b) three dimensional hue, saturation, and value space per 10% (circles), 33% (triangles), and 50% (squares) staining protocols

Table 5: Average distances between features in HSV color space for the10%, 33%, and 50% staining protocols.

Stain Concentration	Average Distance (HSV)	
	Malaria Parasites vs. Background	Malaria Parasites vs. RBCs
10%	0.371 ± 0.0267	0.369 ± 0.0268
33%	0.448 ± 0.0181	0.453 ± 0.0215
50%	0.483 ± 0.0277	0.530 ± 0.0250

In HSV color space, the feature separability increases with the concentration of stain used as shown by the increasing average distances between the malaria parasites and the RBC's and background (**Table 5**). Coefficients of variance for the hue and saturation

of the malaria parasites within each image were < 1 for all three concentrations, and there was no significant difference in the variance of distance between malaria parasites and RBC's for all three concentrations. However, more cells in the 50% images show crenation than in the 33% and 10% images, likely due to the higher methanol concentrations used in the 50% stain (**Figure 16**). These results indicate that the 33% stain concentration protocol gives an optimal blend of enhanced contrast and preserved cellular morphology that is preferable for brightfield staining.

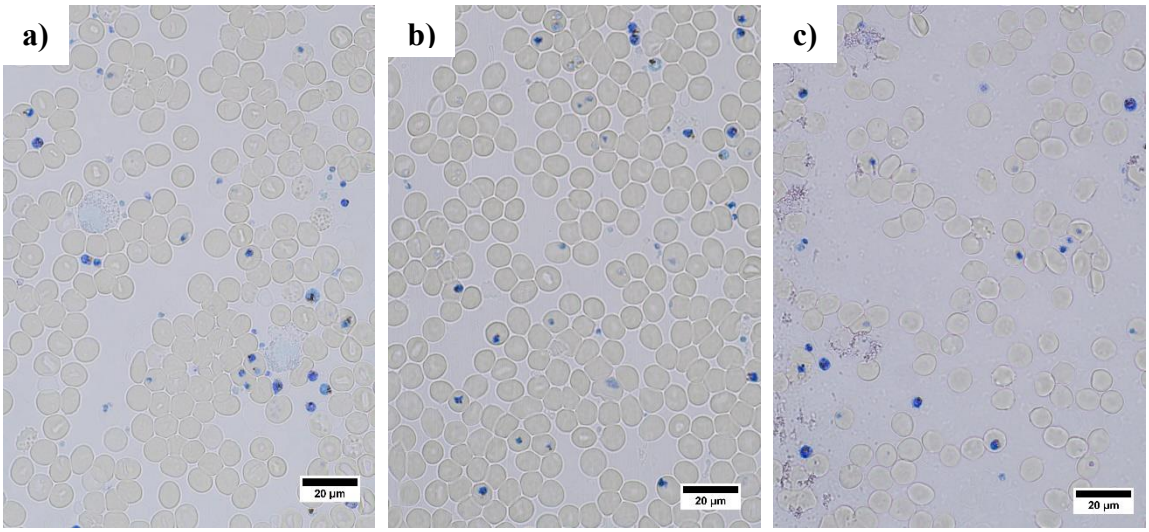

Figure 16. Images in-channel Giemsa stained blood smears using a) 10% stain dilution; b) 33% stain dilution; c) 50% stain dilution

Comparison of Stain within and across Channels. Multiple independent trials of the 33% Giemsa staining protocol were performed to check the variation of staining both

within and between smears from three different channels (ch) (**Figure 17**). The results show that the HSV background for the ch1, ch2, and ch3 of the 33% are, respectively (244, 6%, 80%), (244, 5%, 78%), and (239, 7%, 79%). The HSV of the RBCs for ch1, ch2, and ch3, are (194, 3%, 71%), (210, 3%, 70%), and (149, 3%,70%) respectively, and the malaria parasites HSV values of (216, 48%, 67%) in ch1, (213, 45%, 64%) in ch2, and (219, 45%, 68%) in ch3 (**Figure 18**). Colors and color differentiability were found to be consistent across all three channels, with only a slight variance found in the distance between malaria parasites and the background in HSV color space ($p < 0.002$) between ch1 and ch3 (**Table 6**). The variances of the distances within the HSV color space from the malaria parasites to the RBCs for the 10 images have no significant difference across the channels, which shows the consistency of the 33% staining protocol. The coefficients of variances for hue and saturation calculated for the malaria parasites also show a low variance both within each channel and across channels (**Figure 19**).

Table 6: HSV color space distances for the 33% protocol compared across 3 channels

Channel	Average Distance (HSV)	
	Malaria Parasites vs. Background	Malaria Parasites vs. RBCs
1	0.448 ± 0.0181	0.453 ± 0.0215
2	0.430 ± 0.0279	0.422 ± 0.0327
3	0.406 ± 0.0269	0.444 ± 0.0296

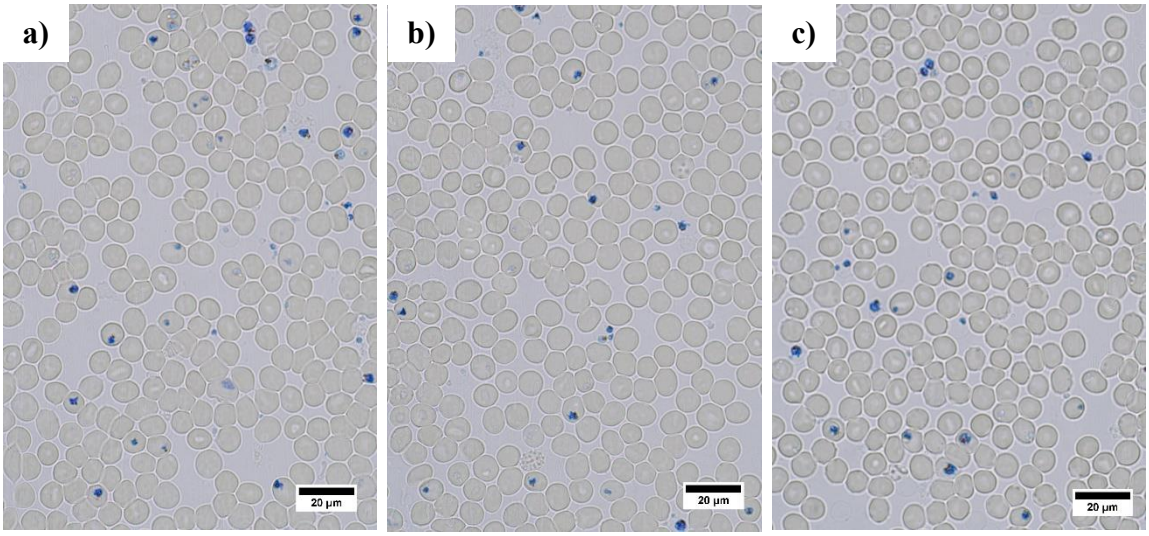

Figure 17. Images of malaria parasites acquired from 33% staining protocol in a) channel 1; b) channel 2; and c) channel 3

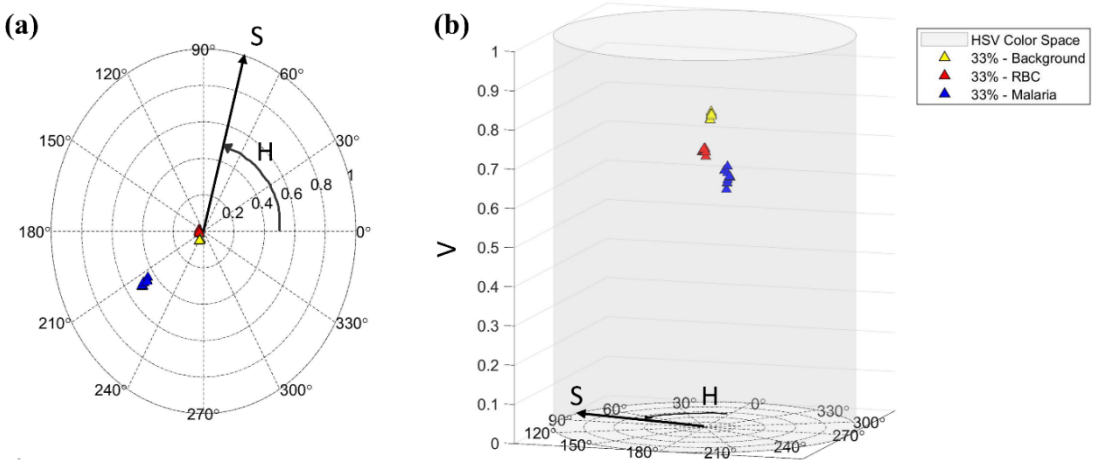

Figure 18. Average HSV colors for the malaria parasites (blue), the background (yellow), and the RBCs (red) for 10 images within a) two-dimensional hue and saturation space and b) three-dimensional hue, saturation, and value space for the 33% staining protocol.

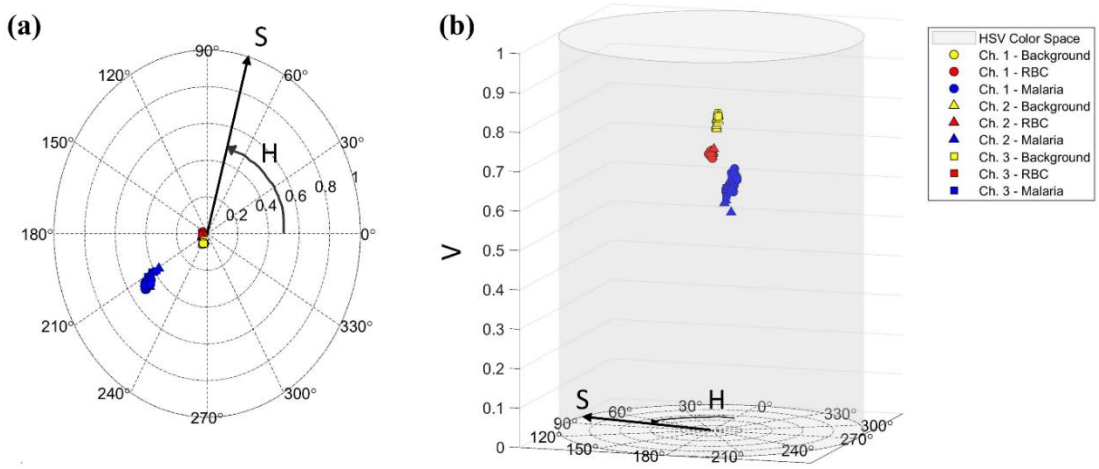

Figure 19. Average HSV colors for the malaria parasites (blue), the background (yellow), and the RBCs (red) for 10 images within (a) two-dimensional hue and saturation space and (b) three-dimensional hue, saturation, and value space per ch1 (circles), ch2 (triangles), and ch3 (squares)

Comparison with Gold-Standard Smear. The 33% concentration was compared to the glass smear, which is considered a gold standard. Background HSV values were found to be (242, 8%, 78%) and (243, 6%, 80%) for the gold-standard and in-channel smears, respectively. The HSV of the RBCs is (303, 8%, 62%) for the gold standard and (194, 3%, 71%) for the 33%, where the color of the glass smear RBCs is purple and the 33% is grey (**Figure 20**). Within the HSV color space, the average distance between the malaria parasites and the background is smaller for the gold-standard smear than for the 33% concentration in-channel smear. Similarly, the distance from the parasites to the RBC of the gold-standard is less than that of the 33% in-channel protocol (**Table 7**). Given these results, it is reasonable to conclude that the parasites in the channel are equally or more distinguishable than the one from the glass smear based on HSV color space

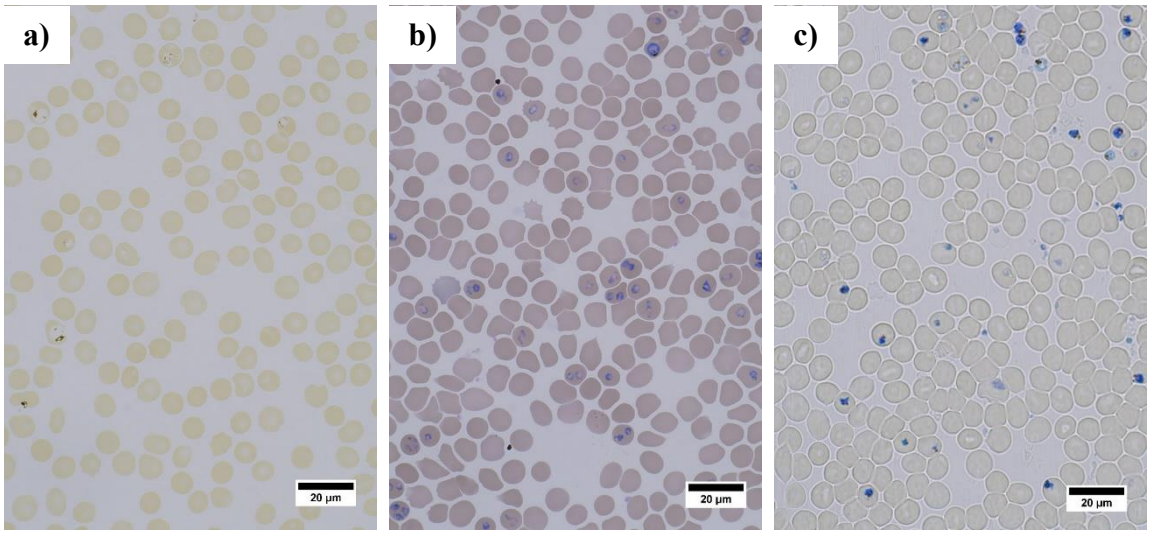

Figure 20. Images of blood smears and malaria parasites acquired from a) unstained gold standard smear; b) gold standard smear and staining; and c) 33% staining in-channel

Table 7: HSV color space distances of the gold standard compared to the 33% protocol

Stain	Average Distance (HSV)	
	Malaria Parasites vs. Background	Malaria Parasites vs. RBCs
33%	0.448 ± 0.0181	0.453 ± 0.0215
Gold Standard	0.337 ± 0.0129	0.381 ± 0.0126

differentiability (**Figure 21**). Both protocols display similar color variances, indicating similar levels of consistency and precision.

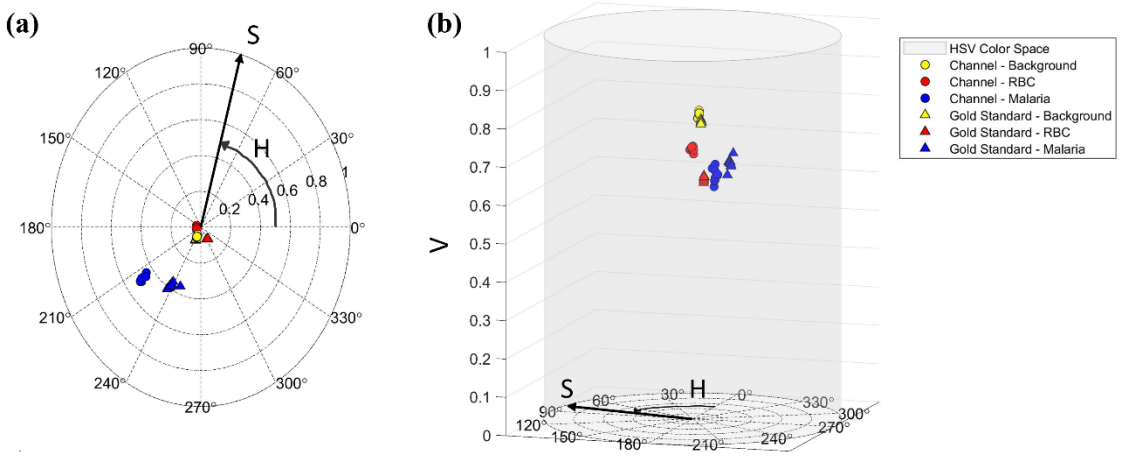

Figure 21. Average HSV colors for the malaria parasites (blue), the background (yellow), and the RBCs (red) for 10 images within a) two-dimensional hue and saturation space and b) three-dimensional hue, saturation, and value space per the 33% (circles) and gold standard (triangles) staining protocols.

Fluorescence Staining. Fluorescently stained samples were imaged in a similar manner to the brightfield images, with images collected at 0.5 mm intervals across the channel, beginning 10 minutes after cells were stained. Acridine Orange stain solution at 12µg/mL was used to stain both in-channel and gold-standard smears. In each, the uptake of AO by parasites allowed them to be clearly seen above RBC and background signals. Although various parasitic features do not differentially stain as in brightfield/Giemsa protocols, it is still easy to distinguish between ring, immature, and mature trophozoite parasitic stages of development (**Figure 22**). Using a 16-bit monochromatic camera, parasitic features in-channel displayed intensities near 4000, while gold-standard smears

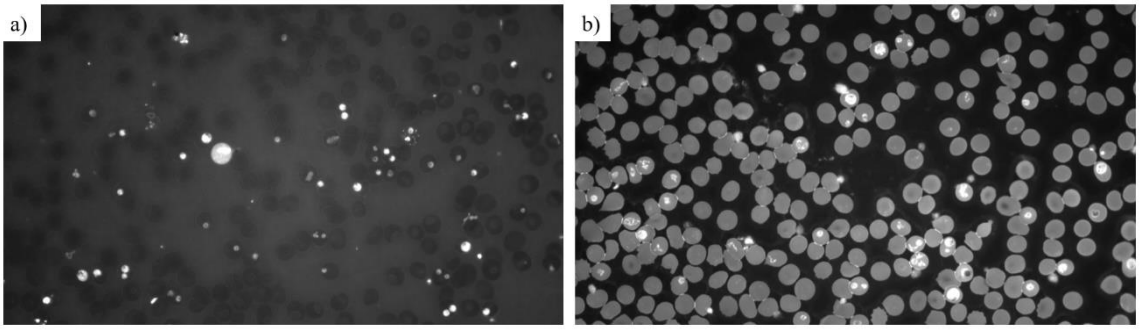

Figure 22. Monochromatic images of samples stained using 12µg/mL Acridine Orange a) in-channel; and b) on a glass slide (gold-standard). Parasites appear brightly in both images, but the contrast of red blood cells and the background are inverted. Images shown with linear contrast enhancement for visibility

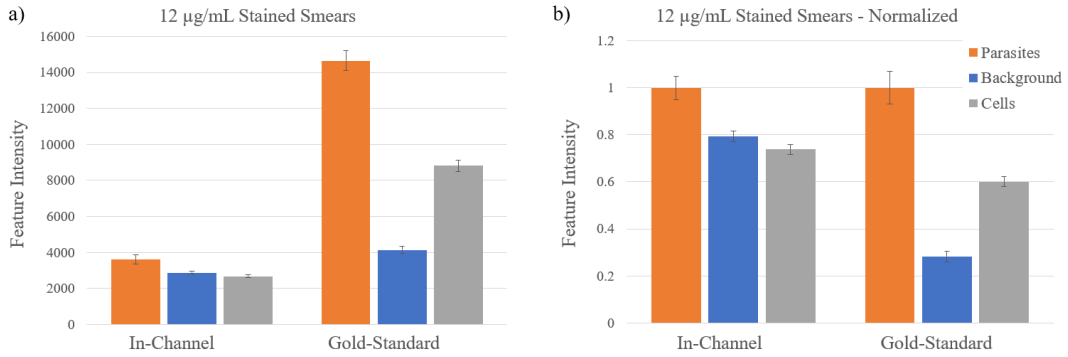

Figure 23. Comparison of fluorescent feature intensities from in-channel and Gold-Standard samples stained with 12 µg/mL of Acridine Orange. a) Absolute feature intensity; b) Relative feature intensity.

displayed intensities near 14000, with comparable coefficients of variation. Smears generated in-channel the RBC's appears darker than the channel background, while in the gold-standard images they appear brighter than the background, likely due to the ability of excess fluorophores to be washed away from glass-mounted gold-standard smears but

not from in-channel smears. Despite these differences, in each image there was a clear separability between the intensities of the parasitic features and those of the RBC's and background (**Figure 23**).

Three independent repetitions of the staining and smear creation process were performed for the 12 µg/mL stain concentration to assess the repeatability of the process. Feature intensity variance was compared within each field-of-view (FOV) and between independently stained channels. As shown in **Figure 24a**, relative feature intensities of parasites, background, and RBC's remain consistent throughout the channel. To better assess staining quality as defined by feature separability, intensities in each FOV were normalized to the intensity of the background to eliminate linear baseline drift that occurred as a gradient along the channel (**Appendix D)**. Due to the differential uptake of stain by parasites of various stages of development and the heterogeneity of fluorescence staining within each individual parasite, a large standard deviation can be observed in the average intensities of populations of parasites from each FOV, however the precision afforded by sampling multiple FOV allows for the clear

separation between the intensities of parasites, RBC's and background in all three (**Figure 24b**).

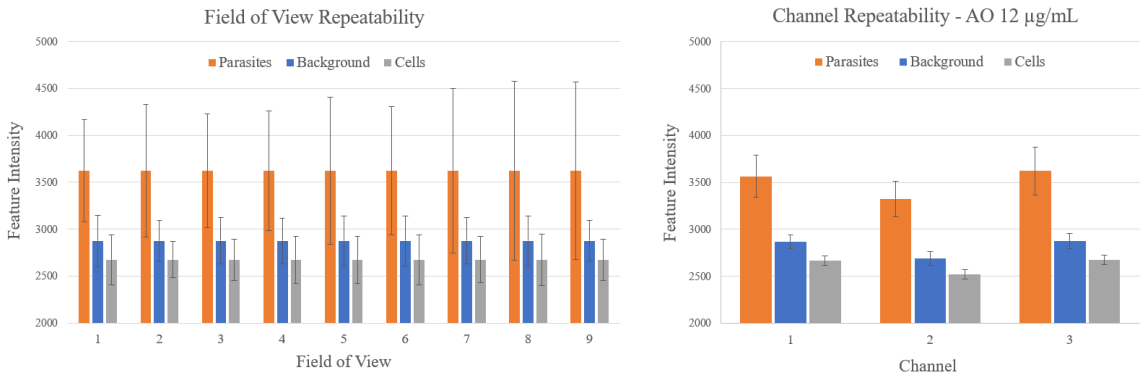

Figure 24. Variance of fluorescence staining shown a) within a single channel, and b) between separate, independent channels

4.5 Conclusion

In this work, whole blood staining procedures for a novel, microchannel-based thin smear generation platform were explored for their applications and impact. In-tube, wet staining techniques were employed instead of the traditional techniques on dried smears to allow samples to flow inside of microfluidic channels instead of the traditional dry blood staining. Staining quality was assessed quantitatively using chromatic and intensity-based feature differentiation for brightfield and fluorescence imaging modalities, respectively. Results confirm that successful differentiation of P. falciparum malarial parasites from red-blood cell and blood plasma is possible during microscopic imaging. Clear relationships between stain concentrations and signal intensities were observed, and quantitative analysis of imaging results give clear evidence that the results are repeatable. It is believed that this combination of staining procedures and smear generation platform

has the potential to improve the consistency and accessibility of high-quality blood films in both laboratory and remote settings.

CHAPTER V

CONCLUSIONS

5.1 Conclusion

Malaria remains a significant global health burden. Despite all the technologies developed to improve malaria diagnosis, the examination of stained smeared blood samples with white light microscopy remains the gold standard. However, this technique requires multiple steps that need to go well for a proper and fast diagnosis. The three steps necessary for the examination of a stained blood smear with light microscopy are 1) smear preparation; 2) fixation and staining or simply staining; and 3) the examination of the stained smear under the microscope which also has three sub-steps (detection, species identification, and parasitemia). Among these three steps, the first two are arguably the most important ones because they both affect the third step. However, most of the efforts to improve the malaria diagnosis were on the third step these past decades. Thus, this work focused on improvements to the first two steps.

In this work, research on the material used for microfluidic diagnosis was performed including modifying PDMS with SMA resulting in an increase in surface hydrophilicity and flow as the concentrations of the SMA increase. Flow control was also achieved with changes in microfluidic channel height. The flow speed increased as the SMA concentration and the channel height increased and the addition of SMA to PDMS did not compromise the optical properties (bright field and fluorescence) of the material. However, the incorporation of the higher concentrations of SMA led to a decrease in modulus. Further, to be able to design a chip that can acquire a thin smear, this flow control

was optimized, including uniform cell distribution, by not only modifying PDMS with the SMA and using a small channel height but also by adding pillars throughout the channel and varying whole blood volume. The results showed that the smear quality decreased as the blood volume increased due to the microfluidic aspect ratio. The results had shown that the combination of SMA of 5 and 7 wt% with 0.3 µl volume, 4.7 µm height with pillars at the inlet outlet and equally spaced in the channel gave the best outcome in terms of a smear with uniform cell distribution and density. The repeatability of the cartridge was tested from chip to chip with the same patient's blood, and the resulting blood smears had cell monolayers, and the cell counts from channel to channel and chip to chip were in the range of 5%. In addition, the blood smears generated from blood samples of different patients, gave a variation in cell counts, as is common due to inherent differences in patient blood (e.g., hematocrit, viscosity, etc.)

A whole blood staining procedure was also developed in the optimized microchannel using flow control. Because it is hard for air to dry samples in a microchannel, a wet blood staining was chosen instead of the traditional dry blood staining. Wet blood staining lead to the dilution of the stain by the whole blood and thus, a 3X stain concentration stock was developed and diluted with DI water to 10%, 33%, 50% concentration as a working solution. The test for the three concentrations was done with malaria parasites and analyzed using HSV color space distances as a form of contrast. The HSV color space distances from the parasites to the RBCs or the background of the 50% protocol was higher than the 33%, and both are higher than the 10% protocol, but the cells at 50% had crenation problems. Thus, the 33% stain concentration protocol was

considered the best for staining wet blood in a microchannel because it had minimal cell crenation and high color differentiability between the malaria parasites and the RBCs. The test for the consistency of the 33% protocol was done in three channels and showed low variance within a channel and across channels in the hue and saturation of the malaria parasites. The 33% protocol was compared to the gold standard stained smear on glass. The results showed that the distances within the HSV color space from the malaria parasites to the RBCs of the 33% are higher than the stained smear on glass. Thus, the parasites of the 33% protocol were more distinguishable than the glass smear.

Overall, the results showed the potential for using a pumpless microfluidic cartridge for automated smear preparation and staining that meets some the WHO ASSURED criteria (Affordable, Sensitive, Specific, User-friendly, Robust and rapid, and Deliverable to remote areas) for malaria diagnosis at the POC

REFERENCES

1. (WHO) WHO. World malaria report 2019 2019, December 4 [Available from: https://www.who.int/publications-detail/world-malaria-report-2019.

2. (WHO) WHO. Malaria 2020, January 14 [Available from: https://www.who.int/news-room/fact-sheets/detail/malaria.

3. Kasetsirikul S, Buranapong J, Srituravanich W, Kaewthamasorn M, Pimpin A. The development of malaria diagnostic techniques: a review of the approaches with focus on dielectrophoretic and magnetophoretic methods. Malaria journal. 2016;15(1):358-.

4. Berzosa P, de Lucio A, Romay-Barja M, Herrador Z, González V, García L, et al. Comparison of three diagnostic methods (microscopy, RDT, and PCR) for the detection of malaria parasites in representative samples from Equatorial Guinea. Malaria Journal. 2018;17(1):333.

5. Tangpukdee N, Duangdee C, Wilairatana P, Krudsood S. Malaria diagnosis: a brief review. The Korean journal of parasitology. 2009;47(2):93-102.

6. Yamamoto T, Hashimoto M, Nagatomi K, Nogami T, Sofue Y, Hayashi T, et al. Field evaluation of a quantitative, and rapid malaria diagnostic system using a fluorescent Blue-ray optical device. bioRxiv. 2019:721076.

7. Moyeh MN, Ali IM, Njimoh D, #xe9, L., Nji AM, et al. Comparison of the Accuracy of Four Malaria Diagnostic Methods in a High Transmission Setting in Coastal Cameroon. Journal of Parasitology Research. 2019;2019:8.

8. Bauserman M, Conroy AL, North K, Patterson J, Bose C, Meshnick S. An overview of malaria in pregnancy. Seminars in Perinatology. 2019;43(5):282-90.

9. Adewoyin AS, Nwogoh B. Peripheral blood film - a review. Annals of Ibadan postgraduate medicine. 2014;12(2):71-9.

10. Nourbakhsh M, Atwood JG, Raccio J, Seligson D. An evaluation of blood smears made by a new method using a spinner and diluted blood. American journal of clinical pathology. 1978;70(6):885-92.

11. Halim S, Bretschneider TR, Li Y, Preiser PR, Kuss C, editors. Estimating Malaria Parasitaemia from Blood Smear Images2006: IEEE.

12. Ross NE, Pritchard CJ, Rubin DM, Dusé AG. Automated image processing method for the diagnosis and classification of malaria on thin blood smears. Medical & biological engineering & computing. 2006;44(5):427-36.

13. Clodfelter RL, Jr. The peripheral smear. Emergency medicine clinics of North America. 1986;4(1):59-74.

14. Obeagu EI, Uo C, Is E. Malaria Rapid Diagnostic Test (RDTs). Annals of Clinical and Laboratory Research. 2018;06(04).

15. Sio SWS, Sun W, Kumar S, Bin WZ, Tan SS, Ong SH, et al. MalariaCount: an image analysis-based program for the accurate determination of parasitemia. Journal of microbiological methods. 2007;68(1):11-8.

16. (WHO) WHO. Guidelines for the treatment of malaria. Third edition April 2015 2015 [Available from: https://www.who.int/malaria/publications/atoz/9789241549127/en/.

17. Bates I, Bekoe V, Asamoa-Adu A. Improving the accuracy of malaria-related laboratory tests in Ghana. Malaria Journal. 2004;3(1):38.

18. Govind D, Lutnick BR, Tomaszewski JE, Sarder P. Automated erythrocyte detection and classification from whole slide images. J Med Imaging (Bellingham). 2018;5(2):027501.

19. Riedl J. Digital imaging/morphology is the next chapter in hematology. MLO: Medical Laboratory Observer. 2018;50(3):28-32.

20. Green JE, Weintraub HA, Donnelly BS, Mordecai BG. Sample preparation variation and its effects on automated blood cell differential analysis. Anal Quant Cytol. 1979;1(3):187-201.

21. Simson E, Gascon-Lema MG, Brown DL. Performance of automated slidemakers and stainers in a working laboratory environment - routine operation and quality control. International journal of laboratory hematology. 2010;32(1 Pt 1):e64-76.

22. Benattar L, Flandrin G. Comparison of the classical manual pushed wedge films, with an improved automated method for making blood smears. Hematology and Cell Therapy. 1999;41(5):211-5.

23. Kull JA, Krawczel PD, Pighetti GM. Short communication: Evaluation of an automated method for assessing white blood cell concentrations in Holstein dairy cows. Veterinary Immunology and Immunopathology. 2018;197:21-3.

24. Fuentes-Arderiu X, García-Panyella M, Dot-Bach D. Between-examiner reproducibility in manual differential leukocyte counting. Accreditation and Quality Assurance. 2007;12(12):643-5.

25. Hattersley SM, Greenman J, Haswell SJ. The Application of Microfluidic Devices for Viral Diagnosis in Developing Countries. In: Jenkins G, Mansfield CD, editors. Microfluidic Diagnostics: Methods and Protocols. Totowa, NJ: Humana Press; 2013. p. 285-303.

26. Peeling RW, Holmes KK, Mabey D, Ronald A. Rapid tests for sexually transmitted infections (STIs): the way forward. Sex Transm Infect. 2006;82 Suppl 5(Suppl 5):v1-v6.

27. Oaks SC, Mitchell VS, Pearson GW. Malaria: Obstacles and Opportunities1991. 0-309 p.

28. Mathison BA, Pritt BS. Update on Malaria Diagnostics and Test Utilization. Journal of Clinical Microbiology. 2017;55(7):2009-17.

29. Talapko J, Skrlec I, Alebic T, Jukic M, Vcev A. Malaria: The Past and the Present. Microorganisms. 2019;7(6):179.

30. Prevention CDCCfDCa. CDC - Malaria - About Malaria - Biology - Malaria Parasites 2020 [updated July 16, 2020. Available from: https://www.cdc.gov/malaria/about/biology/parasites.html.

31. Prevention CDCCfDCa. CDC - Malaria - About Malaria - Biology 2020 [updated July 16, 2020. Available from: https://www.cdc.gov/malaria/about/biology/.

32. Yarnell E. Artemisia annua (Sweet Annie), Other Artemisia Species, Artemisinin, Artemisinin Derivatives, and Malaria. Journal of Restorative Medicine. 2014;3:69-84.

33. White NJ. The parasite clearance curve. Malaria Journal. 2011;10(1):278.

34. Trampuz A, Jereb M, Muzlovic I, Prabhu RM. Clinical review: Severe malaria. Critical care (London, England). 2003;7(4):315-23.

35. Kovacs SD, Rijken MJ, Stergachis A. Treating Severe Malaria in Pregnancy: A Review of the Evidence. Drug Safety. 2015;38(2):165-81.

36. Newton CRJC. Neurological aspects of tropical disease: Cerebral malaria. Journal of Neurology, Neurosurgery & Psychiatry. 2000;69(4):433-41.

37. Chen K, Yuen C, Aniweh Y, Preiser P, Liu Q. Towards ultrasensitive malaria diagnosis using surface enhanced Raman spectroscopy. Scientific Reports. 2016;6(February):20177-.

38. Dharmadhikari AK, Basu H, Dharmadhikari Ja, Sharma S, Mathur D. On the birefringence of healthy and malaria-infected red blood cells. Journal of biomedical optics. 2013;18:125001-.

39. Delahunt C, Horning MP, Wilson BK, Proctor JL, Hegg MC. Limitations of haemozoin-based diagnosis of Plasmodium falciparum using dark-field microscopy. Malaria journal. 2014;13(1):147-.

40. Kantele A, Jokiranta TS. Review of Cases With the Emerging Fifth Human Malaria Parasite, Plasmodium knowlesi. Clinical Infectious Diseases. 2011;52(11):1356-62.

41. Moody A. Rapid diagnostic tests for malaria parasites. Clinical microbiology reviews. 2002;15(1):66-78.

42. Hyde JE. Drug-resistant malaria - an insight. FEBS J. 2007;274(18):4688-98.

43. MenkinSmith L, Winders WT. Malaria (Plasmodium Vivax). StatPearls [Internet]: StatPearls Publishing; 2019.

44. Langhi DM, Orlando Bordin J. Duffy blood group and malaria. Hematology. 2006;11(5-6):389-98.

45. Cowman AF, Healer J, Marapana D, Marsh K. Malaria: Biology and Disease. Cell. 2016;167(3):610-24.

46. Collins WE, Jeffery GM. Plasmodium ovale: Parasite and Disease. Clinical Microbiology Reviews. 2005;18(3):570-81.

47. Okafor CN, Finnigan NA. Malaria (Plasmodium Ovale). StatPearls [Internet]: StatPearls Publishing; 2019.

48. Collins WE, Jeffery GM. Plasmodium malariae: Parasite and Disease. Clinical Microbiology Reviews. 2007;20(4):579-92.

49. Singh B, Daneshvar C. Human Infections and Detection of Plasmodium knowlesi. Clinical Microbiology Reviews. 2013;26(2):165-84.

50. Barber BE, Rajahram GS, Grigg MJ, William T, Anstey NM. World Malaria Report: time to acknowledge Plasmodium knowlesi malaria. Malaria Journal. 2017;16(1):135.

51. Krampa FD, Aniweh Y, Awandare GA, Kanyong P. Recent Progress in the Development of Diagnostic Tests for Malaria. Diagnostics (Basel). 2017;7(3):54.

52. Malpartida-Cardenas K, Miscourides N, Rodriguez-Manzano J, Yu L-S, Moser N, Baum J, et al. Quantitative and rapid Plasmodium falciparum malaria diagnosis and

artemisinin-resistance detection using a CMOS Lab-on-Chip platform. Biosensors and Bioelectronics. 2019;145:111678.

53. Tek FB, Dempster AG, Kale I. Parasite detection and identification for automated thin blood film malaria diagnosis. Computer Vision and Image Understanding. 2010;114:21-32.

54. Amexo M, Tolhurst R, Barnish G, Bates I. Malaria misdiagnosis: effects on the poor and vulnerable. The Lancet. 2004;364(9448):1896-8.

55. Chandramohan D, Jaffar S, Greenwood B. Use of clinical algorithms for diagnosing malaria1. Tropical Medicine & International Health. 2002;7(1):45-52.

56. McCombie SC. Self-treatment for malaria: the evidence and methodological issues. Health Policy Plan. 2002;17(4):333-44.

57. Pagnoni F, Convelbo N, Tiendrebeogo J, Cousens S, Esposito F. A community-based programme to provide prompt and adequate treatment of presumptive malaria in children. Transactions of The Royal Society of Tropical Medicine and Hygiene. 1997;91(5):512-7.

58. (CDC) CfDCaP. Disease 2019, January 4 [Available from: https://www.cdc.gov/malaria/about/disease.html.

59. Guy R, Liu P, Pennefather P, Crandall I. The use of fluorescence enhancement to improve the microscopic diagnosis of falciparum malaria. Malaria journal. 2007;6:89-.

60. CDC. Blood Specimens - Specimen Processing 2019, June 21 [Available from: https://www.cdc.gov/dpdx/diagnosticprocedures/blood/specimenproc.html.

61. World Health O, Research UNUWBWSPf, Training in Tropical D. Microscopy for the detection, identification and quantification of malaria parasites on stained thick and thin blood films in research settings (version 1.0): procedure: methods manual. Geneva: World Health Organization; 2015 2015.

62. World Health Organization. Regional Office for the Western P. Malaria microscopy standard operating procedures. Manila : WHO Regional Office for the Western Pacific; 2016.

63. Rosenthal DS. Evaluation of the peripheral blood smear. UpToDate. 2010.

64. Houwen B. Blood film preparation and staining procedures. Clinics in Laboratory Medicine. 2002;22(1):1-14.

65. Benattar L, Flandrin G. Morphometry and Quality Control For a May-Grunwald Giemsa Stained Preparation. A 40 Centers Cooperative Study. Leukemia & Lymphoma. 1999;33(5-6):587-91.

66. Horobin RW. How Romanowsky stains work and why they remain valuable - including a proposed universal Romanowsky staining mechanism and a rational troubleshooting scheme. Biotechnic & histochemistry : official publication of the Biological Stain Commission. 2011;86(1):36-51.

67. Sathpathi S, Mohanty AK, Satpathi P, Mishra SK, Behera PK, Patel G, et al. Comparing Leishman and Giemsa staining for the assessment of peripheral blood smear preparations in a malaria-endemic region in India. Malaria journal. 2014;13:512-.

68. Berod A, Hartman BK, Pujol JF. Importance of fixation in immunohistochemistry: use of formaldehyde solutions at variable pH for the localization

of tyrosine hydroxylase. Journal of Histochemistry & Cytochemistry. 1981;29(7):844-50.

69. Comar SR, Malvezzi M, Pasquini R. Evaluation of criteria of manual blood smear review following automated complete blood counts in a large university hospital. Revista Brasileira de Hematologia e Hemoterapia. 2017;39(4):306-17.

70. Horning MP, Delahunt CB, Singh SR, Garing SH, Nichols KP. A paper microfluidic cartridge for automated staining of malaria parasites with an optically transparent microscopy window. Lab on a Chip. 2014;14(12):2040-.

71. Wongsrichanalai C, Barcus MJ, Muth S, Sutamihardja A, Wernsdorfer WH. A Review of Malaria Diagnostic Tools: Microscopy and Rapid Diagnostic Test (RDT). Am J Trop Med Hyg. 2007;77(6_Suppl):119-27.

72. Manguin S, Foumane V, Besnard P, Fortes F, Carnevale P. Malaria overdiagnosis and subsequent overconsumption of antimalarial drugs in Angola: Consequences and effects on human health. Acta Tropica. 2017;171:58-63.

73. Antony HA, Parija SC. Antimalarial drug resistance: An overview. Tropical parasitology. 2016;6(1):30-41.

74. Lubell Y, Reyburn H, Mbakilwa H, Mwangi R, Chonya S, Whitty CJM, et al. The impact of response to the results of diagnostic tests for malaria: cost-benefit analysis. BMJ. 2008;336(7637):202-5.

75. (WHO) WHO. Malaria Microscopy Quality Assurance Manual Version 2.

76. Kang JM, Cho PY, Moe M, Lee J, Jun H, Lee HW, et al. Comparison of the diagnostic performance of microscopic examination with nested polymerase chain reaction for optimum malaria diagnosis in Upper Myanmar. Malar J. 2017;16(1):119.

77. (CDC) CfDCaP. Blood Specimens - Microscopic Examination 2016, May 3 [Available from: https://www.cdc.gov/dpdx/diagnosticprocedures/blood/microexam.html.

78. Kakkilaya BS. Rapid Diagnosis of Malaria. Laboratory Medicine. 2003;34(8):602-8.

79. Tek FB, Dempster AG, Kale I. Computer vision for microscopy diagnosis of malaria. Malaria journal. 2009;8:153-.

80. Ohrt C, O'Meara WP, Remich S, McEvoy P, Ogutu B, Mtalib R, et al. Pilot assessment of the sensitivity of the malaria thin film. Malaria journal. 2008;7:22-.

81. Guy R, Liu P, Pennefather P, Crandall I. The use of fluorescence enhancement to improve the microscopic diagnosis of falciparum malaria. Malaria Journal. 2007;6(1):89-.

82. Hassan SE-DH, Haggaz AED, Mohammed-Elhassan EB, Malik EM, Adam I. Fluorescence microscope (Cyscope) for malaria diagnosis in pregnant women in Medani Hospital, Sudan. Diagnostic pathology. 2011;6(1):88-.

83. Jha N, Prasad R, Jana D. Comparison between Quantitative Buffy Coat (QBC) and Optimal Test for malaria diagnosis at DMC, Laheriasarai, Bihar. International Journal of Scientific Research. 2020;9(1).

84. Cunningham J, Jones S, Gatton ML, Barnwell JW, Cheng Q, Chiodini PL, et al. A review of the WHO malaria rapid diagnostic test product testing programme (2008–2018): performance, procurement and policy. Malaria Journal. 2019;18(1):387.

85. Siwal N, Singh US, Dash M, Kar S, Rani S, Rawal C, et al. Malaria diagnosis by PCR revealed differential distribution of mono and mixed species infections by Plasmodium falciparum and P. vivax in India. PloS one. 2018;13(3):e0193046-e.

86. Han TZ, Han KT, Aye KH, Hlaing T, Thant KZ, Vythilingam I. Comparison of microscopy and PCR for the detection of human Plasmodium species and Plasmodium knowlesi in southern Myanmar. Asian Pacific Journal of Tropical Biomedicine. 2017;7(8):680-5.

87. Haanshuus CG, Mørch K, Blomberg B, Strøm GEA, Langeland N, Hanevik K, et al. Assessment of malaria real-time PCR methods and application with focus on low-level parasitaemia. PloS one. 2019;14(7):e0218982-e.

88. (CDC) CfDCaP. Treatment of Malaria: Guidelines For Clinicians (United States) 2019 [Available from: https://www.cdc.gov/malaria/diagnosis_treatment/clinicians1.html.

89. Fallahi H, Zhang J, Phan HP, Nguyen NT. Flexible Microfluidics: Fundamentals, Recent Developments, and Applications. Micromachines (Basel). 2019;10(12).

90. Mark D, Haeberle S, Roth G, von Stetten F, Zengerle R. Microfluidic lab-on-a-chip platforms: requirements, characteristics and applications. Chemical Society reviews. 2010;39(3):1153-82.

91. Smith S, Madzivhandila P, Sewart R, Govender U, Becker H, Roux P, et al. Microfluidic Cartridges for Automated, Point-of-Care Blood Cell Counting. SLAS Technol. 2017;22(2):176-85.

92. Smith S, Sewart R, Land K, Roux P, Gärtner C, Becker H. Blister pouches for effective reagent storage and release for low cost point-of-care diagnostic applications. Proc of SPIE. 2016;9705:97050F-F.

93. Ren K, Zhou J, Wu H. Materials for Microfluidic Chip Fabrication. Accounts of Chemical Research. 2013;46(11):2396-406.

94. Disch A, Mueller C, Reinecke H. Low cost production of disposable microfluidics by blister packaging technology. Conference proceedings : Annual International Conference of the IEEE Engineering in Medicine and Biology Society IEEE Engineering in Medicine and Biology Society Annual Conference. 2007;2007:6323-6.

95. Tsao C-W, Chia W. Polymer Microfluidics: Simple, Low-Cost Fabrication Process Bridging Academic Lab Research to Commercialized Production. Micromachines. 2016;7(12):225-.

96. Pennathur S. Flow control in microfluidics: are the workhorse flows adequate? Lab on a chip. 2008;8(3):383-7.

97. He T, Liang Q, Zhang K, Mu X, Luo T, Wang Y, et al. A modified microfluidic chip for fabrication of paclitaxel-loaded poly(l-lactic acid) microspheres. Microfluidics and Nanofluidics. 2011;10(6):1289-98.

98. Xing Y, Nourmohammadzadeh M, Elias JEM, Chan M, Chen Z, McGarrigle JJ, et al. A pumpless microfluidic device driven by surface tension for pancreatic islet analysis. Biomedical Microdevices. 2016;18(5):80-.

99. Marimuthu M, Kim S. Pumpless steady-flow microfluidic chip for cell culture. Analytical Biochemistry. 2013;437(2):161-3.

100. Yao M, Fang J. Hydrophilic PEO-PDMS for microfluidic applications. Journal of Micromechanics and Microengineering. 2012;22(2):025012.

101. Zhou J, Khodakov Da, Ellis AV, Voelcker NH. Surface modification for PDMS-based microfluidic devices. Electrophoresis. 2012;33(1):89-104.

102. Zhou J, Ellis AV, Voelcker NH. Recent developments in PDMS surface modification for microfluidic devices. Electrophoresis. 2010;31(1):2-16.

103. Maria MS, Rakesh PE, Chandra TS, Sen AK. Capillary flow-driven microfluidic device with wettability gradient and sedimentation effects for blood plasma separation. Scientific Reports. 2017;7(January):43457-.

104. Duffy DC, McDonald JC, Schueller OJA, Whitesides GM. Rapid Prototyping of Microfluidic Systems in Poly(dimethylsiloxane). Analytical Chemistry. 1998;70(23):4974-84.

105. Sackmann EK, Fulton AL, Beebe DJ. The present and future role of microfluidics in biomedical research. Nature. 2014;507(7491):181-9.

106. He J, Mao M, Li D, Liu Y, Jin Z. Characterization of Leaf-Inspired Microfluidic Chips for Pumpless Fluid Transport. Journal of Bionic Engineering. 2014;11(1):109-14.

107. Bakshi S, Pandey K, Bose S, Gunjan, Paul D, Nayak R. Permanent superhydrophilic surface modification in microporous polydimethylsiloxane sponge for multi-functional applications. Journal of Colloid and Interface Science. 2019;552:34-42.

108. Ye Z, Li S, Wang C, Shen R, Wen W. Capillary flow control in nanochannels via hybrid surface. RSC Advances. 2016;6(4):2774-7.

109. Suk JW, Cho J-H. Capillary flow control using hydrophobic patterns. Journal of Micromechanics and Microengineering. 2007;17(4):N11-N5.

110. Zhao B, Cui X, Ren W, Xu F, Liu M, Ye Z-G. A Controllable and Integrated Pump-enabled Microfluidic Chip and Its Application in Droplets Generating. Scientific Reports. 2017;7(1):11319.

111. Tan SH, Nguyen N-T, Chua YC, Kang TG. Oxygen plasma treatment for reducing hydrophobicity of a sealed polydimethylsiloxane microchannel. Biomicrofluidics. 2010;4(3):32204-.

112. Saha AA, Mitra SK, Tweedie M, Roy S, McLaughlin J. Experimental and numerical investigation of capillary flow in SU8 and PDMS microchannels with integrated pillars. Microfluidics and Nanofluidics. 2009;7(4):451-65.

113. Hale RS, Bonnecaze RT, Hidrovo CH. Optimization of capillary flow through square micropillar arrays. International Journal of Multiphase Flow. 2014;58:39-51.

114. Thorslund S, Larsson R, Bergquist J, Nikolajeff F, Sanchez J. A PDMS-based disposable microfluidic sensor for CD4+ lymphocyte counting. Biomedical Microdevices. 2008;10(6):851-7.

115. Du X, Zhang P, Liu Y, Wu Y. A passive through hole microvalve for capillary flow control in microfluidic systems. Sensors & Actuators: A Physical. 2010;165:288-93.

116. Young W-BB. Analysis of capillary flows in non-uniform cross-sectional capillaries. Colloids and Surfaces A: Physicochemical and Engineering Aspects. 2004;234(1-3):123-8.

117. Ichikawa N, Hosokawa K, Maeda R. Interface motion of capillary-driven flow in rectangular microchannel. Journal of colloid and interface science. 2004;280(1):155-64.

118. Zhu Y, Petkovic-Duran K. Capillary flow in microchannels. Microfluidics and Nanofluidics. 2010;8(2):275-82.

119. Mielczarek WS, Obaje EA, Bachmann TT, Kersaudy-Kerhoas M. Microfluidic blood plasma separation for medical diagnostics: is it worth it? Lab on a Chip. 2016;16(18):3441-8.

120. Lehmann M, Wallbank AM, Dennis KA, Wufsus AR, Davis KM, Rana K, et al. On-chip recalcification of citrated whole blood using a microfluidic herringbone mixer. Biomicrofluidics. 2015;9(6):064106-.

121. Liu X, Yuan L, Li D, Tang Z, Wang Y, Chen G, et al. Blood compatible materials: state of the art. J Mater Chem B. 2014;2(35):5718-38.

122. Juncker D. Capillary microfluidic systems for bio/chemistry [Thesis]: Universite de Neuchatel; 2002.

123. Jong WR, Kuo TH, Ho SW, Chiu HH, Peng SH. Flows in rectangular microchannels driven by capillary force and gravity. International Communications in Heat and Mass Transfer. 2007;34(2):186-96.

124. Sewchand LS, Rowlands S, Lovlin RE. Resistance to the Brownian Movement of Red Blood Cells on Flat Horizontal Surfaces. CELL BIOPHYSICS. 1982;4:41-6.

125. Krasowska A, Sigler K. How microorganisms use hydrophobicity and what does this mean for human needs? Frontiers in Cellular and Infection Microbiology. 2014;4:112.

126. Fatona A, Chen Y, Reid M, Brook MA, Moran-Mirabal JM. One-step in-mould modification of PDMS surfaces and its application in the fabrication of self-driven microfluidic channels. Lab on a Chip. 2015;15(22):4322-30.

127. Kim CB, Chun H, Chung J, Song KB, Lee SH. Non-collapsible PDMS nanochannel fabrication with tunable width and height using single master mold. Proceedings of the IEEE Conference on Nanotechnology. 2011:1723-7.

128. Park S-m, Huh YS, Craighead HG, Erickson D. A method for nanofluidic device prototyping using elastomeric collapse. Proceedings of the National Academy of Sciences of the United States of America. 2009;106(37):15549-54.

129. Lake M, Narciso C, Cowdrick K, Storey T, Zhang S, Zartman J, et al. Microfluidic device design, fabrication, and testing protocols. Protoc Exch. 2015;10(10.1038).

130. Morra M, Occhiello E, Marola R, Garbassi F, Humphrey P, Johnson D. On the aging of oxygen plasma-treated polydimethylsiloxane surfaces. Journal of Colloid and Interface Science. 1990;137(1):11-24.

131. Eddington DT, Puccinelli JP, Beebe DJ. Thermal aging and reduced hydrophobic recovery of polydimethylsiloxane. Sensors and Actuators B. 2006;114:170-2.

132. Larson BJ, Gillmor SD, Braun JM, Cruz-Barba LE, Savage DE, Denes FS, et al. Long-Term Reduction in Poly(dimethylsiloxane) Surface Hydrophobicity via Cold-Plasma Treatments. Langmuir. 2013;29(42):12990-6.

133. Liu VA, Jastromb WE, Bhatia SN. Engineering protein and cell adhesivity using PEO-terminated triblock polymers. Journal of Biomedical Materials Research. 2002;60(1):126-34.

134. Wang ZK, Zheng HY, Lim RYH, Wang ZF, Lam YC. Improving surface smoothness of laser-fabricated microchannels for microfluidic application. Journal of Micromechanics and Microengineering. 2011;21(9):095008-.

135. Neff JA, Tresco PA, Caldwell KD. Surface modification for controlled studies of cell–ligand interactions. Biomaterials. 1999;20(23):2377-93.

136. Chen H, Zhang Z, Chen Y, Brook MA, Sheardown H. Protein repellant silicone surfaces by covalent immobilization of poly(ethylene oxide). Biomaterials. 2005;26(15):2391-9.

137. Lee S, Vörös J. An Aqueous-Based Surface Modification of Poly(dimethylsiloxane) with Poly(ethylene glycol) to Prevent Biofouling. Langmuir. 2005;21(25):11957-62.

138. Papra A, Bernard A, Juncker D, Larsen NB, Michel B, Delamarche E. Microfluidic Networks Made of Poly(dimethylsiloxane), Si, and Au Coated with Polyethylene Glycol for Patterning Proteins onto Surfaces. Langmuir. 2001;17(13):4090-5.

139. Chen H, Brook MA, Chen Y, Sheardown H. Surface properties of PEO-silicone composites: reducing protein adsorption. Journal of biomaterials science- Polymer edition. 2005;16(4):531-48.

140. Chen H, Brook MA, Sheardown H. Silicone elastomers for reduced protein adsorption. Biomaterials. 2004;25(12):2273-82.

141. D. B. Thompson, A. S. Fawcett, Brook MA. Silicon Based Polymers: Advances in Synthesis and Supramolecular Organization: Springer Netherlands; 2008.

142. Gokaltun A, Kang YBA, Yarmush ML, Usta OB, Asatekin A. Simple Surface Modification of Poly(dimethylsiloxane) via Surface Segregating Smart Polymers for Biomicrofluidics. Sci Rep. 2019;9(1):7377.

143. Rufin MA, Barry ME, Adair PA, Hawkins ML, Raymond JE, Grunlan MA. Protein resistance efficacy of PEO-silane amphiphiles: Dependence on PEO-segment length and concentration. Acta Biomaterialia. 2016;41:247-52.

144. Hawkins ML, Schott SS, Grigoryan B, Rufin MA, Ngo BKD, Vanderwal L, et al. Anti-protein and anti-bacterial behavior of amphiphilic silicones. Polymer Chemistry. 2017;8(34):5239-51.

145. Klasner SA, Metto EC, Roman GT, Culbertson CT. Synthesis and characterization of a poly(dimethylsiloxane)-poly(ethylene oxide) block copolymer for

fabrication of amphiphilic surfaces on microfluidic devices. Langmuir. 2009;25(17):10390-6.

146. Cai DK, Neyer A, Kuckuk R, Heise HM. Optical absorption in transparent PDMS materials applied for multimode waveguides fabrication. Optical Materials. 2008;30(7):1157-61.

147. Mata A, Fleischman AJ, Roy S. Characterization of polydimethylsiloxane (PDMS) properties for biomedical micro/nanosystems. Biomedical microdevices. 2005;7(4):281-93.

148. Rufin MA, Ngo BKD, Barry ME, Page VM, Hawkins ML, Stafslien SJ, et al. Antifouling silicones based on surface-modifying additive amphiphiles. Green Materials. 2017;5(1):1-10.

149. Thangawng AL, Swartz MA, Glucksberg MR, Ruoff RS. Bond-detach lithography: A method for micro/nanolithography by precision PDMS patterning. Small. 2007;3(1):132-8.

150. Johnston ID, McCluskey DK, Tan CKL, Tracey MC. Mechanical characterization of bulk Sylgard 184 for microfluidics and microengineering. Journal of Micromechanics and Microengineering. 2014;24(3):035017-.

151. Wang Z, Volinsky Aa, Gallant ND. Crosslinking effect on polydimethylsiloxane elastic modulus measured by custom-built compression instrument. Journal of Applied Polymer Science. 2014;131(22):n/a-n/a.

152. Bricaud A, Morel A. Light attenuation and scattering by phytoplanktonic cells: a theoretical modeling. Applied Optics. 1986;25(4):571-80.

153. Hawkins ML, Grunlan MA. The protein resistance of silicones prepared with a PEO-silane amphiphile. Journal of Materials Chemistry. 2012;22(37):19540-6.

154. Bain BJ. Diagnosis from the Blood Smear. New England Journal of Medicine. 2005;353(5):498-507.

155. Gulati G, Song J, Florea AD, Gong J. Purpose and criteria for blood smear scan, blood smear examination, and blood smear review. Annals of laboratory medicine. 2013;33(1):1-7.

156. Whitesides GM. The origins and the future of microfluidics. Nature. 2006;442(7101):368-73.

157. Manz A, Harrison DJ, Verpoorte EMJ, Fettinger JC, Paulus A, Lüdi H, et al. Planar chips technology for miniaturization and integration of separation techniques into monitoring systems. Capillary electrophoresis on a chip. Journal of Chromatography A. 1992;593(1-2):253-8.

158. Moen ST, Hatcher CL, Singh AK. A Centrifugal Microfluidic Platform That Separates Whole Blood Samples into Multiple Removable Fractions Due to Several Discrete but Continuous Density Gradient Sections. PLOS ONE. 2016;11(4):e0153137.

159. Li H, Jayamohan H, Lambert C, Mohanty S, Gale BK. Automated Whole Blood Processing With a Portable Microfluidic Device for Point-of-Care Diagnosis. 2013(October):1758-60.

160. Dogbevi KS, Ngo BKD, Blake CW, Grunlan MA, Coté GL. Pumpless, “Self-Driven” Microfluidic Channels with Controlled Blood Flow Using an Amphiphilic Silicone. ACS Applied Polymer Materials. 2020.

161. Green JE, Weintraub HA, Donnelly BS, Mordecai BG. Sample preparation variation and its effects on automated blood cell differential analysis. Analytical and quantitative cytology
1979;1(3):187-201.
162. Nourbakhsh M, Atwood JG, Raccio J, Seligson D. An Evaluation of Blood Smears Made by a New Method
Using a Spinner and Diluted Blood. American journal of clinical pathology. 1978.
163. Hale RS, Ranjan R, Hidrovo CH. Capillary flow through rectangular micropillar arrays. International Journal of Heat and Mass Transfer. 2014;75:710-7.
164. Maria MS, Chandra TS, Sen AK. Capillary flow-driven blood plasma separation and on-chip analyte detection in microfluidic devices. Microfluidics and Nanofluidics. 2017;21(4):72.
165. Chantiwas R PS, Soper SA, Kim BC, Takayama S, Sunkara V, Hwang H, Cho YK. Flexible fabrication and applications of polymer nanochannels and nanoslits. Chemical Society Reviews. 2011;40(7):3677-.
166. Melin J, Quake SR. Microfluidic large-scale integration: the evolution of design rules for biological automation. Annual review of biophysics and biomolecular structure. 2007;36:213-31.
167. Saurabh V. Manipulating fluids: Advances in micro-fluidics, opto-fluidics and fluidic self assembly [Ph.D. Thesis]: California Institute of Technology; 2006.

168. Kaminaga M, Ishida T, Kadonosono T, Kizaka-Kondoh S, Omata T. Uniform Cell Distribution Achieved by Using Cell Deformation in a Micropillar Array. Micromachines. 2015;6(4):409-22.

169. Tripathi S, Varun Kumar YVB, Prabhakar A, Joshi SS, Agrawal A. Passive blood plasma separation at the microscale: a review of design principles and microdevices. Journal of Micromechanics and Microengineering. 2015;25(8):083001-.

170. Park S, Shabani R, Schumacher M, Kim Y-S, Bae YM, Lee K-H, et al. On-chip whole blood plasma separator based on microfiltration, sedimentation and wetting contrast. Microsystem Technologies. 2016;22(8):2077-85.

171. Dowling MA, Shute GT. A comparative study of thick and thin blood films in the diagnosis of scanty malaria parasitaemia. Bulletin of the World Health Organization. 1966;34(2):249-67.

172. Roland L, Drillich M, Iwersen M. Hematology as a diagnostic tool in bovine medicine. Journal of Veterinary Diagnostic Investigation. 2014;26(5):592-8.

173. Zhu X, Yi Chu L, Chueh B-h, Shen M, Hazarika B, Phadke N, et al. Arrays of horizontally-oriented mini-reservoirs generate steady microfluidic flows for continuous perfusion cell culture and gradient generation. The Analyst. 2004;129(11):1026-.

174. BACUS JW. Erythrocyte morphology and centrifugal "spinner" blood film preparations. Journal of Histochemistry & Cytochemistry. 1974;22(7):506-16.

175. World Health O. Malaria microscopy quality assurance manual. 121- p.

176. Basic Malaria Microscopy: Part I. Learner's Guide. 2nd Edition ed: World Health Organization; 2010.

177. Maguire JD, Lederman ER, Barcus MJ, O'Meara WAP, Jordon RG, Duong S, et al. Production and validation of durable, high quality standardized malaria microscopy slides for teaching, testing and quality assurance during an era of declining diagnostic proficiency. Malaria Journal. 2006;5(1):92.

178. Eltoum I, Fredenburgh J, Myers RB, Grizzle WE. Introduction to the Theory and Practice of Fixation of Tissues. Journal of Histotechnology. 2001;24(3):173-90.

179. Rolls G. Process of Fixation and the Nature of Fixatives Leica Biosystems2012 [cited 2020. Available from: https://www.leicabiosystems.com/knowledge-pathway/fixation-and-fixatives-1-the-process-of-fixation-and-the-nature-of-fixatives/.

180. Singh H, Bishen KA, Garg D, Sukhija H, Sharma D, Tomar U. Fixation and Fixatives: Roles and Functions—A Short Review. Dental Journal of Advance Studies. 2019;07(02):051-5.

181. Kawamoto F. Rapid diagnosis of malaria by fluorescence microscopy with light microscope and interference filter. The Lancet. 1991;337(8735):200-2.

182. Wongsrichanalai C, Pornsilapatip J, Namsiripongpun V, Webster HK, Luccini A, Pansamdang P, et al. Acridine orange fluorescent microscopy and the detection of malaria in populations with low-density parasitemia. American Journal of Tropical Medicine and Hygiene. 1991;44(1):17-20.

183. Lowe B, Jeffa N, New L, Pedersen C, Engbaek K, Marsh K. Acridine orange fluorescence techniques as alternatives to traditional Giemsa staining for the diagnosis of malaria in developing countries. Transactions of the royal society of tropical medicine and hygiene. 1996;90(1):34-6.

184. Guy R, Liu P, Pennefather P, Crandall I. The use of fluorescence enhancement to improve the microscopic diagnosis of falciparum malaria. Malaria journal. 2007;6(1):89.

185. Parsel SM, Gustafson SA, Friedlander E, Shnyra AA, Adegbulu AJ, Liu Y, et al. Malaria over-diagnosis in Cameroon: Diagnostic accuracy of Fluorescence and Staining Technologies (FAST) Malaria Stain and LED microscopy versus Giemsa and bright field microscopy validated by polymerase chain reaction. Infectious Diseases of Poverty. 2017;6(1):1.

186. Park S, Zhang Y, Lin S, Wang T-H, Yang S. Advances in microfluidic PCR for point-of-care infectious disease diagnostics. Biotechnol Adv. 2011;29(6):830-9.

187. Bain BJ, Mitchell Lewis S. Chapter 4 - Preparation and staining methods for blood and bone marrow films. In: Lewis SM, Bain BJ, Bates I, editors. Dacie and Lewis Practical Haematology (Tenth Edition). Philadelphia: Churchill Livingstone; 2006. p. 59-77.

188. Keiser J, Utzinger J, Premji Z, Yamagata Y, Singer BH. Acridine Orange for malaria diagnosis: its diagnostic performance, its promotion and implementation in Tanzania, and the implications for malaria control. Ann Trop Med Parasitol. 2002;96.

189. Besarab A, Bolton WK, Browne JK, Egrie JC, Nissenson AR, Okamoto DM, et al. The Effects of Normal as Compared with Low Hematocrit Values in Patients with Cardiac Disease Who Are Receiving Hemodialysis and Epoetin. New England Journal of Medicine. 1998;339(9):584-90.

190. Steen RG, Xiong X, Mulhern RK, Langston JW, Wang WC. Subtle brain abnormalities in children with sickle cell disease: Relationship to blood hematocrit. Annals of Neurology. 1999;45(3):279-86.

191. BÜYÜKaŞIk Y, Alİ R, Ar C, Turgut M, Yavuz S, Saydam G. Polycythemia vera: diagnosis, clinical course, and current management. Turkish Journal of Medical Sciences. 2018;48(4):698-410.

192. Pearson TC. 2 Rheology of the absolute polycythaemias. Baillière's Clinical Haematology. 1987;1(3):637-64.

193. Çinar Y, Şenyol AM, Duman K. Blood viscosity and blood pressure: role of temperature and hyperglycemia. American Journal of Hypertension. 2001;14(5):433-8.

194. Mayer GA. Blood viscosity and oral anticoagulant therapy. American journal of clinical pathology. 1976;65(3):402-6.

195. Paal P, Brugger H, Strapazzon G. Chapter 33 - Accidental hypothermia. In: Romanovsky AA, editor. Handbook of Clinical Neurology. 157: Elsevier; 2018. p. 547-63.

196. Rogers AP, Estes M. Hyperviscosity Syndrome. StatPearls [Internet]: StatPearls Publishing; 2019.

197. Klabunde RE. Cardiovascular Physiology Concepts 2017 [updated december 08, 2017. Available from: https://www.cvphysiology.com/Hemodynamics/H011.

APPENDIX A

Table A1. Summary of different methods for malaria diagnosis. Reprinted with permission from **(**Tangpukdee, 2009)

Sensitivity and specificity	Depends on malaria endemicity	depends on good technique good reagent and micro microscopist skill	sensitivity and specificity higher than PBS	moderate if more 100 parasites/ µl	relatively high but not correlate to clinical symptom of patients	excellent	excellent	relatively high	variable sensitivity high specific	variable in both sensitivity and specificity	undetermined
time consumed	depends on physician's skill	30-60	< 15	10-15	30-60	45-360 depends on the methods	< 60	< 60	Automated < 1/sample	Automated < 1/sample	Automated < 1/sample
detection limit	undetermined	Expert ~5-10 routinely >50	> 5	50-100	undetermined	> 1	> 5	undetermined	poor correlation	5-20	100 for whole blood
expertise required	high in no endemic areas	high in no endemic areas	moderate	low	moderate	high	high	high	high	high	high
instrument cost	none	low-cost	moderate	moderate	moderate	expensive	moderate	expensive	expensive	expensive	expensive expensive

Table A1 Continued

Other considerations	Easy to follow the diagnostic algorithm; Result in significant over treatment of malaria especially in highly endemic areas but lower estimation in hypoendemic areas	Gold standard method, good for all human species except (P knowlesi) need considerable expertise	Simple and user-friendly electricity is need, limit for species identification and quantitative parasite;	1st line diagnosis in all areas; suitable in field work; possible for differentiation, between P vivax, malaria,	Results can be influenced by trained technician possible for all human species useful for epidemiological survey;	2nd line diagnosis in well-equipped laboratory useful to identify the development of drug resistance	limit for quantifying parasites; possible for all human species clinical trial are need to validate feasibility and clinical utility	Still in the early stage of development of malaria	Useful for diagnosis for clinical unsuspected malaria clinical trials are needed to validate feasibility and clinical utility	Clinical trials are needed to validate feasibility and clinical utility	Still in early stage of development diagnosis of malaria

Table A1 Continued

Other considerations continue	Severe malaria is commonly caused by P. falciparum mixed infection is still problematic	Mixed infection and low parasitemia may cause misdiagnosis	Cannot store capillaries for later reference	Limited for quantifying parasites low parasitemia may cause misdiagnosis	not useful for treatment decision making	Species; identification; and quantifying parasite density at low parasitemia		

Table A2. Severe falciparum malaria definition. Reprinted with permission from (WHO, 2015)

• Impaired consciousness: A Glasgow coma score < 11 in adults or a Blantyre coma score < 3 in children • Prostration: Generalized weakness so that the person is unable to sit, stand or walk without assistance • Multiple convulsions: More than two episodes within 24 h • Acidosis: A base deficit of > 8 mEq/L or, if not available, a plasma bicarbonate level of < 15 mmol/L or venous plasma lactate ≥ 5 mmol/L. Severe acidosis manifests clinically as respiratory distress (rapid, deep, laboured breathing). • Hypoglycaemia: Blood or plasma glucose < 2.2 mmol/L (< 40 mg/dL) • Severe malarial anemia: Hemoglobin concentration ≤ 5 g/dL or a hematocrit of ≤ 15% in children < 12 years of age (< 7 g/dL and < 20%, respectively, in adults) with a parasite count > 10 000/μL • Renal impairment: Plasma or serum creatinine > 265 μmol/L (3 mg/dL) or blood urea > 20 mmol/L • Jaundice: Plasma or serum bilirubin > 50 μmol/L (3 mg/dL) with a parasite count > 100 000/ μL • Pulmonary oedema: Radiologically confirmed or oxygen saturation < 92% on room air with a respiratory rate > 30/min, often with chest indrawing and crepitations on auscultation • Significant bleeding: Including recurrent or prolonged bleeding from the nose, gums or venipuncture sites; hematemesis or melaena • Shock: Compensated shock is defined as capillary refill ≥ 3 s or temperature gradient on leg (mid to proximal limb), but no hypotension. Decompensated shock is defined as systolic blood pressure < 70 mm Hg in children or < 80 mm Hg in adults, with evidence of impaired perfusion (cool peripheries or prolonged capillary refill). • Hyperparasitemia: P. falciparum parasitemia > 10%.

Table A3. Key differences between severe knowlesi and severe falciparum. Reprinted with permission from (WHO, 2015)

• P. knowlesi hyperparasitemia: parasite density > 100 000/μL • Jaundice and parasite density > 20 000/μL.

Table A4. Applications of Microfluidic Systems Made of Different Materials. Reprinted with permission from (Ren, 2013)

Applications	Silicon/glass	Elastomers	Thermoset	Thermoplastics	Hydrogel	Paper
CE	Excellent	Moderate	Good	Good	NA	NA
Electrochemical detection	Good	Limited	Moderate	Moderate	No	Moderate
Organic synthesis	Excellent	Poor	Good	Moderate to Good	NA	NA
Droplets formation [a]	Excellent	Moderate	Good	Good	NA	NA
PCR	Excellent	Good	Good	Good	NA	NA
Protein crystallization	Poor	Good	Poor	Moderate	NA	NA
Bioculture	Moderate	Good	Moderate	Moderate	Excellent, 3D	Good, 3D
Cost of production	High	Medium	High	Low	Medium to High	low
Reusability	Yes	No	Yes	Yes	No	No
Disposable device use	Expensive	Good	Expensive	Good	Hard to store	Good
[a] In the cases of droplet microfluidics, biological or chemical reactions are confined to individual droplets, and the surface properties of the device material only affect the generation of the droplets.						

Table A5. Overview of Materials for Microfluidic Device Fabrication. Reprinted with permission from (Ren, 2013)

property	silicon/glass	elastomers	thermoset	thermoplastics	hydrogel	paper
Young's (tensile) modulus (GPa)	130–180/50–90	~0.0005	2.0–2.7	1.4–4.1	low	0.0003–0.0025
common technique for microfabrication	photolithography	casting	casting, photopolymerization	thermomolding	casting, photopolymerization	photolithography, printing
smallest channel dimension	<100 nm	<1 μm	<100 nm	~100 nm	~10 μm	~200 μm
channel profile	limited 3D	3D	arbitrary 3D	3D	3D	2D
multilayer channels	hard	easy	easy	easy	medium	easy
thermostability	very high	medium	high	medium to high	low	medium
resistance to oxidizer	excellent	moderate	good	moderate to good [c]	low	low
solvent compatibility	very high	low	high	medium to high	low	medium
hydrophobicity	hydrophilic	hydrophobic	hydrophobic	hydrophobic	hydrophilic	amphiphilic
surface charge	very stable	not stable	stable	stable	N/A	N/A
permeability to oxygen (Barrer)	<0.01	~500	0.03–1	0.05–5	>1	>1
optical transparency	no/high	high	high	medium to high	low to medium	low

APPENDIX B

CHAPTER II SUPPORTING INFORMATION

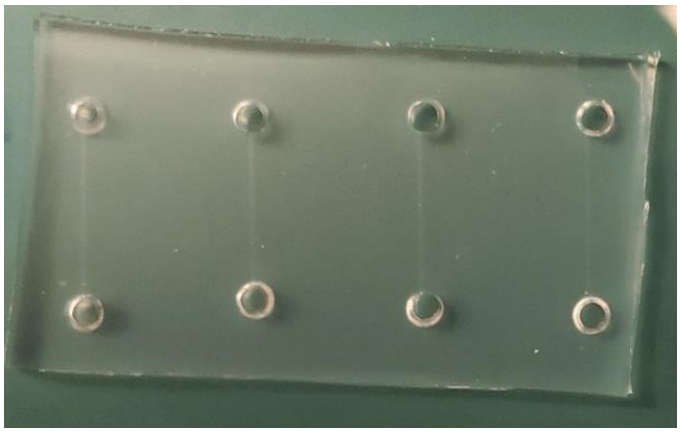

Figure S1. Photograph of a ***14% PEO-PDMS*** microfluidic chip bonded to a glass slide.

Figure S2. Photographs of *unmodified silicone* (i.e. unmodified Sylgard 184), *5% PEO-PDMS*, *7% PEO-PDMS*, and *14% PEO-PDMS* films.

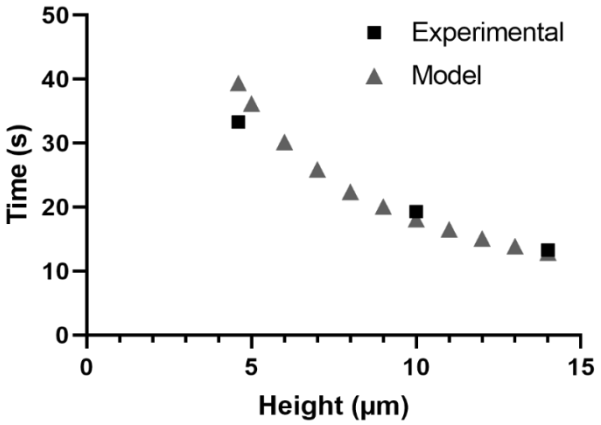

Figure S3. Theoretical model (Jong et al.) and experimental data of whole blood flow in a low height rectangular microchannel.

The equation for this model is $t = \frac{6\eta L^2}{\rho g H h^2 + 2h\sigma cos\theta}$

η: Blood viscosity= 9.834×10^{-3} Pa.S (bovine blood temperature around 10-15 degree was estimated)

L: channel length

ρ: density = 1060 kg/m^3

σ: Surface tension = 0.055 N/m

Θ: angle of 60 degree or 1.047 rad

H: 0.18 μm

h: channel height (4.6-14 μm)

g: gravity 9.8 m/S^2

Table S1. Modulus values of ***unmodified silicone***, ***5% PEO-PDMS***, ***7% PEO-PDMS***, and ***14% PEO-PDMS*** films (t = 0) (corresponding to **Figure 6a**).

Sample	Modulus (MPa)
Unmodified	4.8 ± 0.6
5% PEO-PDMS	3.0 ± 0.2
7% PEO-PDMS	2.3 ± 0.2
14%PEO-PDMS	1.1 ± 0.1

Table S2. Modulus values of the ***14% PEO-PDMS*** throughout aging (corresponding to **Figure 6b**).

Conditioning Time	14% PEO-PDMS (MPa)
Initial	1.1 ± 0.1
2 Weeks	1.4 ± 0.1
1 Month	1.5 ± 0.2
3 Months	1.5 ± 0.2
6 Months	1.6 ± 0.3

Table S3. Static contact angle (θ_{static}) values of ***unmodified silicone, 5% PEO-PDMS***, ***7% PEO-PDMS***, and ***14% PEO-PDMS*** at 15 sec and 1 min following water droplet placement (corresponding to **Figure 7a**).

Sample	15 sec (°)	1 min (°)
Unmodified	112.6 ± 0.4	111.9 ± 0.2
5%PEO-PDMS	107.1 ± 1.3	81.4 ± 3.6
7%PEO-PDMS	105.5 ± 7.3	57.8 ± 2.2
14%PEO-PDMS	19.8 ± 2.7	16.6 ± 1.5

Table S4. Static contact angle (θ_{static}) values of 3 replicate samples of ***14% PEO-PDMS*** at 15 sec, 1 min and 3 min following water drop placement.

Sample	15 sec (°)	1 min (°)	3 min (°)
14%PEO-PDMS_A	22.6 ± 2.2	15.3 ± 0.4	11.2 ± 0.5
14%PEO-PDMS_B	16.9 ± 7.2	12.9 ± 4.3	8.7 ± 1.8
14%PEO-PDMS_C	17.5 ± 2.4	11.2 ± 1.6	7.9 ± 1.5

Table S5. Static contact angle (θ_{static}) values of ***unmodified silicone*** and ***14% PEO-PDMS*** at 15 sec and 1 min following water droplet placement, taken throughout aging (corresponding to **Figure 7b**).

Conditioning Time	Unmodified 15 sec (°)	Unmodified 1 min (°)	14%PEO-PDMS 15 sec (°)	14%PEO-PDMS 1 min (°)
Initial	112.6 ± 0.4	111.9 ± 0.2	19.8 ± 2.7	16.6 ± 1.5
2 Weeks	114.5 ± 0.1	112.1 ± 0.2	21.6 ± 0.2	20.3 ± 0.4
1 Month	114.5 ± 0.2	114.1 ± 0.3	17.8 ± 1.4	12.7 ± 1.9
3 Months	114.7 ± 0.5	114.4 ± 0.5	42.0 ± 13.3	28.5 ± 6.7
6 Months	104.2 ± 2.7	103.8 ± 2.8	71.9 ± 15.5	44.1 ± 5.8

Table S6. Pumpless flow times of blood through microfluidic channels of ***7% PEO-PDMS*** with various heights: ***4.6 µm***, ***10 µm***, and ***14 µm*** (corresponding to **Figure 8a**).

Sample	Flow Time (s)
4.6 µm	33.3 ± 1.5
10 µm	19.3 ± 0.6
14 µm	13.3 ± 0.6

Table S7. Pumpless flow times of blood through microfluidic channels (***channel height = 14 µm***) of ***5% PEO-PDMS***, ***7% PEO-PDMS***, and ***14% PEO-PDMS*** (corresponding to **Figure 8b**).

Sample	Flow Time (s)
5% PEO-PDMS	31.0 ± 0.0
7% PEO-PDMS	13.3 ± 0.6
14% PEO-PDMS	7.7 ± 0.6

Video S1's name: microcarrier1084_middle_initial

Video S1. Video of capillary flow of blood (volume = 5 µL) at the middle of a ***14% PEO-PDMS*** microchannel (h = 14 µm, w = 250 µm) immediately after blood addition to the inlet.

Video S2's name: microcarrier1086_middle after 30min

Video S2. Video of capillary flow of blood (volume = 5 µL) at the middle of a ***14% PEO-PDMS*** microchannel (h = 14 µm, w = 250 µm) 30 min after blood addition to the inlet.

APPENDIX C

As mentioned earlier, every patient has a different blood. Although we cannot test for every blood condition, bellow is described 4 common blood situations or diseases and how those situations could affect the smear quality based on the blood flow model.

Blood with low hematocrit (15-20%) that leads to low blood viscosity (3 mPa.s). This is a situation for patients that are anemic or have kidney failure (189, 190). It is well known that as hematocrit decreases, the blood viscosity will decrease, and the flow rate will increase (i.e., low flow time). It was also shown earlier that increased flow rate could increase the amount cells that come in the channel, thus more cells are depicted per field of view (e.g., 7% SMA study, and worst-case scenario 1 µl study). Although a decrease in hematocrit will decrease the number of cells per field of view, that decrease in hematocrit also increases the flow rate by lowering blood viscosity. Thus, an increase in the number of cells that come in the channel could balance some of the low hematocrit problems and, in a worst-case scenario, would give a smear with low cell count

Blood with high hematocrit (51-78 %) that leads to high blood viscosity (15 mPa.s). This situation is common for patients that have erythrocytosis, polycythemia vera, and other conditions (191, 192). An increase in hematocrit will decrease the flow rate (higher flow time) by increasing the viscosity. Since more elevated hematocrit means more cells in the filed view and low flow rate means fewer cells will come in the channel, the two situations

could balance each other, but in a worst-case scenario, the blood will have difficulty flowing well similar to 3% SMA study.

Blood with a healthy level of hematocrit (40-50%) and low viscosity (3 mPa.s). This is a situation where the blood temperature increases or blood thinner medication is used (193-195). In this situation, the low viscosity by itself will not affect the smear much based on the flow model, which showed a flow time in the range that is believed would give a good quality smear.

Blood with a normal level of hematocrit (40-50%) and high blood viscosity (15 mPa.s). This situation is typical for hypergammaglobulinemia, multiple myeloma patients, or when the blood temperature decreases (195, 196). High viscosity means a low flow rate, so this situation has a normal hematocrit with a low flow rate, which could be similar to the 3% study in a worst-case scenario. Because the blood flow from the model showed a flow time in the range similar to our experimental data, it is believed that a good quality smear will be produced compared to high hematocrit/high viscosity situation.

Flow model assumption. A normal blood viscosity with (40-50 %) hematocrit (HCT) is around (4-6 mPa.s) (192, 197). Cold blood with normal hematocrit has a viscosity of about (9.8 mPa.s) around 10-15 degrees (195). In the model, 15 % HTC was chosen for anemia hematocrit, and this corresponds to around (3 mPa.s) blood viscosity (16, 197). The HTC of disease such as erythrocytosis, polycythemia is around 75%, which has ~ 15 mPa.s viscosity (197)

NOTE: This flow model is done in a channel without pillars compared to the channel used in study 3, so the flow times in the model are 15-30 s reduced compared to what the experimental data would give.

The equation for this model is $t = \frac{6\eta L^2}{\rho g H h^2 + 2h\sigma cos\theta}$

η: Blood viscosity (3, 6, 9.8, 15, 30 mPa.s)

L: channel length :13 mm

ρ: density = 1060 kg/m^3

σ: Surface tension = 0.055 N/m

Θ: angle of 60 degree or 1.047 rad

H: 0.18 µm

h: channel height (~3.5 µm: approximate practical height of the channel because of sagging)

g: gravity 9.8 m/S^2

Blood quality (HCT)	Viscosity	Time (s)
Anemic blood (15% HCT)	3	15
Healthy blood (43%HCT)	6	30
Cold blood ~15^{o} (43% HCT)	9.8	50
Polycythemia (75% HCT)	15	76
very extreme situation (~250% HCT)	30	153

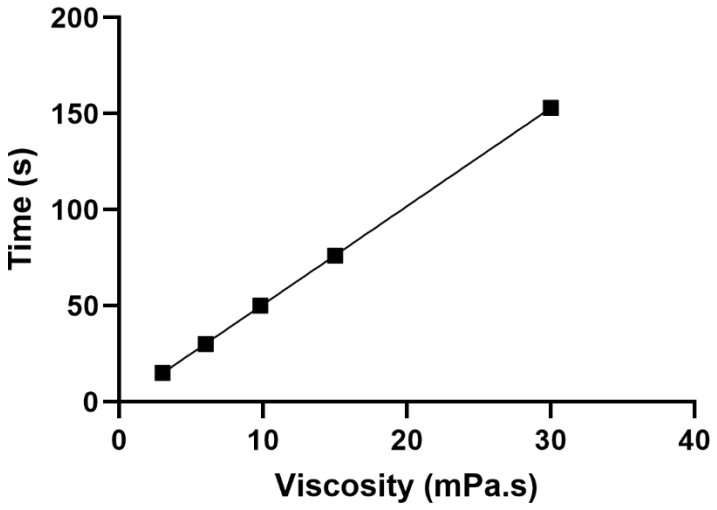

Figure C 1. Theoretical model (Jong et al.) of whole blood flow time as function of viscosity in a low height rectangular microchannel

APPENDIX D

Materials. Allyl methyl PEO (Polyglykol AM 450, M_n = 292–644 g mol^{-1} per manufacturer's specifications; Mn = 424 g mol^{-1} per proton (^1H) nuclear magnetic resonance (NMR) end group analysis) was provided by Clariant. Octamethylcyclotetrasiloxane and tetramethyldisiloxane were purchased from Gelest. $ODMS_{30}$ (M_n = 2354 g mol^{-1} per ^1H NMR end group analysis) was prepared as reported (56). Triflic acid, rhodium (I) tris(triphenylphosphine) chloride (Wilkinson's catalyst), hexamethyldisilazane, tridecafluoro-1, 1, 2, 2-tetrahydrooctyl-1-trichlorosilane, and solvents were obtained from Sigma-Aldrich. All solvents were dried over 3 Å molecular sieves prior to use. Sylgard 184 was purchased from Ellsworth Adhesives, and SU8-5 from Microchem. Glass microscope slides (75 × 25 × 1 mm3) were purchased from Fisher Scientific.

Synthesis of PEO-silane amphiphile (HSi-$PDMS_{30}$-PEO_8). The PEO-silane amphiphile polymer used to create the hydrophilic microchannels, HSi-$PDMS_{30}$-PEO_8, was synthesized as previously reported using a Wilkinson's-catalyzed regioselective hydrosilylation reaction of $ODMS_{30}$ and allyl methyl PEO_8 (1:1 molar ratio) (148). ^1H NMR of the purified product, a clear and colorless liquid, was in agreement with that previously reported.

Master-mold fabrication. The mask channel dimensions are 300 µm wide, 16 mm long. Each channel has 50 µm diameter pillars with 25 µm gaps between pillars at the inlet, outlet and middle of the channel. There are 1.1 mm of pillars, about 19 columns, at the

inlet and outlet. There are 2 sets of pillars with 3 columns in the middle of the channel at 4 mm from the inlet and outlet and 4 mm apart from one another. Master mold fabrication and coating is as described in our previous paper (160)

The mold and chip fabrication. Sylgard 184 "base" was added with the Sylgard 184 "curing agent" at a 10:1 ratio. To this 7% wt (*7% PEO-PDMS.)* HSi-$PDMS_{30}$-PEO_8 was added based on the total weight of the Sylgard base and curing agent. The samples were mixed in a Flacktek mixer for 15 sec at 1000 rpm, then manually ramped to 3000 rpm over 15 second and mixed at 3000 rpm for 4 min. After that, the sample is mixed in a 70 °C water bath before pouring into a 60 °C preheated master mold. The warmed sample was desiccated for 13 min to remove the air bubbles and cured at 130 °C for 1.5 hour. After the sample was cured, the molds were removed from the master molds and were stored for 2-5 days at room temperature. The molds were prepped during this period by creating the inlet and outlet with a 5 mm biopsy punch. The molds after being prepared were bonded to glass using an oxygen oven plasma cleaner (Harrick Plasma PDC-001) with the following protocol: sequential vacuum (10 min), oxygen (2 min), plasma (2 min), and 110 °C oven (2 hr). The bonded molds (chip) were stored in air at room temperature for 24 hours prior to use in the experiment to permit the plasma effect to dissipate from the chip. The dimensions of the chips used for the experiment after prepping were around 300 µm wide, around 13 mm long and around 4.7 µm height, with around 0.75 mm of pillars at the inlet and outlet.

Reconstitution of malaria cultures to replicate parasitized human blood. Cultures of *P. falciparum* malarial parasites were cultured asynchronously *in vitro* to a parasitemia of

approximately 5% in human RBC's Samples of the cultured cells suspended in growth media were centrifuged for 2 minutes at 2,000 rcf to form a loose pellet of parasitized RBC's in the base of the tube. The supernatant media was removed, and the process repeated twice more to form a non-packed, un-lysed collection of parasitized RBC's. This pellet was resuspended 1:1 by volume in fresh human blood plasma, and the resulting resuspended culture was mixed 1:1 with whole blood to create a physiologically accurate sample of human blood doped with *P. falciparum*. Control smears from each stage of sample reconstitution were created and examined to ensure that cellular morphology and hematocrit were preserved.

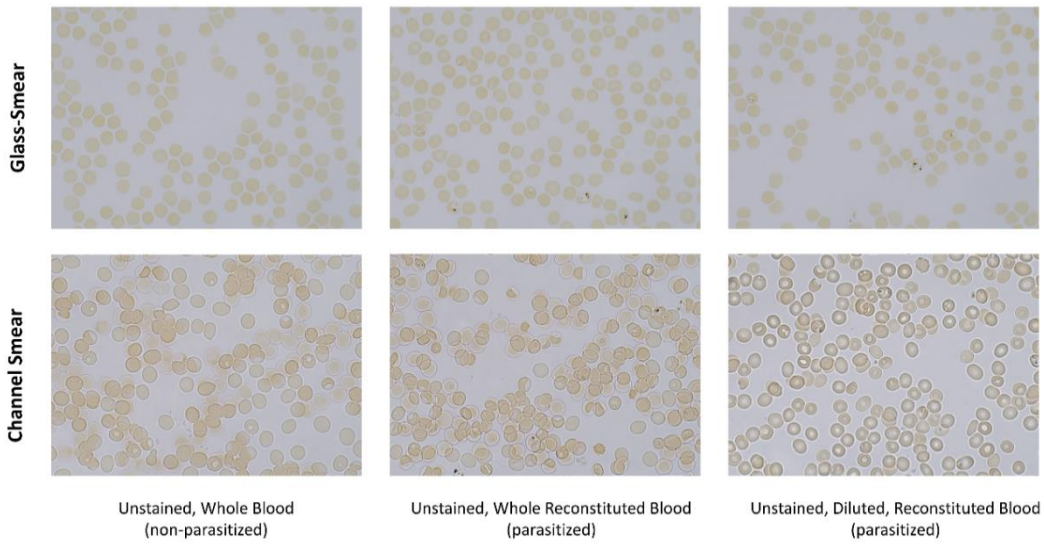

Figure D1. Assessment of reconstitution quality

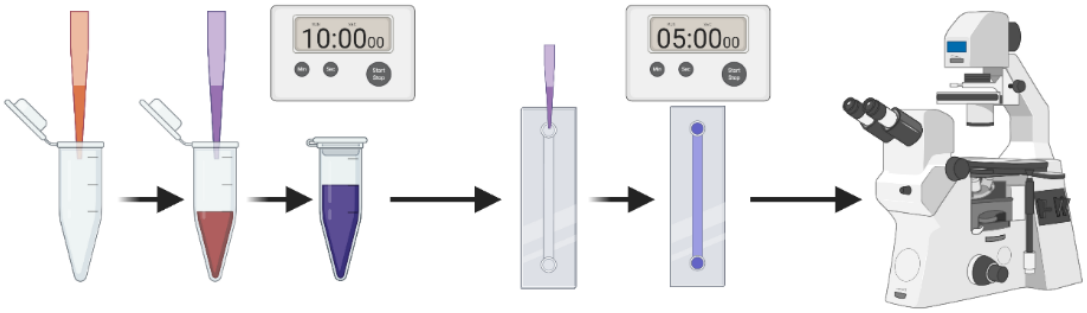

Figure D2. Overview Experimental Process Diagram

Effect of varying fluorescent stain concentrations during in-channel staining. Channels stained using 6 µg/mL, 12 µg/mL, and 96 µg/mL Acridine Orange were collected to assess staining quality for several concentrations of stain. Results show the relationship between increased stain concentration and fluorescent intensity, with the highest concentration of stain showing comparable parasitic intensity to that of the gold-standard images with much greater contrast between parasites and background

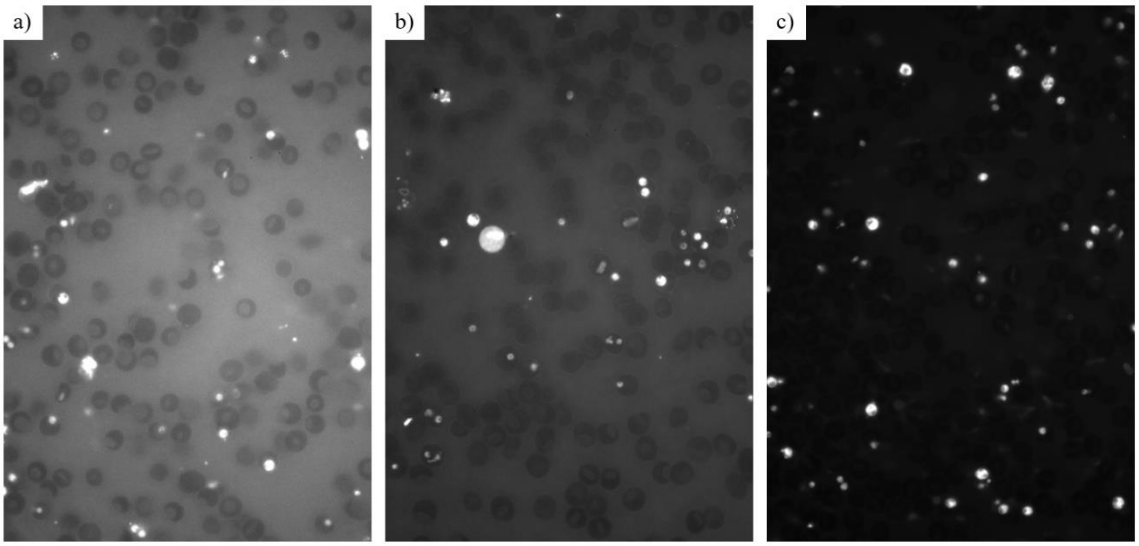

Figure D3. Monochromatic images of in-channel samples fluorescently stained using a) 6µg/mL, b) 12µg/mL, and c) 96µg/mL Acridine Orange. Greater contrast between parasites and background can be seen with higher stain concentration. Images shown with linear contrast enhancement for visibility.

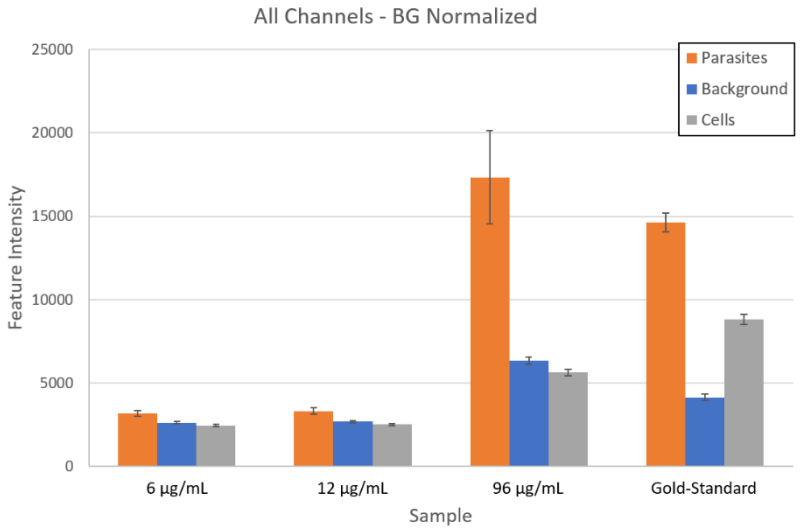

Figure D4. Values of fluorescence features as functions of Acridine Orange stain concentration and smear type